Fusion techniques for iris recognition in degraded sequences

Nadia Othman

NNT : 2016SACLL003

THESE DE DOCTORAT
DE
L'UNIVERSITE PARIS-SACLAY
PREPAREE A
TELECOM SUDPARIS

ÉCOLE DOCTORALE N°580
Sciences et technologies de l'information et de la communication

Spécialité de doctorat : Informatique

Par

Mme Nadia Othman

Fusion techniques for iris recognition in degraded sequences

Thèse présentée et soutenue à Evry, le 11 mars 2016 :

Composition du Jury:

Mme Florence TUPIN , Professeure, Télécom ParisTech, France - Présidente du Jury
M. Amine NAIT-ALI , Professeur, Université Paris-Est Créteil, France - Rapporteur
Mme Stephanie SCHUCKERS , Full Professor, Clarkson University, Etats-Unis - Rapporteur
Mme Maria DE MARSICO , Associate Professor, Sapienza Università Di Roma, Italie - Examinatrice
M. Emine KRICHEN, Docteur, MORPHO GROUPE SAFRAN, France - Examinateur
Mme Bernadette DORIZZI , Professeure, Télécom SudParis, France - Directrice de thèse

Acknowledgments

Preparing a thesis is a challenging task, but I have been lucky to be professionally and personally well-supported.

First and foremost, I would like to thank to my supervisor Prof. Bernadette Dorizzi for guiding and supervising me throughout the thesis. I am especially grateful for her valuable advices, comments, analyses and encouragements. Our discussions were very beneficial for me, which has contributed to the success of this thesis. I have a great respect for her not only for teaching me research skills but also for taking care personally.

I add a special thank to Dr. Nesma Houmani for her technical advices and remarks that have been valuable to me.

I would like to thank Prof. Florence Tupin, Prof. Amine Nait-ali, Prof. Stephanie Schuckers, Prof. Maria De Marsico, and Dr. Emine Krichen for being members of my PhD committee and for their comments and suggestions for improving this doctoral work.

I would like also to thank Prof. Stephanie Schuckers for providing us QFIRE database which was very useful to my research.

Special thanks go to all my colleagues of Télécom SudParis at Nano-INNOV for making enjoyable and friendly my daily environment.

Finally, I acknowledge the support of my relatives during all my scholarship. In particular, I dedicate this thesis to my parents.

Abstract

Among the large number of biometric modalities, iris is considered as a very reliable biometrics with a remarkably low error rate. The excellent performance of iris recognition systems are obtained by controlling the quality of the captured images and by imposing certain constraints on users, such as standing at a close fixed distance from the camera. However, in many real-world applications such as control access and airport boarding these constraints are not suitable due to the fact that the acquisition can be done at a large distance, with possible subject's movement. In such non ideal conditions, the resulting iris images suffer from diverse degradations such as a lack of resolution, low contrasts and strong occlusions. All these disturbances have a negative impact on the recognition rate.

One way to try to circumvent this bad situation is to use some redundancy arising from the availability of several images of the same eye in the recorded sequence. Therefore, this thesis focuses on how to fuse the information available in the sequence in order to improve the performance. In the literature, diverse schemes of fusion have been proposed at different levels (score, pixel, feature and bit). However, all these works agree on the fact that the quality of the used images in the fusion process is an important factor for its success in increasing the recognition rate. Therefore, researchers concentrated their efforts in the estimation of image quality to weight each image in the fusion process according to its quality. There are various iris quality factors to be considered and diverse methods have been proposed for quantifying these criteria. These quality measures are generally combined to one unique value: a global quality. However, there is no universal combination scheme to do so and some a priori knowledge has to be inserted. Moreover, whatever the method used, the fusion process requires previously a normalization step on the quality values, which is not a trivial task either.

To deal with these disadvantages, in this thesis we propose of a novel way of measuring and integrating quality measures in the image fusion scheme aiming at improving the performance. More precisely, we propose quality-based super-resolution approaches. This strategy can handle two types of issues for iris recognition: the lack of resolution and the presence of various artifacts in the captured iris images.

The first part of the doctoral work consists in elaborating a relevant quality metric able to quantify locally the quality of the iris images. Our measure relies on a Gaussian Mixture

Model estimation of clean iris texture distribution. A global quality can be defined by using the different local quality measures estimated on different sub-parts of the iris image. The interest of our quality measure is 1) its simplicity, 2) its computation does not require identifying in advance the type of degradations that can occur in the iris image, 3) its uniqueness, avoiding thus the computation of several quality metrics and associated combination rule and 4) its ability to measure the intrinsic quality and to specially detect segmentation errors.

In the second part of the thesis, we propose two novel quality-based fusion schemes. Firstly, we suggest using our quality metric as a global measure in the fusion process in two ways: as a selection tool for detecting the best images and as a weighting factor at the pixel-level in the super-resolution scheme. In the last case, the contribution of each image of the sequence in final fused image will only depend on its overall quality. Secondly, taking advantage of the localness of our quality measure, we propose an original fusion scheme based on a local weighting at the pixel-level, allowing us to take into account the fact that degradations can be different in diverse parts of the iris image. This means that regions free from occlusions will contribute more in the image reconstruction than regions with artefacts. Thus, the quality of the fused image will be optimized in order to improve the performance.

The effectiveness of the proposed approaches is shown on several databases commonly used: MBGC portal, Casia-Iris-Thousand and QFIRE at three different distances: 5, 7 and 11 feet. We separately investigate the improvement brought by the super-resolution, the global quality and the local quality in the fusion process. In particular, the results show the important improvement brought by the use of the global quality, improvement that is even increased using the local quality.

Keywords : Iris recognition; Data fusion; Global and local quality; Texture pattern; Super-resolution; Gaussian mixture model.

Résumé

Parmi les diverses modalités biométriques qui permettent l'identification des personnes, l'iris est considéré comme très fiable, avec un taux d'erreur remarquablement faible. Toutefois, ce niveau élevé de performances s'obtient en contrôlant la qualité des images acquises et en imposant de fortes contraintes à la personne (être statique et à proximité de la caméra). Cependant, dans de nombreuses applications de sécurité comme les contrôles d'accès, ces contraintes ne sont plus adaptées car l'utilisateur peut se trouver loin de l'objectif ou en mouvement. Les images résultantes souffrent alors de diverses dégradations : manque de résolution, faibles contrastes et occlusions importantes. Toutes ces perturbations ont un impact négatif sur les taux de reconnaissance.

Pour contourner ce problème, il est possible d'exploiter la redondance de l'information découlant de la disponibilité de plusieurs images du même œil dans la séquence enregistrée. Cette thèse se concentre sur la façon de fusionner ces informations, afin d'améliorer les performances. Dans la littérature, diverses méthodes de fusion ont été proposées à différents niveaux (score, pixel, descripteur et bits). Cependant, tous ces travaux s'accordent sur le fait que la qualité des images utilisées dans la fusion est un facteur crucial pour sa réussite. Plusieurs facteurs de qualité doivent être pris en considération et différentes méthodes ont été proposées pour les quantifier. Ces mesures de qualité sont généralement combinées pour obtenir une valeur unique et globale. Cependant, il n'existe pas de méthode de combinaison universelle et des connaissances a priori doivent être utilisées ainsi qu'une étape de normalisation qui rendent le problème non générique et non trivial.

Pour faire face à ces limites, nous proposons une nouvelle manière de mesurer et d'intégrer des mesures de qualité dans le schéma de fusion d'images. Plus précisément, nous proposons des approches de super-résolution complétées par des critères de qualité. Cette stratégie permet de remédier à deux types de problèmes courants en reconnaissance par l'iris: le manque de résolution et la présence d'artefacts dans les images d'iris.

La première partie de la thèse consiste en l'élaboration d'une mesure de qualité pertinente pour quantifier la qualité d'image d'iris. Elle repose sur une mesure statistique locale de la texture de l'iris grâce à un modèle de mélange de Gaussienne. Une qualité globale peut aussi être définie à partir de ces différentes mesures locales, effectuées sur les sous-parties de l'iris. L'intérêt de notre mesure est 1) sa simplicité, 2) son calcul ne nécessite pas d'identifier a

priori les types de dégradations, 3) son unicité, évitant ainsi l'estimation de plusieurs facteurs de qualité et un schéma de combinaison associé et 4) sa capacité à prendre en compte la qualité intrinsèque des images mais aussi, et surtout, les défauts liés à une mauvaise segmentation de la zone d'iris.

Dans la deuxième partie de la thèse, nous proposons de nouvelles approches de fusion basées sur des mesures de qualité. Tout d'abord, notre métrique est utilisée comme une mesure de qualité globale de deux façons différentes: 1) comme outil de sélection pour détecter les meilleures images de la séquence et 2) comme facteur de pondération au niveau pixel dans le schéma de super-résolution. Dans le deuxième cas, la contribution de chaque image de la séquence dans la reconstruction de l'image finale dépendra uniquement de sa qualité globale. Puis, profitant du caractère local de notre mesure de qualité, nous proposons un schéma de fusion original basé sur une pondération locale au niveau pixel, permettant ainsi de prendre en compte le fait que les dégradations peuvent varier d'une sous partie à une autre. Ainsi, les zones de bonne qualité contribueront davantage à la reconstruction de l'image fusionnée que les zones présentant des artéfacts. Par conséquent, l'image résultante sera de meilleure qualité et pourra donc permettre d'assurer de meilleures performances en reconnaissance.

L'efficacité des approches proposées est démontrée sur plusieurs bases de données couramment utilisées: MBGC portal, Casia-Iris-Thousand et QFIRE à trois distances différentes. Nous étudions séparément l'amélioration apportée par la super-résolution, la qualité globale et la qualité locale dans le processus de fusion. En particulier, les résultats montrent une amélioration importante apportée par l'utilisation de la qualité globale, amélioration qui est encore augmentée en utilisant la qualité locale.

Mots-clés : Reconnaissance par l'iris; Fusion d'information; Qualité globale et locale; Motif de texture; Super-resolution; Mélange de Gaussienne.

Contents

List of Tables

List of Figures

Acronyms and abbreviations

Organizations/Benchmarks	
IREX	IRis EXchange
MICHE	Mobile Iris CHallenge Evaluation
NIST	National Institute of Standards and Technology
NICE	Noisy Iris Challenge Evaluation

Metrics	
DET	Detection Error Trade-off
EER	Equal Error Rate
FAR	False Acceptance Rate
FMR	False Match Rate
FNMR	False Non Match Rate
FRR	False Rejection Rate
FTA	Failure To Acquire
GAR	Genuine Acceptance Rate
iFMR	image False Match Rate
iFNMR	image False Non Match Rate
ROC	Receiver Operating Characteristic

Models/Programs/Algorithms	
EM	Expectation Maximization
GMM	Gaussian Mixture Model
OSIRIS	Open Source for IRIS
SVM	Support Vector Machine

Databases	
CASIA	Chinese Academy of Sciences Institute of Automation
ICE2005	Iris Challenge Evaluation 2005
ICE2006	Iris Challenge Evaluation 2006
MBGC	Multiple Biometrics Grand Challenge
QFIRE	Quality Face and Iris Research Ensemble

Abbreviations	
Def	Definition
GLCM	Gray Level Co-occurrence Matrix
GMM4obs	Gaussian Mixture Model with an observation vector of 4 elements
GMM5obs	Gaussian Mixture Model with an observation vector of 5 elements
GQ	Global Quality
HR	High-resolution

IOM	Iris-On-the-Move
LBP	Local Binary Pattern
LR	Low-Resolution
LQ	Local Quality
MGMP	Multi-Gallery Multi-Probe
NIR	Near InfraRed
QAoT	Quality Assurance of Texture
QMA	Quality Measurement Algorithm
SR	Super-resolution
UIA	Usable Iris Area
uirLBP	uniform invariant rotation Local Binary Pattern

Chapter 1. Introduction

Reliable methods for automatic identification of individuals meet the increasing demand for security in applications such as ID cards, border crossings, access control and forensics. Traditional authentication methods based on knowledge (passwords, PIN number...) and tokens (identification cards) suffer from several limitations. Indeed, cards are vulnerable to being stolen, lost or even shared and passwords can be easily forgotten. In contrast, human identifications based on physiological and behavioral characteristics are great alternatives to verify the identity of a person. In fact, such methods called biometrics, do not require knowledge and tokens, and thus become more convenient and friendly for users. Biometric traits such as face, iris, voice, fingerprint, and palmprint have also proved to be unique to each person and constant throughout its lifetime [1]. For all these reasons, a growing attention has been devoted to biometric methods.

This thesis exclusively addresses iris trait for human identification, namely iris recognition. Among all biometric characteristics, iris pattern has been revealed as one of the most reliable biometric trait to distinguish among different persons [2]. Large scale evaluations have demonstrated remarkable performance in terms of recognition accuracy [3].

The iris is an "annular structure of elastic connective tissues forming a rich pattern of random texture, visible in the eye" as defined in [3]. It is located between the pupil (dark region) and the sclera (bright region). The border between the iris/pupil and the iris/sclera are respectively called pupillary and limbic boundaries. The iris surface is characterized by diverse patterns e.g. radial and contraction furrows, crypts... They represent the iris texture. A schematical anatomy of the human eye is provided in Figure 1-1.

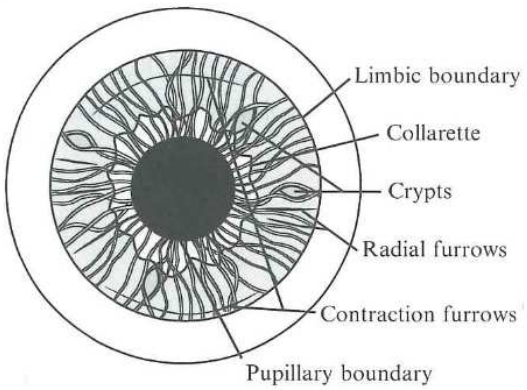

Figure 1-1: Frontal view of a schematical human eye [3]

Iris has several interesting properties. In contrast to other biometric traits such as fingerprint and face, the iris is an internal organ, highly protected and thus cannot be easily altered [4]. It also satisfies the requirements of uniqueness for biometric purpose. In fact, the iris texture is revealed to be a random pattern of great complexity and randomness. More precisely, the texture is epigenetic (not genetic determined, except for eye color), and developed from the third to eighth month of the gestation [5]. Moreover, the iris assures stability throughout life [6]. For all these reasons, the iris allows distinguishing between different people, even in the case of monozygotic twins. Moreover the iris texture of the right and the left eyes belonging to the same person is different [7].

In Section 1.1, we relate the origin of recognizing people by their iris by citing the major key dates in the iris recognition history. The major deployments of iris recognition systems in real applications are reported in Section 1.2. After that, Section 1.3 explains how iris acquisition can be achieved in operational systems. Classical iris recognition systems usually follow four main steps. They are briefly described in Section 1.4. The objective and the contributions of the thesis are presented in Section 1.5. Then, the structure of the report is described in Section 1.6. Finally, the publications that have been published as part of this doctoral work are listed in Section 1.7.

1.1. History of iris recognition

Iris recognition is based on the analysis of iris patterns by mathematical pattern recognition techniques. This modality is actually relatively recent, since the first automatic system able to identify people based on iris texture was developed and patented by John Daugman in the last decade of twentieth century.

However, the concept of recognizing people by their iris dates back to the nineteenth century. In 1886, Alphonse Bertillon was the first to propose properties of the human eye (color) for arrestee identification [8]. The idea of exploiting iris patterns was founded latter with the ophthalmologist James H. Doggart in 1949 who had written [9]:

"Just as every human being has different fingerprints, so does the minute architecture of the iris exhibit variations in every subject examined. [Its features] represent a series of variable factors whose conceivable permutations and combinations are almost infinite."

In 1953, Francis H. Adler also referred to this fact in a clinical textbook [10]:

"In fact, the markings of the iris are so distinctive that it has been proposed to use photographs as a means of identification, instead of fingerprints.".

Much later in 1987, the concept of using iris in automatic recognition system founded its origin through two ophthalmologists: Leonard Flom and Aran Safir [11]. In fact, they patented the conjecture of Adler and Doggart that iris texture could be used for identification but without proposing an algorithm or an implementation to perform it. Less than ten years after, John Daugman developed and patented the first automatic iris recognition system in 1994 [12] and details on the algorithm were published in [13]. Most of the current iris recognition solutions are still based on Daugman' approach.

1.2. Deployments of iris recognition systems: Security applications

Many real-world security applications, such as financial transactions, access control, crossing international borders and so on, require reliable personal identification. Due to the impressive uniqueness of the texture, iris biometric systems have been successfully adopted in several large-scale applications, especially at airports for borders crossing in lieu of passport presentation for frequent travelers.

For instance, the UK IRIS project (Iris Recognition Immigration System) has been deployed at many airports, including Heathrow, Manchester, Birmingham and Gatwick, to identify frequent travelers by their iris [14]. The system requires a priori registration (between five and ten minutes) in order to store their irises in an enrolled database. After that, the enrolled travelers just have to look at the front of the camera, crossing an IRIS gate (about twenty seconds) to perform the automatic identification: the iris is compared to all that are present in the enrollment database. Consequently, frequent passengers can travel without having to wait in a queue to have their passport stamped. Figure 1-2 illustrates an example of the IRIS gate in a United Kingdom airport terminal for enrolled frequent travelers.

This technology is also employed in other countries for controlling border access such as Schiphol airport in Netherlands [15], twenty-nine national airports in Canada [16], and also in the United States [17] [16].

In the United Arab Emirates, iris-based border security systems are widely used to track expellees and to perform access control [18]. The project is deployed at 32 air, land and sea ports. Over

one million of iris templates are saved in a "watch-list". Each day, about 12,000 irises are compared to that list, leading to 14 billion of comparison. Since 2001, all expellees have been enrolled in order to track illegal re-entry to UAE.

Figure 1-2: An example of IRIS gates used at an airport terminals for registered frequent travelers in lieu of passport presentation [19].

The most largely deployed biometric system is set up in India. The project UIDIA (Unique Identification Authority of India) [20] started in 2009 and is still in progress. For each Indian resident, a unique number, called Aadhaar number, is attributed to provide a form of identity in order to facilitate medical and financial aids, government use (national ID card, driver's license...)... Each number is linked to biometric data (face, fingerprints and irises). More than 200 million citizens have been enrolled since 2012, and the final goal of UIAID is to record about 1.2 billion persons.

The major projects based on iris recognition are listed in Table 1-1.

Due to the current success of iris recognition in many real-world applications, there is a clear trend toward less controlled iris acquisitions. Scenarios such as portal-based, at-a-distance, and on-the-move are more and more frequent in biometric system.

Table 1-1: Summary of public deployment of iris biometric systems (data from [1]).

Project	Country	Enrollments	Purpose
UIDAI Aadhaar	*India*	*>200 million (2012)*	*National identity number for financial aids, governance, etc. [20]*
UNHCR Repatriation	*Afghanistan*	*>2 million (2008)*	*Refugee registration for aid (assistance package, food, etc.) [21]*
UAE Border control	*UAE*	*>1.5 million (2008)*	*Expellees tracking and border control in the United Arab Emirates [18]*
TSA CLEAR	*US*	*>175 thousand (2008)*	*Frequent traveler border crossing at major US airports [17]*
National Airport Sec.	*Canada*	*>150 thousand (2010)*	*Security solution at 29 Canadian airports [16]*
IRIS	*UK*	*>100 thousand (2009)*	*Heathrow, Manchester, Birmingham and Gatwick airports border control [14]*
NEXUS	*US, Canada*	*>100 thousand (2006)*	*Frequent traveler border-crossing [22]*
York County Prison	*US*	*>35 thousand (2012)*	*Inmates registration [16]*
Privium	*Netherlands*	*>30 thousand (2009)*	*Frequent traveler border control at Schiphol airport using smartcard [15]*

1.3. Iris acquisition

Acquiring iris images of high quality is not an evident task. The iris relatively represents a small part of the face, with a diameter approximately equals to 11 mm. Moreover, iris is an internal organ, situated behind the cornea, which is strongly reflective.

Most commercial iris acquisition systems work in near infrared (NIR) band. The illumination source emits a light with a wavelength in the range of 700-900 nm. At those wavelengths, the structure of iris patterns are visible, even for highly pigmented irises (dark eyes), and the reflection of the light is widely reduced, in contrast to visible wavelength light. Figure 1-3 shows an example of an iris image acquired in near infrared. The iris texture is well revealed under such wavelengths.

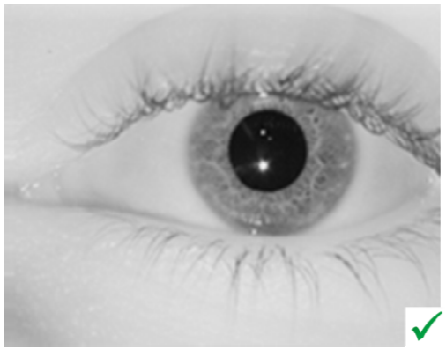

Figure 1-3: Iris image acquired in near infrared band with LG2200 sensor.

1.3.1. Controlled mode: conventional acquisition

The acquisition conditions of the iris images play a crucial role in the iris recognition. In fact, the quality of the captured images is closely linked to recognition rate as pointed out by many biometric researches.

First conventional systems have been very restrictive: the user is fully cooperative during the acquisition process. He is asked to stand close to the camera at a fixed distance, and to look straight at it. The eye has to be wide open and located in the center of the image. The specular reflections should appear inside the region of the pupil and not on the pupillary boundary or inside the iris region.

A series of algorithmic measurements of the image quality, such as focus, pupillary and limbic contrasts, illumination and iris resolution, are also used in such controlled acquisition scenario. Technical guidance for iris image collection were established in the IRis EXchange (IREX) program [23], more precisely in the IREX V [24]. The project was organized by the National Institute of Standards and Technology (NIST). An example of a "correct" iris acquisition is illustrated in Figure 1-4.

All these recommendations were suggested in order to give guidance for avoiding the collection of poor quality iris samples. Consequently, the resulting images are of good quality but with a lack of user-friendliness during the acquisition.

There are principally two different types of camera for iris acquisition in controlled mode:

- *Access control*: Wall-mounted camera with moderate focal volume as illustrated in Figure 1-5-a.
- *Handheld:* Portable camera with small focal volume as depicted in Figure 1-5-b.

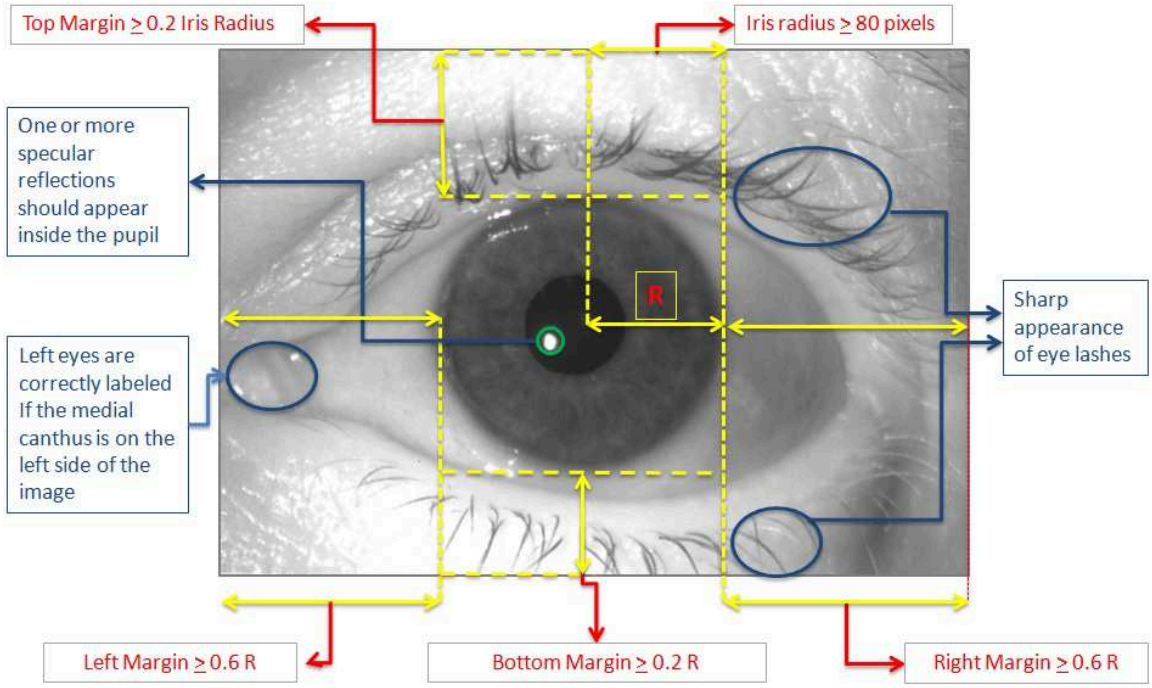

Figure 1-4: An example of a correct iris acquisition, with some of its desirable properties marked up [24].

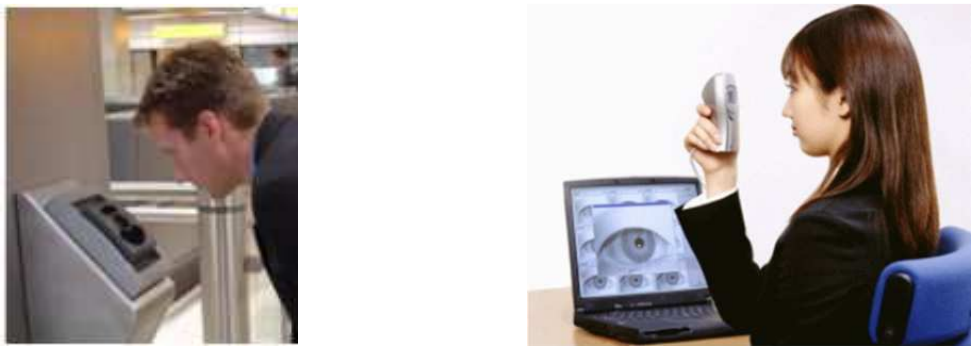

(a) (b)

Figure 1-5: Examples of iris acquisition devices: (a) IrisAccess2200 from LG/IrisID with an acquisition range between 8 to 25 cm, and (b) IRISPASS-H from OKI with an acquisition distance of approximately 3 cm.

1.3.2. Uncontrolled mode: less constrained acquisition

However, in many real-world security applications as presented in Section 1.2, many of these constraints become impossible to impose on the user, especially for iris recognition at a distance and

on-the-move. Relaxing acquisition conditions is an active field of research. Various iris recognition systems have been designed and developed, such as IOM system (Iris On the Move), working with moving subject passing through a portal at 3 meters [25], Eagle-Eyes operating at 3-6 meters [26], Stand-off system with iris acquisition at 1.5 meters [27] and 3 meters [28], Pan tilt zoom camera operating at 1.5 to 3 meters [29], and finally long range iris acquisition system (video surveillance) at 8 to 12 meters [30] and 30 meters [31]. Such systems will be described in details in Chapter 3.

The scenarios addressed by such systems correspond to more realistic conditions. However, as the degree of freedom of the subject's movement and position increase, the expected variation in the images acquired by such systems increases too. These changes lead to potentially strong differences in resolution, illumination and eye pose between different acquisitions. As pointed in [32], this fact has a negative impact on the recognition accuracy. In particular, the similarity between two irises of the same eye considerably decreases when the environment acquisition differs, leading to eventual confusion regarding the biometric decision (iris from the same person or not). Moreover, the resulting images often suffer from a lack of resolution and contrast between the pupillary and limbic boundaries. Strong occlusions (e.g. eyelids, eyelashes, specular reflections) frequently occur in such uncontrolled acquisition mode. Examples of degraded iris images are given in Figure 1-6. For all these reasons, iris recognition in such conditions becomes a very challenging task.

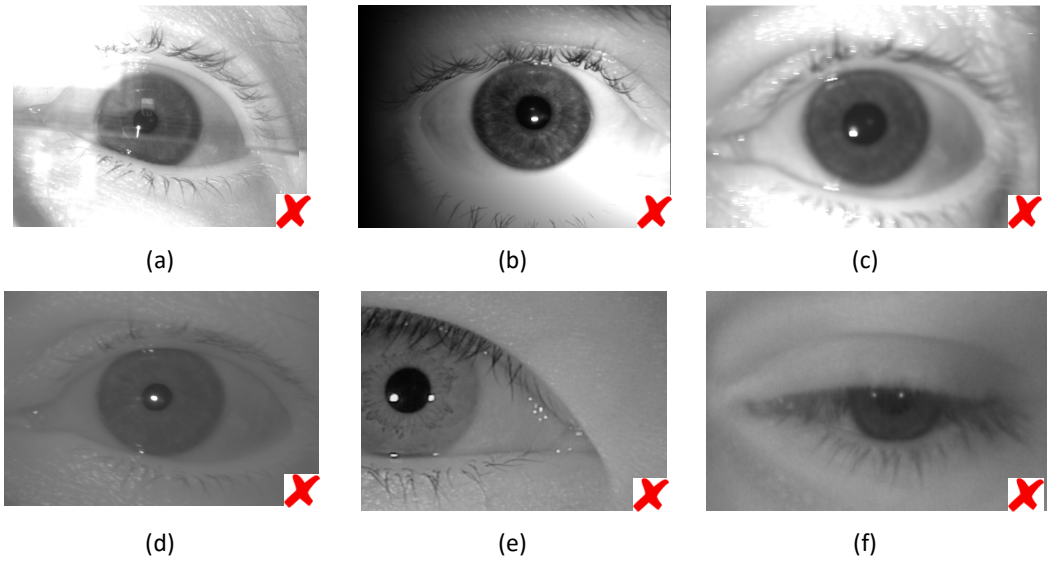

Figure 1-6: Examples of degraded iris images: (a) Specular reflection, (b) Irregular illumination, (c) Out of focus, (d) Low contrast, (e) Off-center and (f) Occlusions.

1.4. Iris recognition

In 1993, Daugman [13] was the first to propose a complete iris recognition system. Most of current systems are inspired from it. They are usually divided into the four following steps:

1. Iris segmentation

The first task consists in isolating the iris texture from other elements of the image such as eyelids, eyelashes, spotlights and/or shadows. These elements are considered as artifacts and have to be handled at this stage. The pupillary and limbic boundaries are usually modeled by a parametric shape such as circles or ellipses. In addition, the segmentation module generates a binary mask to indicate which pixels of the image belong to iris texture in order to remove noisy information in the further steps.

2. Normalization

The iris region is mapped into a size-invariant band called the normalized iris image. This dimensionless coordinate system of the resulting image copes with the problem of pupil dilation. This transformation is carried out by exploiting a parameterization of the iris boundaries obtained by the segmentation module. The normalization process allows the alignment of any two iris images to be compared.

3. Feature extraction

This stage aims at extracting the texture characteristics of a given iris. Discriminative features of iris texture are the basis for the comparison (also called matching) of any two images. The resulting template is usually represented by using a binary code composed of bits, called irisCode. These bits are obtained by the quantization of the iris features.

4. Template matching

The final stage of iris recognition systems consists in deciding whether two templates belong to the same iris or not. To this end, a similarity or dissimilarity score is computed between the two binary codes to be compared. The decision of acceptance or rejection is taken by comparing the matching score to a threshold. The key at this stage is to fix this threshold appropriately, in order to take the correct decision.

We note that several levels are used for representing the iris during these four stages: (1) the pixel-level (in the segmentation and normalization steps), (2) the feature-level (in the feature extraction

stage), and finally (3) the bit-level (in the matching step). Figure 1-7 shows the standard elements given by a classical iris recognition system.

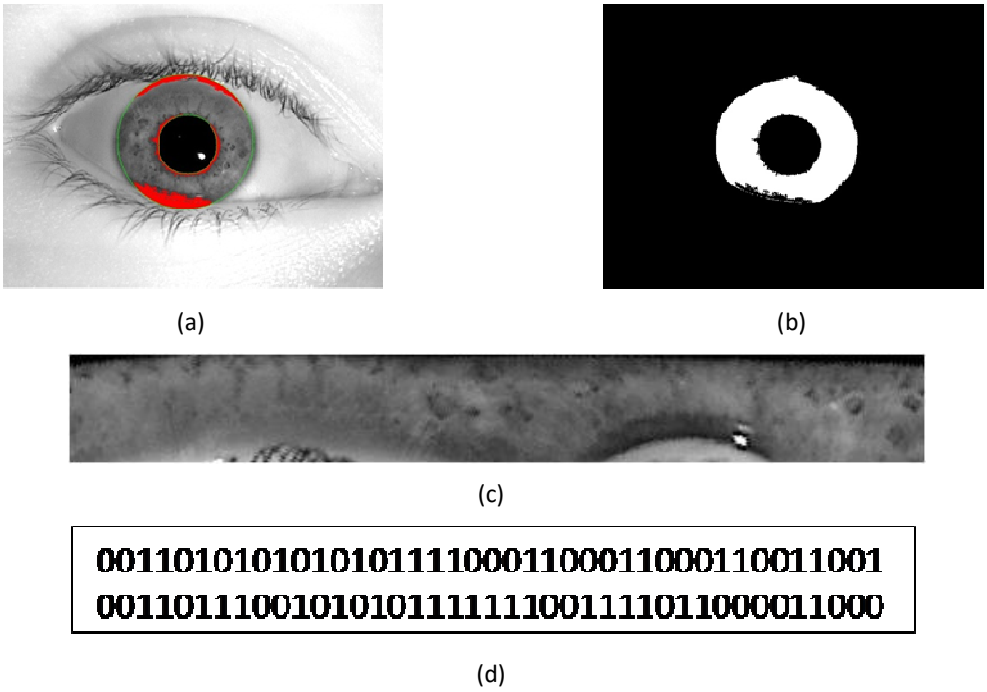

Figure 1-7: Standard components in a classical iris recognition system: (a) Iris segmentation: the red regions correspond to the artifacts, detected by the iris recognition system. The green circles delimit the iris area. (b) Iris mask: The white pixels belong to the iris, the remaining black pixels are considered as noisy regions, (c) Normalized iris image, and (d) IrisCode [33].

1.5. Objective and contributions of the thesis

Ideally, an iris recognition system would operate with un-cooperative users, and acquire images of subjects possibly on the move and at a significant distance. However due to the difficulty in obtaining images of good quality, environmental conditions must be constrained e.g. NIR illumination, close acquisition distances, frontal gaze and user collaboration. Nevertheless, dealing with real scenarios, it becomes impossible to impose these constraints to the users. Consequently, the resulting iris images tend to suffer from imperfections as depicted in Figure 1-6. All these degradations significantly decrease iris recognition performance. In fact, it is well known that recognition performance is strongly related to the quality of the biometric samples [34].

In line with this problematic, in this doctoral work we have addressed NIR video based iris recognition in such non-ideal condition, which corresponds to more realistic applications. Our objective consists in proposing a solution to overcome the degradation of the performance that is caused by the low quality of the resulting iris images. In such situations, two main aspect have to be taken into account:

- *Iris resolution:* A minimal resolution has to be respected. The International Standards Organization (ISO) Iris Image Standard released in 2005 [35] suggested a minimum of 100 pixels across the iris diameter. Under this value, the recognition performance is dramatically degraded. Images that contain irises with 200 pixels in the diameter are considered of high quality.
- *Iris quality:* Due to the relaxation of the constraints imposed on the users during the acquisition, the quality of the captured irises may change from a frame to another. Blur resulting from out-of-focus or/and motion blur, eyelids and eyelashes occlusions, specular reflections, shadows, off angles, uneven illumination, low contrasts between the boundaries are generally present in the images. All these factors affect the accuracy of the recognition.

Instead of keeping only one high quality iris image such as done in controlled mode, in unconstrained scenarios, we consider the whole series of frames containing eventual degradations as cited before. One way to try to circumvent this bad situation is to use some redundancy arising from the availability of several images of the same eye in the recorded video sequence. Therefore, our research activities focus on how to fuse the information available in the sequence in order to improve as much as possible iris recognition.

In the state-of-the-art, different schemes of fusion have been proposed. These methods can be achieved at different levels such as score and signal levels i.e. pixel, feature, or bit levels (see Section 1.4.). However, researchers agree that the quality of images used in the fusion process is a very important factor for its success, and for obtaining an improvement in the recognition performance. Therefore, they concentrated their efforts in the estimation of the image quality of each image in the sequence in order to give it less or more weight in the fusion process according to its quality. The principal iris quality components to be considered are: defocus/motion blur, occlusion/specular reflection, lighting, resolution and iris/pupil-iris/sclera contrasts. Various methods have been proposed for quantifying these criteria. These quality measures are generally combined in order to give one unique value: **a global quality**. There is no universal combination scheme to do so and in general some

a priori knowledge is inserted. The combination method can be a simple multiplication or a more sophisticated method such as the theory of Dempster–Shafer. Moreover, whatever the used method, the fusion process requires previously a normalization step on the quality values, which is not a trivial task either.

To deal with most of the disadvantages mentioned before, we propose a different approach for computing the quality of an iris image. In the thesis, we concentrate our efforts on proposing of a novel way of measuring and integrating quality measures in the image fusion scheme, aiming at improving the poor performance resulting from the image degradations obtained from unconstrained acquisitions.

Therefore, we have first elaborated a relevant local quality metric to assess the amount of good texture in the normalized iris images. This measure relies on a Gaussian Mixture Model (GMM) estimation of a clean iris texture distribution. Our idea is to exploit this quality in the fusion process. The GMM has been carefully designed in order to characterize the iris texture patterns in non-ideal captured images. This local quality can be used to compute a global quality measure of the normalized iris image. This new metric has been compared to most influential quality factors that are mentioned in the state-of-the-art. We will also see that our quality measure is well correlated to the recognition performance.

After that, we have proposed two novel schemes based on a super-resolution technique applied at the pixel-level, on the different frames of a video, improved by taking into account our quality measure in the fusion process. More precisely, our first contribution is the proposition of a global quality measure of iris images, that we will use in two ways: as a selection tool and as a weighting factor at the pixel-level in the super-resolution scheme. The interest of our quality measure compared to what is done in the literature is (1): its simplicity, (2): the fact that its computation does not require identifying in advance the type of degradations that can occur in the iris images, (3) its uniqueness (to avoid combination method). The super-resolution was carried out in order to remedy the poor resolution of iris images in videos acquired at a significant distance.

Taking benefit of this local measure, we explore as a second novel contribution a **local weighting** strategy at the pixel-level, allowing us to handle local degradations of the iris images. Indeed, we assume that the quality in a given iris image can be different in diverse sub-regions. Therefore, by performing a local weighted scheme, regions free from occlusions will contribute more in the reconstruction of the fused image than regions with artefacts. Thus, the quality of the

reconstructed image will be optimized in order to improve the performance. To our knowledge we were the first to propose a local weighted scheme at the pixel-level in the literature.

The effectiveness of the proposed approaches has been demonstrated on several iris databases that are collected under different unconstrained scenarios: iris-on-the-move (MBGC portal database [36]), with intra-class variations (CASIA-Iris-Thousand [37]) and at different significant distances (collections of QFIRE database [38] [39]). We have analyzed separately the iris recognition improvement brought by the use of the super-resolution, the global quality and then the local quality for determining the best strategy of fusion that leads to the best performance. This variability of the acquisition protocols allows us to determine the robustness of the proposed approaches and determining the best strategy of fusion regarding the specificity of the acquisition scenario.

To our knowledge, only a few works have been assessed on the QFIRE database for the iris modality [40] [41] [42] and no protocols have been yet defined for this database. The database contains a large number of acquisition scenarios. Therefore, we selected the scenarios and we defined some protocols that seemed interesting for assessing our contribution in the fusion process. Note that we would be happy to share them with the iris community so that they could be used for benchmarking other iris recognition systems in video. Note that providing novel assessment protocols for the QFIRE database is another contribution of the doctoral work.

Finally, we will demonstrate the advantage of performing a weighted fusion scheme at the pixel-level in unconstrained iris acquisition compared to another level which is the bit-level as proposed in recent works of the state-of-the-art. To this end, we have integrated our local quality in the matching score computation stage. More precisely, the local quality measures the reliability of the bit-pair comparisons. Then, we will also demonstrate the limitation of recent methods performing at the bit-level.

Throughout the thesis, we have used two iris recognition systems developed by our research group before my arrival: OSIRISV2 and the novel one OSIRISV4.1. These two systems are open source and they are available on the website of Biosecure [43]. However, I have been involved into recent works related to OSIRIS. We have published a paper which presents a comparison between the different OSIRIS's versions [33]. Moreover, we have submitted the last version: OSIRISV4.1 to the ICB Competition on Iris Recognition 2013 [44]. The obtained results show that OSIRISV4.1 can be considered as an efficient iris recognition system.

1.6. Thesis organization

The thesis is organized as follows:

Chapter 2. Evaluation of iris recognition systems, presents the methods and tools we used in the thesis to evaluate the performance of biometrics systems and quality measurement algorithms. After that, the public iris databases that have been selected to assess our algorithms are described. The major benchmarks in the field of iris recognition are then given to highlight the interest of the research community in iris recognition in non-ideal situations.

Chapter 3. Fundamentals in iris acquisition and recognition systems, focuses on the state-of-the-art of iris acquisition and recognition systems. First, the most important iris recognition systems in the literature are described. Next, we present the designed open source recognition systems we used in the thesis. Finally, a literature review on iris acquisition systems in less constrained environments is reported.

Chapter 4. Design of a quality measurement algorithm for improving iris recognition, has as center point our quality measurement algorithm. Related works to iris image qualities are first presented. Iris quality components and their usage in recognition systems are explained. From this, we will define what a relevant quality metric for iris recognition should be and design the proposed quality measurement algorithm that will be used throughout the thesis. Details on the statistical model that we have elaborated to quantify the amount of iris texture are then given. Besides, we present how we have used it to measure locally the quality of the iris images. A global quality metric is also defined. We will show that our global metric is well correlated to the performance of the system. Moreover, a comparative study between our quality and most of the quality components that are shown in the literature to influence significantly iris recognition is then given. From this study, we will deduce the effectiveness of the proposed quality assessment algorithm in characterizing iris pattern of good quality.

Chapter 5. Fusion approaches of iris sequences for improving the recognition, presents the main contribution of the work. First, an overview of the methods used for the fusion of iris sequences captured in less constrained acquisition is given. We will see that all these works agree on the fact that the key of a successful fusion scheme lies in the good quality of the iris images. This will lead us to propose quality-based fusion schemes in order to improve iris recognition. Our main novelty is the introduction of a local quality measure (presented in Chapter 4) in the fusion scheme. It can also be

exploited for computing a global quality measure of the iris image which can be used either for the selection of the best images or for weighting the images in the fusion scheme. Finally, extensive experiments on challenging iris databases acquired under different real-world scenarios are reported. Experimental studies on the impact of the sequence fusion, the super-resolution and the introduction of the global and local quality are carried out. Depending on the specificity of each database, we will underline which strategy of fusion can lead to best performance.

Chapter 6. Quality assessment at the bit-level, reports comparisons between introducing our quality measure at two different levels in the fusion scheme: the pixel and bit levels. This comparison allows us to determine which strategy can lead to best performance. We will also see the limitations of some recent works that perform fusion at the bit-level.

Finally, **Chapter 7** closes this thesis with conclusions and perspectives.

1.7. List of publications

The publications that have been published as part of this doctoral work are as follows:

International conferences:

- Nadia Othman, Nesma Houmani, Bernadette Dorizzi: *Improving Video-based Iris Recognition Via Local Quality Weighted Super Resolution*, in International Conference on Pattern Recognition Applications and Methods (ICPRAM), Barcelona, Spain, 2013.
- M. Zhang, J. Liu, Z. Sun, T. Tan, W. Su, F. Alonso-Fernandez, V. Nemesin, N. Othman, K. Noda, P. Li, E. Hoyle, A. Josh: *The First ICB Competition on Iris Recognition*, in international Joint Conference on Biometrics (IJCB), Florida, USA, 2014.

Book chapter:

- Nadia Othman, Nesma Houmani, and Bernadette Dorizzi: Quality-Based Super Resolution for Degraded Iris Recognition, in Advances in Intelligent Systems and Computing, Series “Pattern Recognition Applications and Methods”, vol. 318, Springer, Jan. 2015.

International journals:

- Nadia Othman, and Bernadette Dorizzi: Impact of Quality-Based Fusion Techniques for Video-Based Iris Recognition at a Distance, in Information Forensics and Security, IEEE Transactions on , vol.10, no.8, pp.1590-1602, Aug. 2015

- Nadia Othman, Bernadette Dorizzi, and Sonia Garcia-Salicetti: OSIRIS: An Open Source Iris Recognition Software, in Pattern Recognition Letters (accepted in Sept 2015).

Chapter 2. Evaluation of iris recognition systems

Biometric systems have been widely deployed in many real-world security applications as described in Chapter 1. Different levels of security are required according to the application's domain. Most systems should perform very high recognition performance to guarantee security task. Failure of those systems can lead to severe consequences. Therefore, disposing of an estimation of the expected accuracy of a given system on large databases is crucial. We explain in Section 2.1 how performance of biometric recognition algorithms can be measured.

As explained in Chapter 1, in operational applications, the users are less cooperative during the acquisition. Relaxing capture conditions introduces strong degradations in the biometric samples. As the sample's quality is a fundamental factor in the accuracy of the recognition, disposing of relevant quality measurement algorithms is very interesting. In Section 2.2, we explain how such algorithms can be evaluated and used for improving the recognition performance.

All these evaluations can be performed only if the algorithms are benchmarked on given databases, preferably public and with a large number of biometric samples of various quality levels. Section 2.3 describes the databases we have used in this doctoral work for evaluating our approaches. Details on the conditions of acquisition for each dataset are given to show the diversity of the scenarios that we have studied in the thesis. The characteristics of the resulting images are also presented to insist on the difficulty of recognizing people in such conditions.

Finally in Section 2.4, we will present the major campaigns of evaluation in the area of iris recognition. We will see that the quality of the iris images is a recurring topic addressed by mostly benchmarks.

2.1. General evaluation of biometric systems

Biometric systems follow three main steps:

- *Enrollment:* It consists in collecting the biometric samples of the system' users.
- *Storage:* The captured samples are then converted into digital representations named templates and stored in the reference database (also called gallery).
- *Comparison:* Finally, the biometric authentication is performed. There are two possible operation modes:
    - *Verification:* In such mode, the individual claims to be a certain person which has previously been recorded in the system during the enrollment. Its corresponding

biometric sample is captured in order to generate its template which is then compared to the stored ones belonging to the claimed person. Each comparison results in a matching score which quantifies the dissimilarity between the templates (or similarity). When several templates of the same person are registered, several matching scores are computed and then combined by averaging them or by taking the minimum value (or maximum) [45]. Then, a biometric decision is taken by comparing this dissimilarly score to a threshold value τ as follows:

- ✓ If the matching score is smaller than τ, then the two templates match;
- ✓ If the matching score is greater than τ, then the two templates do not match.

This biometric decision is then taken for permitting or denying the access of the person to the system.

- *Identification:* In this case, the identity of the individual is not known a priori. Its biometric sample is first acquired. From it, a template is created and then compared to every template in the reference database. Usually, a list of the *k* most probable identities for the test individual is suggested by the biometric system [46].

In this doctoral work, we will perform only verification mode. We note also that the matching scores reflect dissimilarity values.

When working with biometric systems, there are two elementary questions to be addressed:

- ✓ How the accuracy of a given biometric system can be measured?
- ✓ How different systems can be compared to each other?

In this sub-section we will answer to these questions.

2.1.1. Score distributions

Reference databases usually contain a large number of subjects. Several samples are acquired for each person. Such databases are often used offline for evaluating biometric systems. Each template of each person is compared to every other stored element in the database. Theses comparisons can be separated into two categories:

- Genuine comparison when the two samples belong to the same person (also called intra-class comparison);

- Impostor comparison when the two samples belong to different persons (also named inter-class comparison).

As explained above, a matching score is associated to each comparison. For evaluating the accuracy of biometric systems, a large number of those scores should be generated for genuine and impostor distributions. The reliability of the system relies on its ability for separating the two scores distributions: a threshold should be properly defined to take the correct biometric decision.

When the two distributions do not overlap, the system can entirely differentiate between them by easily setting a threshold as illustrated in Figure 2-1-a. However, this never occurs in real conditions as no biometric system is completely truthful. Indeed, the two distributions overlap, and there is consequently no possible threshold able to perfectly separate them as shown in Figure 2-1-b. By varying the threshold, some of the genuine comparisons will be incorrectly classified as a non match (producing false rejection error) and some impostor comparisons will be incorrectly taken as a match (generating false acceptance error).

Therefore, this threshold plays a key role in the accuracy of a biometric system. If the threshold is set very low, the system will be strict, rejecting many genuine users. Otherwise, if the threshold is very high, the system will be more indulgent, letting many impostors pass as genuine. We note that those two errors are linked to each other: if one increases, the other decreases and vice-versa.

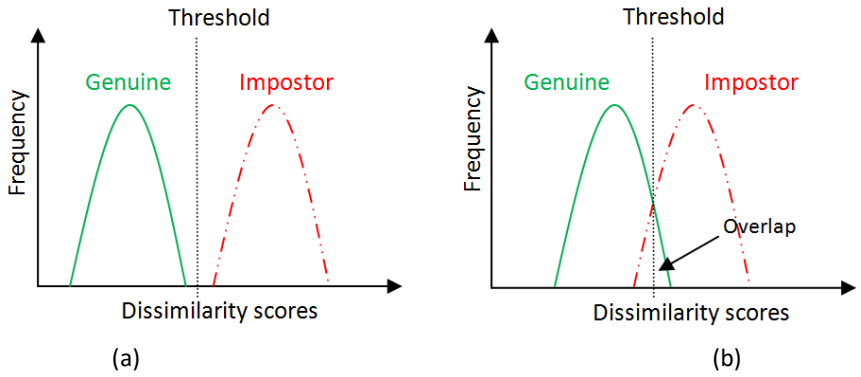

Figure 2-1: Genuine and impostor distributions for (a) an ideal system, and (b) a real system.

2.1.2. Accuracy rates

There are several metrics to measure the performance of a given biometric systems. Probably, the most essential indicators are False Acceptance Rate (FAR), False Rejection Rate (FRR), and Equal Error Rate (EER):

- FAR defines "the portion of verification transactions with wrongful claims of identity that are incorrectly confirmed" (ISO/IEC 19795-1 [47]). This error is also named Type I.
- FRR represents "the portion of verification transactions with truthful claims of identity that are incorrectly denied" (ISO/IEC 19795-1 [47]). This error is also called Type II.
- When the distributions of the genuine and the impostor overlap, FRR and FAR intersect at a specific point called the EER of the system. In other terms, the ERR is the point where the proportion of the FRR and FAR are equals.

The Genuine Acceptance Rate (GAR) may also be used. It is defined as follows: $GAR = 1 - FRR$. According to genuine and impostor accumulation scores given by the recognition system, FRRs and FARs are adjusted by varying thresholds as explained in the previous section. Figure 2-2 shows the relationships between FRR, FAR and EER.

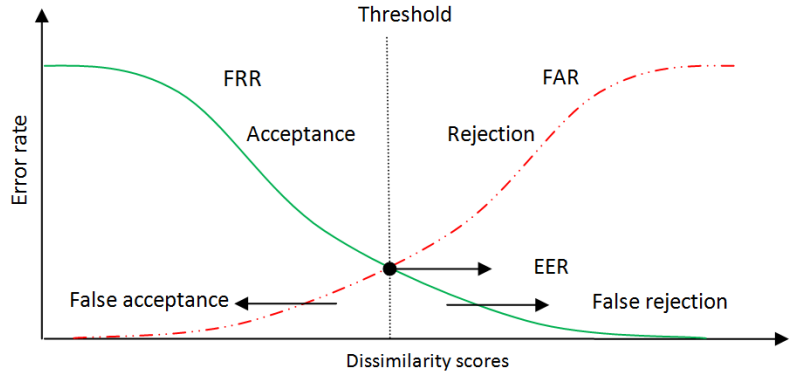

Figure 2-2: Performance of a biometric system: Relationship between FAR, FRR and EER.

We note that False Match Rate (FMR) and False Non Match Rate (FNMR) could be used as error rates instead of FRR and FAR. The difference between them is that FMR and FNMR do not include errors specific to biometric applications such as the proportion of Failure To Acquire (FTA) due to the insufficient quality of the acquired sample. The relationships between FRR/FNMR and FAR/FMR can be expressed as follow:

$$FRR = FTA + FNMR \times (1 - FTA) \quad (2.1)$$

$$FAR = FMR \times (1 - FTA) \quad (2.2)$$

In general, the results of a given biometric system are presented as FRR values at certain levels of FAR. For example, a $FRR = 10^{-2}$ @ $FAR = 10^{-4}$ means that: one out of 10^4 impostor attempts is

considered as a match, and one out 10^2 of the genuine attempts is considered as a non match. These possible couples of values are called operating points.

2.1.3. Performance curves

For visualizing performance results, receiver operating characteristic (ROC) curves are often used. ROC curve plots pairs of GAR (vertical axis) and FAR (horizontal axis) for varying thresholds describing a biometric system. When the system is accurate, the curve is near the coordinate axes. Therefore, it is useful to use logarithmic scale for one or both axis to highlight regions of interest on the graph and operating points (EER, FRR at different FAR levels). For that reason, Detection Error Trade-off (DET) curve is usually used instead of ROC curve. Each point of the graph exhibits the FAR (vertical axis) and FRR (horizontal axis) associated with a certain threshold value, using logarithmic scales (or at least for one axis). As ROC curve, DET curve covers the whole range of possible threshold values which is the interval of the matching scores. (Remark: the FMR and FNMR could be respectively used instead of FAR and FRR.)

Figure 2-3-a shows an example of DET curves for two different biometric systems. System 1 has a lower FRR than System 2 at a specified level of FAR (target 1). Consequently, System 1 is more accurate than System 2. We can also note that in this case, System 1 is always more effective that System 2 at every FAR. This does not always happen. For example in Figure 2-3-b, at target 1 System 2 is more accurate than System 1 while at target 2 the reverse occurs. This demonstrates the important choice of the operating points according to the desired level of security/convenience of the application.

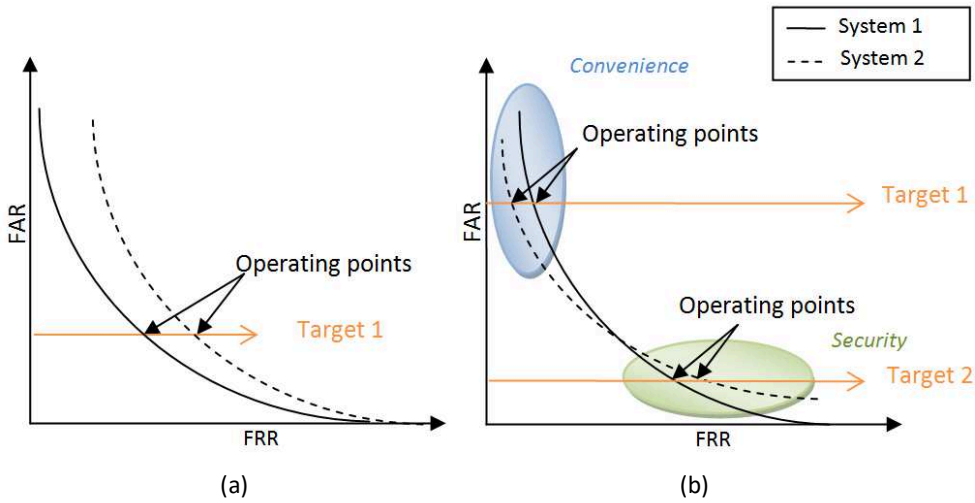

Figure 2-3: Example of DET curves and some operating points for two distinct biometric systems.

2.1.4. Image specific evaluation

The tools previously explained provide global evaluations about the overall performance of a given biometric system. However, it is interesting to note that some persons (or images) are more difficult to recognize than other ones. Many researches in biometrics have addressed performance variability among different users, suggesting that some of them contribute disproportionately to the two error rates: Type I (FAR) and Type II (FRR) of a biometric system. An analogy between these errors heterogeneities and the existence of biometric menagerie was investigated in different modalities such as speech, fingerprint, and face [48] [49] [50].

Doddington et al. [48] were the first authors who applied biometric zoo to the area of speaker recognition by developing a framework able to identify four categories of speakers based on the recognition errors for each individual:

- *Sheep:* Group of subjects that dominate the population and perform recognition easily;
- *Goats:* Group of subjects that are particularly difficult to recognize;
- *Lambs:* Group of subjects that are easy to imitate;
- *Wolves:* Group of subjects those are remarkably good at imitating others.

Goats cause the major portion of FRR but do not affect the FAR. They are especially problematic for systems which the main interest is convenience issue (low FRR desirable at a fixed FAR as illustrated in Figure 2-3-b). Paradoxically, lambs and wolves affect the security of the system by generating high FAR.

In addition to performance variations among the users, different images belonging to the same person can lead to significant difference in the matching scores. This intra-class variability is frequently assigned to the acquisition device (different imaging systems, sensors...), the environment (controlled/uncontrolled capture, illumination variation…) or the user itself (squinting, blinking…). Disposing of assessment tools for measuring performance variations among the images is very interesting for developing algorithms that are more robust to such variations, aiming at improving the overall accuracy of the system.

In [50], novel tools were proposed to perform this type of evaluation. Two new metrics named image False Match Rate (iFMR) and image False Non Match Rate (iFNMR) were introduced by inheriting concepts from the biometric menagerie. To our knowledge, it is also the first work that

investigated the existence of biometric zoo in the field of iris modality. These errors are defined as follows:

- *iFMR* is defined as "the proportion of comparison for which an image produces false matches", i.e. impostor comparison scores are at or below the operating threshold (in the case of dissimilarity scores).
- *iFNMR* is defined as "the proportion of comparison for which an image produces false non matches", i.e. genuine comparison scores are above the operating threshold (in the case of dissimilarity scores).

Explicitly, let be s_{kl}^{ij} the comparison score of the k^{th} image of subject i with l^{th} image of subject j. The set of impostor scores of the k^{th} image of subject i for comparison against all N_j images of all J persons in the database is:

$$I(i,k) = \left\{ s_{kl}^{ij}, i \neq j, j = 1 \ldots J, l = 1 \ldots N_j \right\} \quad (2.3)$$

The iFMR at a certain threshold τ is then expressed as follows:

$$iFMR(\tau, i, k) = \frac{\sum_{s \in I(i,k)} 1 - H(s - \tau)}{\sum_{s \in I(i,k)} 1} \quad (2.4)$$

where H is the step function defined as:

$$H(x) = \begin{cases} 0 & if\ x \leq 0 \\ 1 & if\ x > 0 \end{cases} \quad (2.5)$$

In a similar way, the set of genuine scores of the k^{th} image of subject i is defined as follows:

$$G(i,k) = \left\{ s_{kl}^{ii}, l = 1 \ldots N_i, k \neq l \right\} \quad (2.6)$$

And, the iFNMR at a given τ threshold is:

$$iFNMR(\tau, i, k) = \frac{\sum_{s \in G(i,k)} H(s - \tau)}{\sum_{s \in G(i,k)} 1} \quad (2.7)$$

Aggregating these two image-specific error rates, the author was able to classify the images according to their level of recognition difficulties into four categories, like the Doddington's concept (combinations of low or high iFNMR and iFMR) [50].

The threshold τ is set regarding a given value of achieved FMR (for example at $FMR = 10^{-3}$ as proposed in [50]).

These image-specific error rates are not only able for partitioning a corpus into sub-sets but they are also useful for:

- Quantifying the level of difficulty of an image, and so a overall dataset;
- Assessing the predictive power of iris image quality scores (correlation between the iFMR/iFNMR and the estimated quality component);
- Detecting errors in the acquisition and the segmentation (images with high value of iFNMR).

iFNMR and iFMR are interesting for us as one axe of the thesis's research is to develop approaches for evaluating the quality of the images. Average of iFNMR and iFMR are relevant indicators on the overall difficulty of the images in the database for recognizing the subjects.

2.2. Evaluation of quality measurement algorithms

Dealing with real-world deployment of biometric systems, the biometric samples often suffer from various degradations, leading to acquired biometric data of different quality levels. When the capture is done under strict conditions (controlled mode), the samples are usually of good quality. However in uncontrolled mode, many factors such as user's behavior, environmental conditions and sensor designs can affect negatively the performance of the system [34].

The biometric community including academics, industrials and government, agrees on the fact that the performance of biometric systems is dependent to the quality of the acquired signal. Therefore, relevant quality measurement algorithms (QMAs) for assessing the quality of a sample are of crucial importance. QMAs will be useful for improving the overall performance of a given iris recognition system by detecting sample of "bad" quality in order to:

- Recapture of the biometric sample of insufficient quality or to select the best sample in live during the enrollment phase;
- Identify the quality factors that influence iris recognition [51];
- Predict the performance of a given iris system via the quality of the images [52] [53];

- Discard images of low quality in a video;
- Assign different weights to the images according to their quality in an image fusion procedure [54]. By this way, images of best quality will contribute more than the other ones in the reconstructed image.

But, the legitimate questions that may arise are "*what means a sample of good quality*?" and *"what is a relevant QMA?*".

It is important to differentiate between the visual human quality of the biometric sample and its quality for matching performance as outlined in [34]. For example for fingerprints modality, if an observer notes that the image contains clear ridges, well contrasted, he may reasonably judge that the sample is of good quality. However, if the recognition algorithm is based on minutia and the image contains insufficient of them, the performance would be degraded. Another example, for face modality: if the image presents sharp details, the observer may pretend that the image is of good quality too. Nevertheless, if the recognition system benefits from a slight blurring, the human perception is not appropriate in that case [34]. As the ultimate goal is to improve [33] the overall accuracy of the recognition system, QMA should be developed with the respect to the target which is the matching error rates, and not with the visual human's statement of the sample's quality.

Quantifying the association between the quality measure of the two images to be compared and the resulting score comparison, is a good way for evaluating the effectiveness of a given QMA. Biometric matching involves in general two samples d_k and d_l. The goal is then to relate their corresponding qualities q_k and q_l to their matching score s_{kl}. To simplify the analysis, it is judicious to combine the qualities into one unique value q_{kl}:

$$q_{kl} = H(q_k, q_l) \quad (2.8)$$

Thus, q_{kl} represents the pairwise quality of the two samples d_k and d_l being compared. Several choices of H are investigated in [34]:

- Minimum: $H(x, y) = min\,(x, y)$
- Arithmetic function: $H(x, y) = (x + y)/2$
- Geometric function: $H(x, y) = \sqrt{xy}$
- Difference function: $H(x, y) = |x - y|$

The choice of H is not limited to these propositions. But the authors considered them for their relevance to real biometric scenarios and ease of implementation. The results show little difference between them [34]. In the doctoral work, similar results were observed by performing these choices of H. We arbitrary decide to choose the minimum function. In this case, the worst sample drives the matching score as only one of the two samples being of low quality is sufficient to degrade the performance.

In the rest of the sub-section, we will present the proposed tools introduced in [34] to assess QMAs, also used in the IREX II - IQCE (Iris Quality Calibration and Evaluation) benchmark [51] organized by the NIST. These methods will be exploited for evaluating our proposed quality measure in Chapter 4.

2.2.1. Ranked DET

As explained in Section 2.1.3, DET curve plots pairs of FMR and FNMR (or FAR and FRR) using logarithmic scales at certain threshold values. A QMA is considered to be useful if it can at least provide a ranking of the system's performance. Stated another way, for L quality levels, L corresponding DETs curves are plotted and they should not cross each other.

As proposed in the IREX II - IQCE, to generate ranked DETs, the matching scores are divided into three groups based on their pairwise quality q_{kl} . These three partitions represent samples of low, medium and high quality. The set of lowest (resp. highest) quality contains a matching score with pairwise qualities in the lowest (resp. highest) 15 percentile. The rest of the matching scores constitutes the medium quality set (70%). Hence, three DET curves are generated, one per set. Illustrations of ranked DET curves based on a good and a weak QMAs are given in Figure 2-4. The dependence of FNMR and FMR on quality at a fixed threshold τ can be shown by plotting connections between the ranked DETs (black lines of Figure 2-4). The connection points correspond to a FNMR and FMR that are observed at the same threshold values.

A QMA is considered as effective if the ranked DETs are well separated. The generated DET curve for the low quality set should appear above the other curves. In contrast, the DET curve of the high quality set should be located below the others. In fact, the proper behavior consists in the observation of expected lower FNMR and FMR as the pairwise quality of the samples increases. If the ranked DETs overlap, then the QMA is not efficient. The more the separation of the ranked DETs is high, the more the QMA is effective. If the DET curves are correctly ranked, the connected lines are

expected to have a positive slope. In this case, the images of high quality generate low FMR, which is a desired behavior.

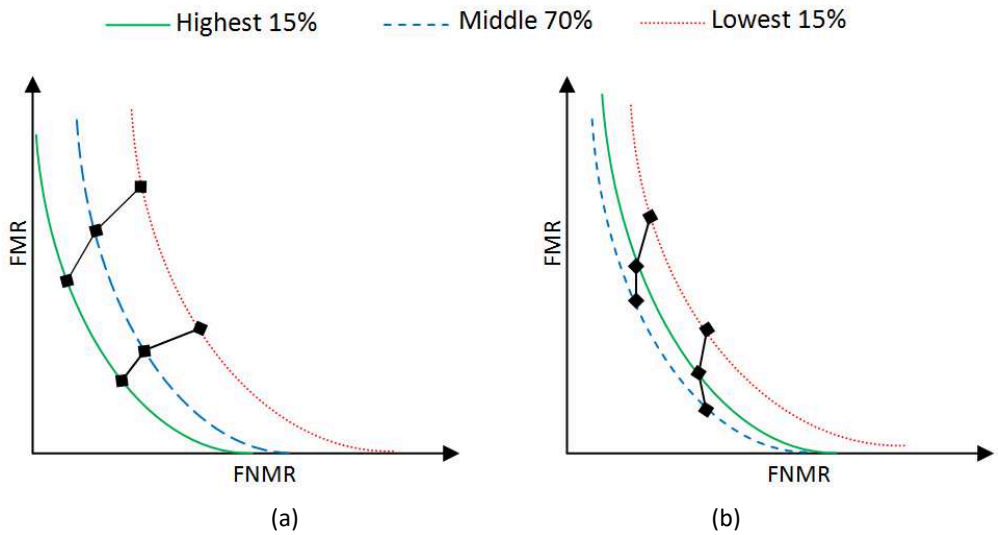

Figure 2-4: Illustration of ranked DET curves: (a) Relevant QMA: A proper behavior is observed and (b) Irrelevant QMA: the ranked DET curves are incorrectly ordered.

2.2.2. Error versus reject curves

Error versus Reject curve is an alternative mean of assessing quality measurement algorithms. It demonstrates how efficiently the rejection of lower quality samples can improve the accuracy of the overall performance of a given recognition system. By detecting the samples of low quality, in an operational scenario for example, the quality measure can drive the re-acquisition of a sample. Moreover, the quality measure can be used to reject a sample in the post processing steps.

The curve plots error rate in function of the percentage of retrieved comparisons in the database. If the QMA is effective, the error rate should decrease quickly as the rejection percentage increase. A flat curve suggests that the QMA is not effective in predicting the performance of recognition.

2.3. Reference iris databases

After describing how to evaluate the performance of biometric recognition systems and quality measurement algorithms, we will present in this section the iris databases we used in this doctoral work to validate our approaches.

Databases are essential for evaluating recognition algorithms. There are two types of data: public and proprietary. Obtaining excellent performance by a certain method on a proprietary database is difficult to reproduce. In contrast, public databases facilitate the evaluation of a proposed system, by comparing it with existing approaches, which make this type of dataset a valuable means for benchmarking purposes and for the state-of-the-art's progress in iris recognition field.

According to [55], biometric databases should satisfy the following criteria:

- *Relevant:* The dataset must contain a large number of biometric samples per subject, in identification mode;
- *Large:* A large number of comparisons are required;
- *Representative:* The demographics properties (age, gender, race…) of the acquired subjects should vary;
- *Targeted* by the sensor types, model, etc;
- *Tagged*: Meta information are provided with the data;
- *Time variant:* The dataset should be acquired over large period;
- *Un-edited* (without pre-processing).

There are several different iris databases available to iris recognition topic. Size samples and target image characteristics (resolution and format, sensor, acquisition conditions) of the databases represent a decisive element in the selection of the dataset, influencing recognition accuracy.

As explained in Chapter 1 in this doctoral work, we focus on improving iris recognition in sequences acquired with low or even poor conditions. We have chosen the portal dataset of the Multiple Biometrics Grand Challenge [36], CASIA-IrisV4-Thousand [37], and a collection of datasets taken from QFIRE database [38] [39]. These databases are interesting for us because they contain sequences (videos or multi images per subject) with various degradations as illumination in-homogeneities, low resolution, occlusions, blur, specular reflections, etc. It is interesting to note that those selected databases present different scenarios of acquisition and difficulties, allowing us to study diverse problems and evaluating the robustness of the proposed approaches in function of these problems. We also notice that different sensors were employed to acquire theses databases allowing the validation of our results in these different conditions.

In the rest of this sub-section, we present the selected databases in details. Some examples of images are given to show the difficulties present in the databases.

2.3.1. Multiple Biometrics Grand Challenge: Portal dataset

Between 2007 and 2009, the National Institute of Standards and Technology (NIST) conducted the Multiple Biometric Grand Challenge (MBGC) [56]. It consists in several sub-challenges to evaluate face and iris recognition in realistic scenarios (less constraint imposed on the participants during the acquisition).

Exploring more realistic low resolution and on the move, we chose to work with the portal dataset of MBGC [36] that is composed of NIR faces videos. This MBGC portal dataset was collected by capturing facial videos of 129 subjects walking through a confined portal located at 3 meters from a NIR camera as depicted in Figure 2-5.

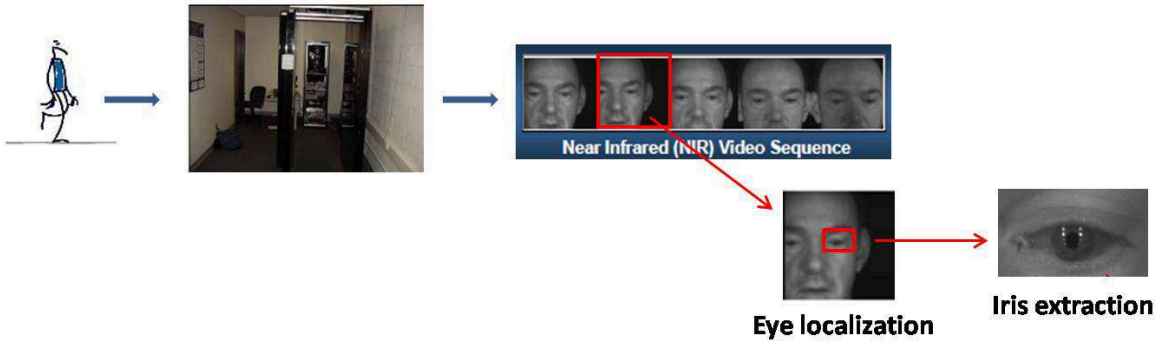

Figure 2-5: Illustration of MBGC portal acquisition.

Although the resolution of the frames in the video is $2048x2048$, the number of pixels across the iris is between 90 to 120, which is below the minimum of 140 pixels recommended by Daugman in [32] as the minimum to ensure a good level of performance.

The images in this dataset contain a large variety of artifacts. They suffer not only from low resolution but also from motion blur, occlusion, specular reflection and high variation of illumination between the frames. Examples of bad quality images are shown in Figure 2-6.

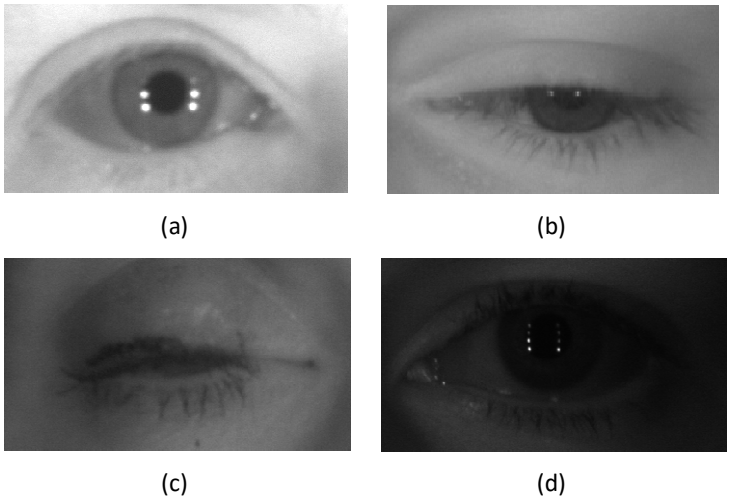

Figure 2-6: Examples of bad quality images taken from MBGC portal: (a) out of focus, (b) eyelid and eyelashes occlusions, (c) closed eye, and (d) dark image (low contrast).

2.3.2. CASIA-IrisV4-Thousand

CASIA-IrisV4-Thousand was collected by the Chinese Academy of Sciences Institute of Automation (CASIA) [37]. The complete database includes 20000 iris images from 2000 eyes of 1000 persons, mainly composed of Asian people. This population tends to have droopy eyelids and eyelashes oriented downwards covering a significant ratio of the iris region, leading to challenging recognition task. The images are captured using the dual-eye iris camera using IKEMB-100 produced by IrisKing. Each subject has 10 instances of both left and right eye.

The main sources of variations in a given sequence are eyeglasses, specular reflections and dilation, which make the iris segmentation particularly difficult. Figure 2-7 illustrates an example of a sequence from CASIA-IrisV4-Thousand. We note the significant difference of the pupil's size in the sequence and in particular between images S5025L03.jpg and S5025L04.jpg. In some images in the sequence the subject is asked to wear eyeglasses, which causes strong specular reflections.

Even if the database does not contain videos, we decided to work with it. Indeed, the intentional intra-variability in the images considerably degrades the recognition accuracy, essentially by introducing iris segmentation errors. Therefore, by using this database for test, we will see how our proposed approaches are robust to segmentation errors.

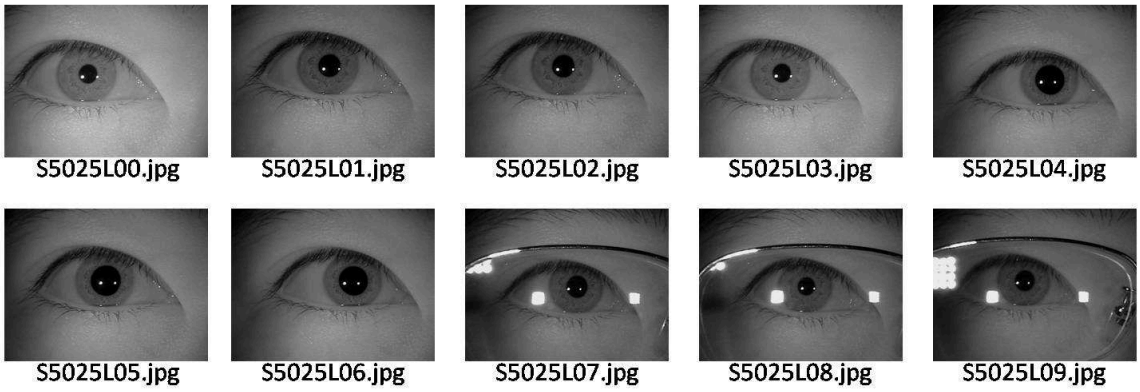

Figure 2-7: Sequence of images for the subject S5025L from CASIA-IrisV4-Thousand.

2.3.3. QFIRE database

Quality Face and Iris Research Ensemble (QFIRE) [38] [39] was collected by Clarkson University. The acquisition was funded by the Department of Homeland Security (DHS) Science and Technology (S&T) Directorate in cooperation with the National Science Foundation. QFIRE is a multimodal database composed of iris and face image sequences captured at varying distances and at different quality levels totally controlled at the acquisition. The iris subsets were particularly used in the IREX II - IQCE benchmark [51] to evaluate the impact of different factor quality on iris recognition.

Apart from this, to our knowledge, only a few works have been assessed on this database for the iris modality [40] [41] [42] and no protocols have been yet defined for this database. The QFIRE database contains a large number of various acquisition scenarios. To study the contribution of the proposed fusion method we chose an acquisition context which differs from the one used in the previous databases mentioned in Sections 2.3.1 and 2.3.2. We decided to work with iris acquisition of stationary subject taken at different significant distances. This variation introduces different iris resolutions between the sequences.

More precisely, we selected 3 subsets composed of NIR videos, captured with a Dalsa 4M30 infrared camera with a Tamron AF 70-300mm 1:4.5-5.6 LD DI lens, taken at a distance of 5, 7, and 11 feet. This variability in the distance was introduced to generate respectively high, medium and low-resolution iris images as classified in [35]. The quality factor "resolution" is defined as the maximum number of pixels across the horizontal diameter of the iris.

Using different distances allows us to study the impact of the proposed fusion schemes for different iris resolutions. Indeed, as the resolution decreases, the iris area in the image is getting less textured and with less distinctive details, as illustrated in Figure 2-8.

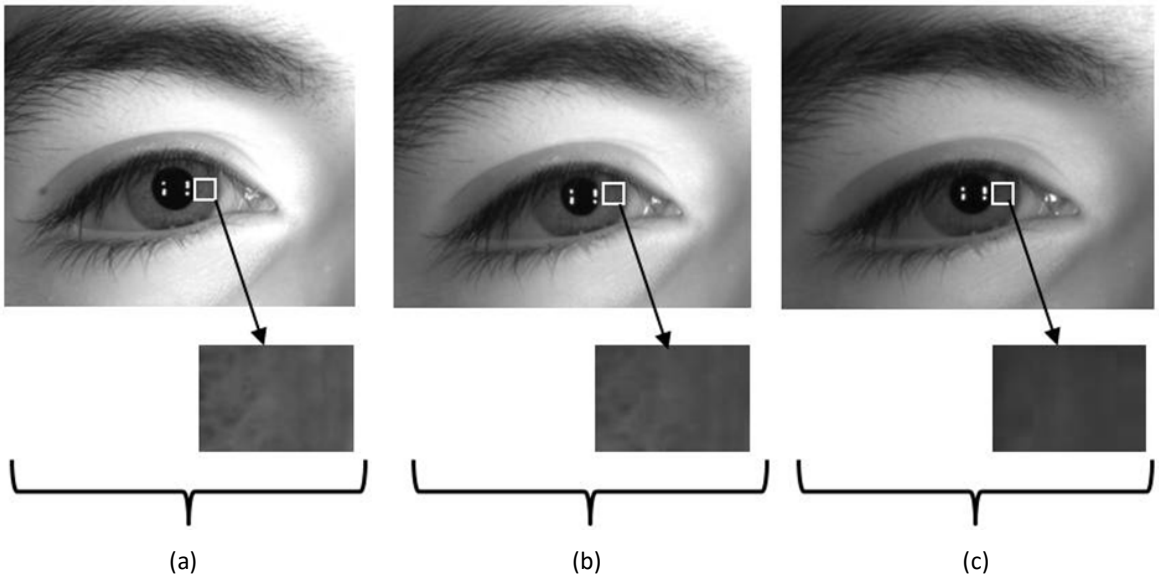

Figure 2-8: Degradation of the iris texture since the distance of the acquisition increases. The selected images correspond to best image in the sequence.

This lack of resolution leads to blurred images. Moreover, during the acquisition procedure of QFIRE in order to generate some non-uniformity in each videos sequence, an intentional defocus blur was added to each sequence by manually turning the focus ring of the iris camera.

The publicly released part of QFIRE consists of 90 subjects with two visits. In all, for each person, two videos of 6 seconds in length were acquired at each distance at a certain illumination level (low, medium and high). Varying levels of illumination are achieved through fixed illumination plus varying levels of lights based on a LED-based portal positioned at 3 feet from the subject as presented in Figure 2-9. This portal is composed of 8 LEDs, which can be turned off or on. For the medium level, 6 LEDs are switched on.

This level of illumination corresponds to the lower bound of contrast suggested by the current ISO iris image standard requirements [35]. The contrast is defined as the difference in gray level between the iris/pupil and the iris/sclera, which are respectively proposed to be at least 50 and 70 gray levels. To make a compromise, we choose the medium illumination level for all the distances.

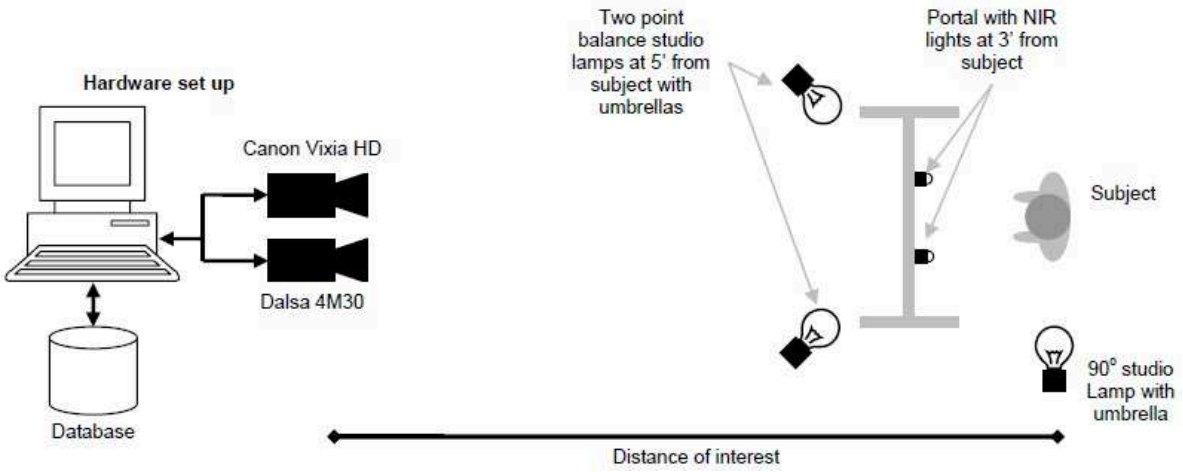

Figure 2-9: QFIRE acquisition [39].

We expect an important decrease in the recognition performance with the decrease of resolution and we want to assess and quantify to what extent the fusion schemes we propose can cope with these degradations. Table 2-1 summarizes the characteristics of each subset. We respectively call QFIRE05, QFIRE07 and QFIRE11 the datasets taken at 5, 7 and 11 feet.

Table 2-1: Characteristics of each of the 3 subsets of QFIRE database.

Subset notation	**QFIRE05**	**QFIRE07**	**QFIRE11**
Distance	*5 feet*	*7 feet*	*11 feet*
Resolution metric range	*280 to 300*	*200 to 220*	*100 to 120*
Quality level	*High*	*Medium*	*Low*
Subset comparable to	*Higher quality of UBIRIS datasets*	*Medium quality of CASIA and BioSecure datasets*	*Low quality MBGC dataset (NIR face camera)*

As the datasets are composed of face videos, we first have to detect and extract the eyes. In particular, the sequences contain entire (at long distances) or partial faces (at close distance). To localize the eyes, in the case of entire faces, we used the Matlab code developed in [57] based on an enhanced pictorial structure model for precise eye localization. In order to track the eyes in partial faces, we used a simple implementation based on a Hough transform. In this way, we obtain eye images on which we can apply a standard processing: segmentation, normalization, feature extraction and then template matching as explained in Section 1.4. False detections were manually discarded. In

addition, due to the intentional defocus blur added at the beginning and the end during the sequence acquisition in the QFIRE database, we have to discard unusable frames and for this, we used wavelet transform.

In order to increase the number of intra-class comparisons, we divided the sequences with a large number of usable frames into multiple sequences. After all these pre-processing processes, the database we used in our experiments is composed of 676, 453 and 361 sequences for respectively QFIRE05, QFIRE07 and QFIRE11. Each sequence has at least 10 frames. For more details on the used dataset and protocols, see appendix B.

Table 2-2 summarizes the dataset's characteristics and lists subjectively the perceived noise factors in the datasets we used in this doctoral work. We can note the variety of scenarios and difficulties which allowed us an extensive evaluation of our fusion methods.

Table 2-2: Characteristic and noise factors in open iris databases.

Database	MBGC	CASIA-IrisV4-Thousand	QFIRE05	QFIRE07	QFIRE11
Acquisition scenario	*At a distance and on the move*	*Intra-class variations, static subject*	*At a distance, static subject*	*At a distance, static subject*	*At a distance, static subject*
Format	*NIR face videos*	*NIR images (jpg)*	*NIR face videos*	*NIR face videos*	*NIR face videos*
Sensor	*MBGC-Portal (IOM system)*	*Irisking IKEMB-100*	*Dalsa 4M30 infrared camera*	*Dalsa 4M30 infrared camera*	*Dalsa 4M30 infrared camera*
Resolution	*low*	*medium*	*high*	*medium*	*Low*
Reflections	**	**	**	**	**
Occlusions	**	*	*	*	*
Blur	*		*	*	**
Illumination	*	**			

*present, **problematic

2.4. Benchmarks

Taking into consideration all the various iris recognition algorithms available in the state-of-the-art, it can be difficult to decide which one provides the best results. To compare the performance of two iris recognition systems, the same protocol and the same data must be used. For these reasons, international

campaigns of benchmarks are frequently organized. They are in general public and are coordinated by an independent organism. In this sub-section, we will present several benchmarks that have taken place in the area of iris recognition.

Most of the benchmark campaigns that have addressed iris recognition were conducted by the National Institute of Standards and Technology (NIST). One of the first open challenges was the Iris Challenge Evaluation 2005 (ICE2005) [58] initiated by NIST. The main goal of this benchmark was to encourage the development of iris recognition systems and to defend this biometric modality in front of the US government. The ICE2005 challenge provided the first largest public dataset, a common experimental protocol for measuring the performance and a baseline iris recognition system (irisBEE). The provided dataset contains 2953 iris images from 132 subjects, organized into two experiments: left and right eyes. Twelve algorithms from nine submitters were benchmarked from August 2005 until March 2006. At a FAR of 0.001 the verification rate on right irises is above 0.995 (for the 5 top algorithms) and on the left irises between 0.990 and 0.995. The results of the evaluation showed correlations between the right and left irises for match and non-match scores, and quality measures. More details about the experimental results can be found in [59].

Soon after, NIST organized a second Iris Challenge Evaluation: ICE 2006 combined with Face Recognition Vendor Test (FRVT) 2006 between June 2006 and March 2007. The objective of this challenge was to alleviate comparison between the biometric modalities face and iris by defining a common testing protocol. Contrary to ICE2005, ICE2006 proposed an independent evaluation with sequestered data (not previously seen by the researchers). The dataset used for this benchmark is larger than ICE2005 since it contained 59558 iris images. The experimental results are presented in [60].

The Multiple Biometric Grand Challenge (MBGC) conducted by NIST took place from 2007 to 2009 [56]. Three challenges were addressed: portal, still face and video. The main interest of this project was to investigate, test and improve performance of face and iris recognition in both still images and videos towards less restrictive acquisition environment. The challenge problems focused on:

- Face recognition on still frontal images of high and low resolution;
- Iris recognition from off-angles images and videos;
- Face and iris fusion at score and image levels;
- Unconstrained face recognition from still image and video;

- Recognition from NIR and HD video streams taken through portals.

Experimental results of the portal challenge are summarized in Table 2-3. GARs were nearly perfect for the face modality and promising for the iris modality.

Table 2-3: Results of the MBGC portal workshop.

Portal challenge's protocol	GAR
Still iris vs. NIR video	*20--95% at 1% FAR*
Video iris vs. NIR video	*20--95% at 1% FAR*
Still face vs. HD video	*15--100% at 1% FAR*
Still iris and still face vs. NIR video and HD video	*80--100% at 0.1% FAR*

In 2007 to 2009, the Noisy Iris Challenge Evaluation (NICE) was the first initiative towards iris recognition with unconstrained data, using visible wavelength instead of NIR iris images. Organized by University of Beira Interior's the SOCIA Lab in Portugal (Soft Computing and Image Analysis Group), it was conducted in two separate parts: NICE I [61] and NICE II [62]. The first challenge focused only on iris segmentation and noise detection by classifying the pixels of the image into iris class or non-iris class. All participants were evaluated by comparing the classification error rate (portion of pixels that disagree with respect to the ground truth manually determined on 500 images). The evaluation was reported on iris images similar to the ones of UBIRIS.v2 dataset [63]. Over than ninety contestants from 20 different countries participated to this challenge. The best performance was achieved by the work of [64] with an error rate of 0.0131%. The global results pointed out that most errors were caused by the failure of detecting accurate pupillary boundaries in contrast to what occurs with NIR data.

The subsequent NICE II challenge conducted between 2009 and 2011 addressed the feature extraction algorithms and comparison techniques of degraded iris images in visible wavelength, already segmented accordingly to the best algorithm [64] of NICE I. The images used in the benchmark are the same as those in NICE I. The challenge attracted 67 contestants. The evaluation was based on the decidability index defined in [65]. Tan et al. [66] were the winner of the competition with a decidability of 2.5748 (vs. 1.8213 for the second place). The approach considers multi-biometric combination of iris and periocular data based on global color-based features and local ordinal measures.

Starting in 2007, NIST has conducted a program entitled The IRis EXchange (IREX) [23] in several instances with specific objectives:

- *IREX I* addresses compression effects on the performance of commercial algorithms and the interoperability of formats. It also summarizes the performance of iris recognition algorithms submitted to NIST since 2009.
- *IREX II - IQCE* defines several iris quality factors and investigates their influence on iris recognition accuracy.
- *IREX III* targets a large scale performance evaluation of iris recognition algorithms published in the academic literature in order to prove the effectiveness of iris recognition as a powerful biometric modality.
- *IREX IV* extends IREX III evaluations of iris identification algorithms for large scale applications. It is composed of two parts. The first part explores the prospective of using cost estimation model as a new performance metric in order to optimize the algorithm for a specific application. The cost corresponds to a trade-off between security and convenience. The second part establishes compression profiles for the compact representation of iris images.
- *IREX V* outlines recommendations and simple procedures for the camera operator, the subject behavior and the iris camera allowing a proper collection of iris images of good quality.
- *IREX VI* investigates the temporal stability of iris recognition accuracy to determine whether the performance decreases with the lapse of time between the enrollment and the test stage. It intends to quantify natural ageing effect of the iris in a healthy population.
- *IREX VII* will intent to define a framework for communication and interaction between the components in an iris recognition system. The goal is to facilitate the development of more flexible, extensible and modifiable systems. The report is not yet published.

It is interesting to note that the quality of iris images has been studied in most benchmarks projects cited in this sub-section. This shows the importance of the quality in the recognition accuracy.

Recent competitions have been organized in conjunction with international conferences on diverse problems:

- *LivDet-Iris 2013* (Iris Liveness Detection Competition 2013 [67]) aimed at developing approaches able to detect imitations of biometric characteristics to prevent from presentation attacks. The competition was composed of two sub-competitions: Software-based and System-based test. The competition provides public iris databases that contain spoof and live images. The spoof images are obtained by using patterned contact lenses and printed iris images. Only three contestants have participated to the competition. The results were presented in the international conference on Biometrics: Theory, Applications and Systems (2013) and are available online [67].

- *ICIR 2013* (ICB Competition on Iris Recognition 2013 [44]) was organized by the Chinese Academy of Sciences' Institute of Automation (CASIA) in 2013. It was the ICB Competition on Iris Recognition. The competition aimed at collecting recent state-of-the-art algorithms of iris recognition. The submitted algorithms were evaluated on a sequestered subset of CASIA-Iris-Thousand database [37]. The iris images suffer from motion blur, non-linear deformation, eyeglasses and specular reflections. Eight teams including our research group have participated. The experimental results were presented in the International Joint Conference on Biometrics (2014) and are available in [44]. In particular, our algorithm [33] have given an EER of 3.02% (second best rate) and a FNMR of 31.41% at a FMR=0.01% (third best rate).

Today, a particular interest is devoted to iris recognition on mobile devices, some benchmarks have already addressed this new issue:

- *MobILive 2014* (Mobile Iris Liveness Detection Competition 2014 [68]) covers also anti-spoofing attack. The goal is to classify the images into fake and real images acquired by mobile devices. The fake images are printed images. The dataset is composed of a subset of iris images taken from MobBIO database and its corresponding fake images.

- *MICHE-I* (Mobile Iris Challenge Evaluation, Part I [69]) was organized in 2014. Its goal consists in tracking the most pertinent contributions in the field of iris recognition on mobile devices (smartphone or tablet). It includes iris detection, segmentation and recognition tasks. To this end, a database captured under uncontrolled settings using mobile devices was provided (MICHE BIPLAB [70]). Nevertheless, participants were also encouraged to provide new datasets with the characteristics of the devices used to capture the images. The contestants were asked to provide their algorithms (executable codes). In

fact, this special issue on iris recognition on mobile devices aimed also at promoting the reproducibility of the research results. An overview of the participants and the datasets they used for their experiments is given in [71].

2.5. Conclusion

In this chapter, several tools for evaluating biometric recognition and quality measurement algorithms were described in details. These tools are commonly used in the biometric community to assess the effectiveness of the developed algorithms. The evaluations are done on a large number of biometric samples. We also presented the different iris databases we have used in the thesis, namely MBGC, CASIA-IrisV4-Thousand and collections taken from QFIRE. For each database, we presented the specific degradations present in the images in order to highlight in which aspect iris recognition is challenging. We insisted on the fact that these databases cover different types of scenarios, leading to various difficulties, in order to show the effectiveness of our results. Finally, we cited the major public evaluation campaigns on iris recognition. We note that iris recognition in less constrained environment and quality assessment are two topics often addressed in the literature. This shows that the research community is concerned about these two issues.

In the next chapter, we will explain how iris recognition works. We describe in particular the pioneer algorithm which has inspired most of the current iris recognition systems. Several recent iris recognition algorithms and open source systems will also be presented. Then, we will describe the reference iris recognition systems developed in our team, and more precisely those used in the thesis. A literature review on iris acquisition systems in less constrained environments will close the next chapter.

Chapter 3. Fundamentals in iris acquisition and recognition systems

This chapter provides basic considerations about iris recognition. Questions like "*How does iris recognition work?*", «*What are the iris recognition systems available in the literature?*" , and "*What are today's challenges in iris acquisition and recognition?*" will be discussed in this chapter.

As explained in Chapter 1, authentication by biometric verification is becoming increasingly common in security applications such as banking, border and access control, forensics and so on. Today, a particular attention is given to iris biometrics, due to its high reliability for personal identification. This modality is relatively recent since the first automatic system able to identify people based on iris texture was proposed by John Daugman in 1993. Later on, alternative solutions have been proposed in the literature aimed at improving the performance of the recognition. To our knowledge, there are only few open source algorithms for iris recognition. Such systems are extremely useful for the research community. Indeed, they provide an accessible tool for comparative evaluation (baseline) of other algorithms. They also encourage development through the modification of some of their components, contrary to commercial products which are in general “black-box” systems.

Details on pioneer algorithms for iris recognition, as well as recent methods and existing open source systems are given in Section 3.1.

Moving forward in this direction, the BioSecure Association, maintained by our research team [43], has proposed an Open Source IRIS recognition system (OSIRIS), in 2007, aiming at providing a reference for the scientific community. OSIRIS is designed as a modular software system, adequate to study modifications of its components and their effects on performance. Several versions of OSIRIS have been implemented, aiming at improving recognition accuracy. In Section 3.2, we detail the evolution of the open source iris recognition system OSIRIS through its more relevant versions, as well as the latest versions we have employed for performing iris recognition in this thesis.

To satisfy recent applications requirements, iris acquisition conditions have been gradually relaxed. Indeed, less intrusive and more fluid acquisition systems would be appreciated in many iris recognition applications. A literature review on iris acquisition systems in less constrained environment: at a distance, with eventually mobile subjects is related in Section 3.3. We insist on the challenging task of designing iris recognition and acquisition systems. The relaxation of the constraints on the subject leads to images of low quality, affecting negatively the performance obtained by usual iris recognition systems. This will lead us to underline what contributions this doctoral work makes in

the management of the issue of iris recognition improvement in less restrictive acquisition environment.

3.1. Iris recognition systems in the literature

3.1.1. Daugman's iris recognition system

The first operational iris recognition system was proposed in 1993 by John Daugman [13] who later patented it in 1994 [12]. As mentioned in Section 1.4, he divides the problem into four parts: segmentation, normalization, feature extraction and template matching [13].

Initial method:

To segment the iris region, Daugman assumes that it can be modeled by two non-concentric circles. The pupillary and the limbic boundaries are approximated by theses circles thanks to an integro-differential operator according to the following formula:

$$\max_{r,x_0,y_0}\left|G_\sigma(r)*\frac{\partial}{\partial r}\oint_{r,x_0,y_0}\frac{I(x,y)}{2\pi r}ds\right| \qquad (3.1)$$

where * denotes convolution, I represents the original iris image and $G_\sigma(r)$ symbolizes a Gaussian filter used for smoothing, σ being the standard deviation.

This operator searches over the whole image for the maximum in the blurred partial derivative, with respect to increasing radius r, of the normalized contour integral of $I(x,y)$ along a circular arc ds of radius r and center (x_o, y_o).

In order to overcome the fact that the size of the iris can change from an image acquisition to another the iris region should be normalized. Indeed, iris dilation/contraction are caused by illumination variations during the acquisition. To handle this issue, the iris area is transformed into a rectangle image of a pre-determined dimension so that it can be used in the template matching module. Such transformation can be seen as an unwrapping of the iris texture delimited by the two pupillary and the limbic boundaries, obtained in the segmentation module as illustrated in Figure 3-1.

More precisely, the normalization technique transforms the iris image I from cartesian coordinates (x,y) to the dimensionless polar coordinates (r,θ). This mapping can be expressed as follows:

$$I(x(r,\theta), y(r,\theta)) \rightarrow I(r,\theta) \quad (3.2)$$

where r is in the range of $[0,1]$; θ is an angle in the range of $[0,2\pi]$; $x(r,\theta)$ and $y(r,\theta)$ consist in linear combination of the set of pupillary boundary points $\left(x_p(\theta), y_p(\theta)\right)$ and the set of limbic boundary points $\left(x_i(\theta), y_i(\theta)\right)$, such that:

$$x(r,\theta) = (1-r)x_p(\theta) + rx_i(\theta) \quad (3.3)$$

$$y(r,\theta) = (1-r)y_p(\theta) + ry_i(\theta) \quad (3.4)$$

This normalization is often referred to, as the rubber-sheet model of the iris. Such mapping has many benefits. The normalized iris image is invariant to iris size and/or dilation/contraction and eye image translation. Moreover, it transforms eye image rotation into normalized iris translation (horizontal axis). In addition, in the template matching module, the normalized irises can be easily compared thanks to the common fixed size.

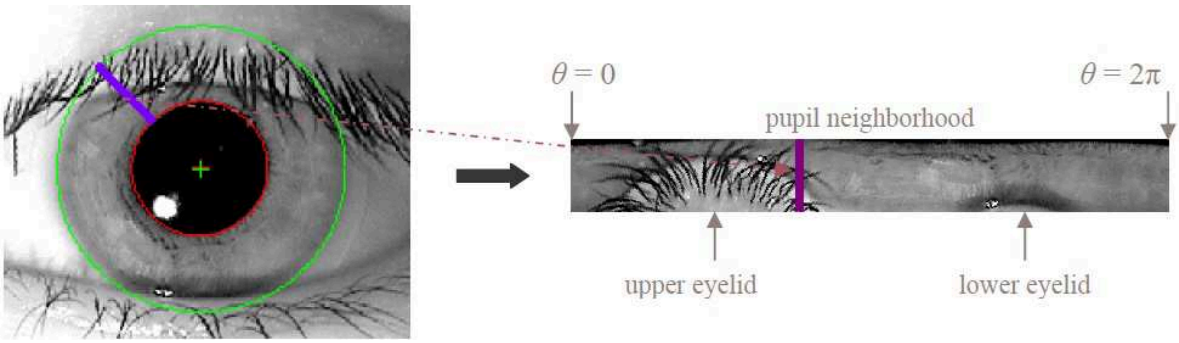

Figure 3-1: Illustration of the transformation procedure proposed by Daugman's normalization [33]. On the left, the original image. The iris is segmented by two circles. On the right, the corresponding unwrapped texture according to Daugman's rubber sheet.

Then, the feature extraction module's purpose consists in generating a compact representation of the characteristics of the iris texture aiming at facilitate the comparison. In Daugman's approach, these characteristics results in a binary code called irisCode, representing frequency information. More precisely, the irisCode is built by applying a set of Gabor filter at different scales and orientations at predetermined points of the normalized image. Then, only the phase of the resulting coefficients is used to represent the iris. For compression information purpose, the phases are quantized: a pair of bits is assigned to each coefficient depending on the sign of its real part and imaginary part as depicted in Figure 3-2. By keeping only the phase information, illumination/contrast, camera gain and other noise

factors, which typically influence magnitude information, are avoided [13]. The irisCode's length depends on the number of Gabor filters applied. Daugman used a binary code of 2048 bits.

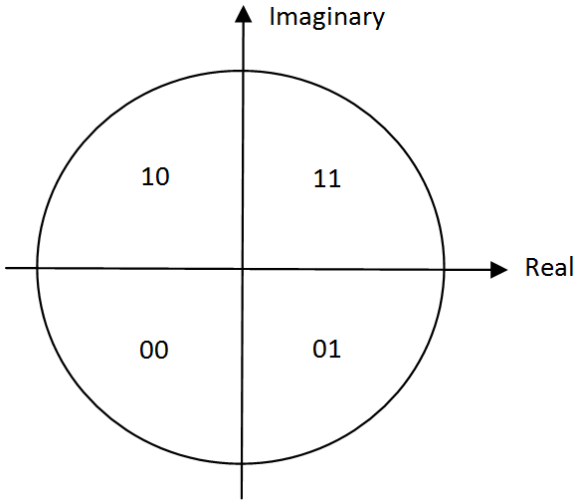

Figure 3-2: Illustration of the phase quantization.

Finally, template comparison is achieved by a bitwise comparison between two binary codes associated to two irises. The Hamming distance is used to evaluate the dissimilarity between the two irisCodes (*A* and *B*), resulting in a matching score according to the following formula:

$$HD = \left\| IrisCodeA \otimes IrisCodeB \right\| \qquad (3.5)$$

where $\otimes$ denotes the XOR operator.

This score represents the ratio of the number of bits that disagree on the length of the irisCodes. The score is 0 if the two irisCodes are identical, and 1 if all the bits disagree. Since each bit has equal a priori odds of being a 1 or a 0, the probability that any pair of bits from different irisCodes disagrees is 0.5. If all the 2048 bits were completely independent, the expected impostor distribution of observed Hamming distances would be a binomial distribution with p = 0.5 and N = 2048. However, the set of Gabor filters used in the feature extraction introduces intrinsic correlation between the bits. In addition, there is some spatial correlation between the pixels of the iris image [13]. Due to these two factors, Daugman shows that there are only 173 independent binary degrees of freedom in the irisCode. Consequently, the impostor matching scores can be modeled by a binomial distribution with p = 0.5 and N = 173 and the likelihood that two irisCodes obtained from two different irises fully agrees is approximately one in $2^{173} \approx 10^{-52}$ [13].

In practice, the iris texture can be affected by non ideal acquisition conditions such as head rotation. A rotation of the iris texture in the original image introduces a horizontal shift of the texture in the normalized image. In that case, binary codes are not aligned and the comparison is biased. To overcome this issue, Daugman proposes to perform different shifts to one of the irisCode of the pairwise to be compared, before evaluating the Hamming distance between the irisCodes. The minimum score corresponds to the correct alignment of the two images.

Performance's improvement:

Since 1993, Daugman has proposed several techniques that can improve the performance given by his first iris recognition algorithm. For example in [72], Daugman proposed to improve the segmentation stage by adding the localization of the upper and lower eyelids by curvilinear edges detection. By this way, he created a binary mask which is then unwrapped according to the rubber sheet. This normalized mask is associated to the corresponding irisCode, aiming at eliminating the bits generated from noisy regions in the iris from the comparison. The Hamming distance between iris *A* and iris *B* is then computed as follows:

$$HD = \frac{\left\| (IrisCodeA \otimes IrisCodeB) \cap maskA \cap maskB \right\|}{\left\| maskA \cap maskB \right\|} \qquad (3.6)$$

where $\otimes$ denotes the XOR operator and $\cap$ the intersection operator (to insure that the distance is only performed on non noisy region of irisCodes *A* and *B*).

The latest improvements of his iris recognition system were presented in [73]. Daugman proposed four supplementary enhancements:

- A segmentation based on active contours aiming at modeling the pupillary and limbic borders more faithfully;
- A Fourier-based method for detecting off-angles in the iris images in order to handle them by rotating the eye into orthographic perspective;
- A statistical inference technique for identifying and eliminating eyelashes;
- A score normalization method based on the amount of iris texture that is available in the images and the required scale of database search.

The new Hamming distance is obtained according to Formula 3.7, in which HD represents the hamming distance previously calculated in Formula 3.6, n is the number of available bits that are

considered in the comparison, and finally the number '911' is the mean of the number of available bits for all the comparisons of the database.

$$HD_{norm} = 0.5 - (0.5 - HD)\sqrt{\frac{n}{911}} \qquad (3.7)$$

The Hamming distance has been normalized for the following reason. The number of bits that contributes in the computation of the Hamming distance in Formula 3.6 depends on the two masks associated to the irisCodes. Consequently, this number varies from one comparison to another. When an importance fraction of occluded pixels is present in the iris image, fewer bits will be used for computing the Hamming distance. This matching score can therefore be biased. To avoid this phenomenon, Daugman proposed to take into account the variations of the number of bits available by normalizing the Hamming distance thanks to Formula 3.7.

3.1.2. Wildes' approach

The iris recognition system proposed by Daugman was followed by Wildes' system based on a distinct approach in 1997 [74]. To our knowledge he is the only one who has proposed a complete alternative solution to iris recognition system. The algorithm included new proposals for iris acquisition, segmentation, normalization, feature extraction and template matching.

Firstly, the author suggested acquiring not only the iris area but also the surrounding elements of the eye during the acquisition stage. The segmentation is based on Circular Hough Transform (CHT) for finding the two boundary circles [75]. To this end, Wildes first searches for edges in the image by using an edge detector (Canny in [74]). In addition, the eyelids are detected by using linear Hough transform in order to remove this area in the comparison stage. The critical issue of this method relies on choosing an accurate edge detector. There are two possible problems: (i) if the iris's edges are not present in the edge map, then the Hough Transform will not be able to find iris boundaries, (ii) if the edge detector is not selective enough, then the computation time of the Hough Transform will drastically increase.

The normalization stage is based on a registration process in which a mapping function is applied to the original image in order to rectify eventual translation and scale differences between the acquired images. This mapping function is selected so that the intensity of the pixels of the acquired image is as close as possible to the corresponding ones in the reference image.

The feature extraction step is based on real-valued feature vectors instead of binary codes such as proposed by Daugman. A multi-spectral analysis is carried out on the registered iris images by using Laplacian of Gaussian (LoG) filters at four resolutions. The filtered images represent the feature vector. A similarity score based on normalized correlation between the vectors of the reference and the test images is computed in the template matching stage.

Compared to the initial Daugman's system [13], Wildes' approach leads to higher EER as pointed in [76]. In addition, the system is more complex than [13]: a less compact representation of iris features is used and a correlation step is performed to obtain a matching score instead of a simple Hamming distance. Nevertheless, Wildes' segmentation is considered to be more stable to noise perturbations (thanks to CHT method) than [13] and is also able to obtain finer distinctions between the irises (no quantization step).

3.1.3. Recent algorithms

Several researches have proposed alternative solutions especially to segmentation and feature extraction stages, aiming at improving the performance of the recognition. However, in general the majority of the existing works on iris recognition used Daugman's rubber-sheet [13] to perform normalization.

Segmentation:

In the literature, there is a large variety of segmentation methods. The pupillary and limbic boundaries can be detected by circles or ellipses fitting techniques. For instance, CHT was widely used with some variations in several works [76] [77] [78] [79] [80] in order to perform iris segmentation. In [81], Zuo and Schimd proposed to segment the iris by fitting rotated ellipse on pre-processed iris images: the noise was considerably reduced thanks to inpainting, and contrast enhancement algorithms. Uhl and Wild presented in [82] a four steps iris segmentation framework: (i) inpainting process for reflection removal, (ii) initial center detection by using feedback on edge magnitude and orientation given by Weighted Adaptive Hough Transform, and (iii) detection of potential boundaries in the polar and ellipsopolar domains and (iv) selection of the best candidate.

Since the iris is neither circular nor elliptical, several authors proposed methods based on active contours aiming at approximating real iris boundaries by curve fitting techniques by using: pulling and pushing elastic model (He et al. [83]), active contours (Vatsa et al. [84]), and geodesic active contours (Shah et al. [85] and Roy et al. [86]).

Other techniques use texture analysis to perform iris segmentation. For example, in [87] Benboudjema et al. exploited a Triplet Markov Field (TMF) for unsupervised segmentation of the eyes in non ideal acquisition condition. A Hidden Markov Field (HMF) and a graph cut based energy minimization algorithm were also proposed by Pundlik et al. in [88] to perform eye segmentation. Recently, Hidden Markov Chain (HMC) and Pairwise Markov Chain (PMC) were also investigated to segment irises in challenging iris images.

A wide literature exists on iris segmentation approaches. See [89] for a more extensive selection of algorithms.

Feature extraction and template matching:

Several researchers have kept the representation of the iris template in binary codes, thus allowing low memory (compact representations) and fast template matching (simple distance). However, alternative ways to extract the iris texture features were proposed. For example, Sun et al. [90] proposed to exploit ordinal measures i.e. relative comparison, between sub-parts of the normalized iris image. To this end, multi-lobe differential filters (MLDF) are employed to extract ordinal iris features. Several parameters such as scale, inter-lobe distance, orientation and number of lobes are set for defining the MLDF allowing flexible filter construction. Consequently, MLDF may be more adaptive to specific texture patterns. The response of the filter is then quantized into a binary code as done in Daugman's approach. Others filters have also been tested for extracting iris features: Discrete Cosine Transform (DCT) as proposed by Monro et al. [91], and dyadic wavelet transforms as suggested by Ma et al. [92]. A comparison study between several filters has been investigated by Thornton et al. [93] in order to determine which filter leads to best recognition performance. The tested filters are: Daubechie's wavelet, bi-orthogonal wavelet, Coiflet wavelet, Symlet wavelet, Haar wavelet, circular symmetric filters and Gabor wavelet, and the best results were obtained by using Gabor wavelets. In all these approaches, filters' responses are quantized into a series of bits from which a similarity/dissimilarity score can be easily computed between the two iris templates to be compared.

As in Wildes' approach [74], several authors exploited real-valued features instead of binary ones. For example, a phase correlation technique in Fourier domain was proposed by Miyazawa et al. [94]. Kumar et al. [95] proposed to generate specific correlation filters for each iris class. Several intra-class images are required at the learning phase for designing the filter. In the test phase, the filter is applied to the test iris image to determine if the two iris images come from the same person. If the resulting correlation contains a narrow peak, then a good match exists between the test and the

reference iris images. Otherwise, there is no match. To build the correlation filter, the authors used Optimal Trade-off Synthetic Discriminant Function (OTSDF) [96] which aims at minimizing the Average Correlation Energy (ACE) and the Output Noise Variance (ONV). In [77], Krichen et al. exploited real-valued features obtained by Gabor-filtered phase. Then, local normalized cross-correlations are performed between sub-parts of the two templates to be compared. The values of the different peaks and their position are used to evaluate a similarity matching score.

The previous listed works are not exclusive. More feature extraction techniques can be found in [89].

3.1.4. Open source systems for iris recognition

It is interesting for the research biometric community to have access to free iris recognition systems in which each module can be studied and examined independently. Moreover, the code can be extracted or/and re-used for other issues. However, to our knowledge only few open source reference systems for iris recognition are available.

Probably, the most widespread open source iris recognition system was supplied by Masek and Kovesi [79] in 2003. The approach is inspired from the first system proposed by Daugman [13]. It was developed as a part of Masek Master's thesis [97]. The source code, written in MATLAB®, has been largely employed by the research community for comparative evaluations and testing purpose. The code is designed as a modular software system. It includes functions for segmentation, normalization, feature extraction, and template matching. The segmentation is based on the Circular Hough Transform to detect the iris region, restricted to an interval of interest, which is manually set, depending on the database used. Eyelids are isolated by performing line Hough Transforms and Canny edge detection. The eyelashes and eventual reflections are removed by a threshold. The extracted iris area is then normalized into a rectangular image following Daugman's rubber sheet model [13]. The features are obtained by convolving each row of the normalized image with 1D Log-Gabor filters. The phase coefficients are then quantized to four levels, resulting in a binary template as proposed by Daugman. Finally, a bitwise template containing a certain number of bit information (iris features), and a corresponding noise mask (non iris regions) are produced. To classify the iris templates, the Hamming distance is used to evaluate dissimilarity scores. Another implementation of the Masek's system is available in C language. The code was rewritten by Liu et al. [98]. This iris recognition system has been largely used by the research community for comparative evaluations. However, its performance has become obsolete relatively to recent state-of-the-art results, obtained by more robust and accurate algorithms.

Recently, for iris recognition in less constrained acquisition environment, NIST provided an open source iris recognition system namely VASIR (Video-based Automated System for Iris Recognition) [99]. VASIR is the first public open source system for video-based iris recognition taken at a distance using an IOM system (Iris On the Move). The still image scenario is also supported. The software was used as a baseline reference for MBGC challenge. The software is composed of 5 modules: acquisition loading (video or still image), eyes regions detection based on Haar-like features [100] and left/right iris images extraction, image quality assessment for best image selection (based on an edge density method for face image quality [101]), segmentation, normalization, feature extraction, and template comparison. The segmentation is based on Circular Hough Transform for detecting the iris, and line Hough Transform for eyelids detection. The rest of the modules are largely similar to Masek's algorithm.

Our research team has also proposed an open source iris recognition system based on Daugman's approach, called OSIRIS (Open Source for IRIS) [102]. OSIRISV1.0 was the first version [102]. The segmentation module used the Circular Hough Transform for retrieving the iris contours. The remaining modules are similar to Daugman's system [13]. No masks were created. OSIRISV1.0 is now obsolete and not yet available online. Since then, other versions were developed and they are explained in the next sub-section.

3.2. Reference systems developed by our research team

In 2007, our research team has proposed the first version of an open source iris recognition system namely “OSIRIS” which is now distributed via the BioSecure Association [43]. The system is free and licensed under the GNU General Public License. The software is mainly composed of four key modules, namely segmentation, normalization, feature extraction and template matching, as classical iris recognition systems.

Several versions of OSIRIS have been developed. From a version to another, some modules have been modified in order to decrease the error rate of the overall recognition system. OSIRISV2 is the first relevant version available online since 2009. Its implementation is basic and simple. The segmentation module is based on a Hough transform. OSIRISV2 was largely used in the past due to its competitive results relatively to the state-of-the-art and in particular relatively to Masek reference system. However, with the progress of research, it became obsolete due to its weakness at the segmentation step, which led to high error rates at the recognition step.

For this reason, this module has been completely modified in the more recent version OSIRISV4 and replaced by a more sophisticated approach. Consequently, the performance has been greatly enhanced and for further improvement, OSIRISV4 has been upgraded by modifying the normalization module. Indeed, to unwrap the iris texture, a novel contour description, relaxing the geometric (circles or ellipses) parameterization constraints is proposed instead of circles as done in OSIRISV2 and OSIRISV4. This parameterization provides more accurate iris boundaries (closer to the real contours) allowing a more efficient matching. This version, namely OSIRISV4.1, is the latest open source software for automated iris recognition and is available online since 2013.

The different versions were developed by other members of our team before my arrival. However, I made some modifications and adaptations of the last version in order to make the system open source (+ documentation) and available online and participate to the ICB competition.

In this doctoral work, we have used both versions i.e. OSIRISV2 and OSIRISV4.1. Details on their implementations are given in this sub-section.

3.2.1. Relevant versions: OSIRIS's evolution

3.2.1.1. OSIRISV2

OSIRISV2[1] has been developed in 2009. The segmentation is done in 2 steps: (i) a rough localization of iris contours is performed by using circular Hough transform; (ii) these two circles are then used to initialize an active contour following the method proposed by Xu and Prince in [103], in order to refine the iris contours as displayed in Figure 3-3. The refined contours are then exploited for generating a mask that indicates those regions containing only iris texture. These two non-concentric circles are used to model the iris borders. According to Daugman's rubber sheet, the iris texture is unwrapped with respect to these two circles as previously explained in Section 3.1.1.

[1] *http://svnext.it-sudparis.eu/svnview2-eph/ref_syst/Iris_Osiris/.*

The next module consists in the extraction of iris features by filtering the normalized image with a bank of 2D Gabor filters of different resolutions and orientations, applied at specific points of the normalized iris image. These points of interest were used in OSIRISV2 are illustrated in Figure 3-4.

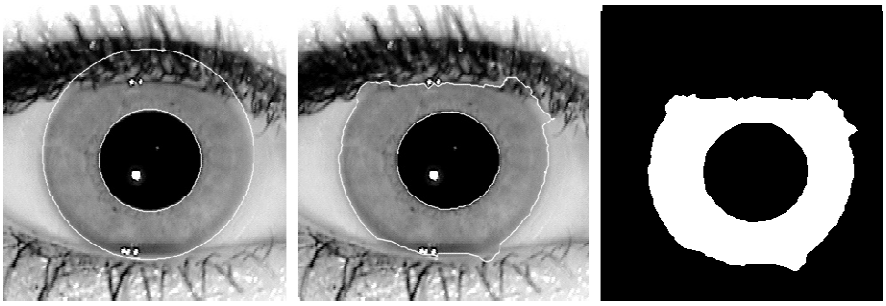

Figure 3-3: Segmentation results in OSIRISV2: (a) Initial contours, (b) accurate contours, and (c) the associated mask [33].

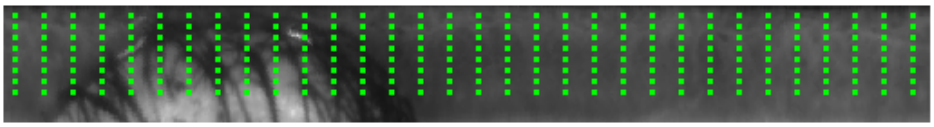

Figure 3-4: Application points uniformly distributed in a normalized iris image.

The phase of each resulting Gabor coefficient is then encoded on two bits, depending on the sign of its real and imaginary parts, resulting in a binary template, the irisCode. In the matching module, the comparison is based on the Hamming distance. This score measures the dissimilarity between the two irisCodes (low (resp. high) when they come from the same (resp. different) iris). These two modules are inspired by Daugman's approach.

In practice, the evaluation of OSIRISV2 has shown the weakness of the segmentation phase. For instance, on the ICE2005 database [58] the EER was 5.41% and the FRR at FAR of 0.001, was 17.46%. This weakness motivated the following new version of OSIRIS which presents an improved accuracy of the segmentation process.

3.2.1.2. OSIRISV4

This version uses the same normalization, feature extraction and matching modules as OSIRISV2. However, the segmentation part has been greatly improved. Indeed, the contours of the iris in this version correspond to an optimal path retrieved by the Viterbi algorithm for joining in an optimal way,

the points of high gradients under the constraint that the resulting curve has to be closed [104]. The Viterbi algorithm is then exploited at two resolutions: at a high resolution, accurate contours are recovered, while at a low resolution the optimal path corresponds to coarse contours. More precisely, at a high resolution, the contour is searched by exploiting all the pixels in the image. In the low resolution case, fewer points on noisy regions (close to the eyelids and the eyelashes) are used to retrieve the contour. Consequently, the coarse contour is non-regularly sampled, contrary to the accurate contour, as represented in Figure 3-5.

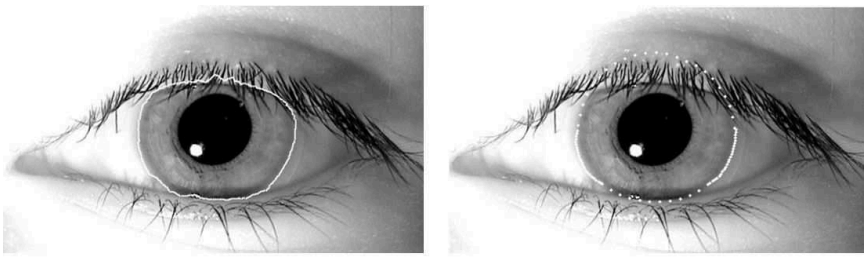

(a) (b)

Figure 3-5: Examples of accurate (a) and coarse (b) iris borders for a given eye image extracted from [104].

The normalization that follows is based on a modelization of the borders by circles, as in OSIRISV2. Such circles are computed from the coarse contours detected by the Viterbi algorithm at low resolution, using a least-square based method for circle fitting. Note that such circles do not need to match exactly with the maximum of pupil and iris gradient points, contrary to the circles obtained through the Circular Hough Transform in OSIRISV2. Moreover, due to the sensitivity of least-square fitting methods to outliers, coarse contours, which contain less noisy points in regions showing occlusions (eyelids and eyelashes zones), are used instead of accurate contours. The two non-concentric resulting circles are then used to unwrap the texture.

For recognition purpose, non-iris regions have to be masked. To this end, this version of OSIRIS exploits the accurate contours found by the Viterbi algorithm to mask the eyelashes. However, this mask is not efficient to detect all the occlusions in the image. Therefore, another mask based on an adaptive filter is generated in order to remove the remaining eyelashes and other occlusions such as shadows and specular reflections. This mask results from a simple classification of pixels (iris or non-iris), and corresponds to the Full Width at Half Maximum (FWHM) of the Gaussian density function, modeling the histogram of iris pixel intensities. This mask is then combined to the segmentation mask given by the accurate contours in order to build a final mask. As shown by Sutra et al. [104],

performance of iris recognition improves when using the refined final mask instead of the mask based only on accurate contours. The difference between OSIRISV2 and OSIRISV4 is illustrated in Figure 3-6-a and Figure 3-6-b.

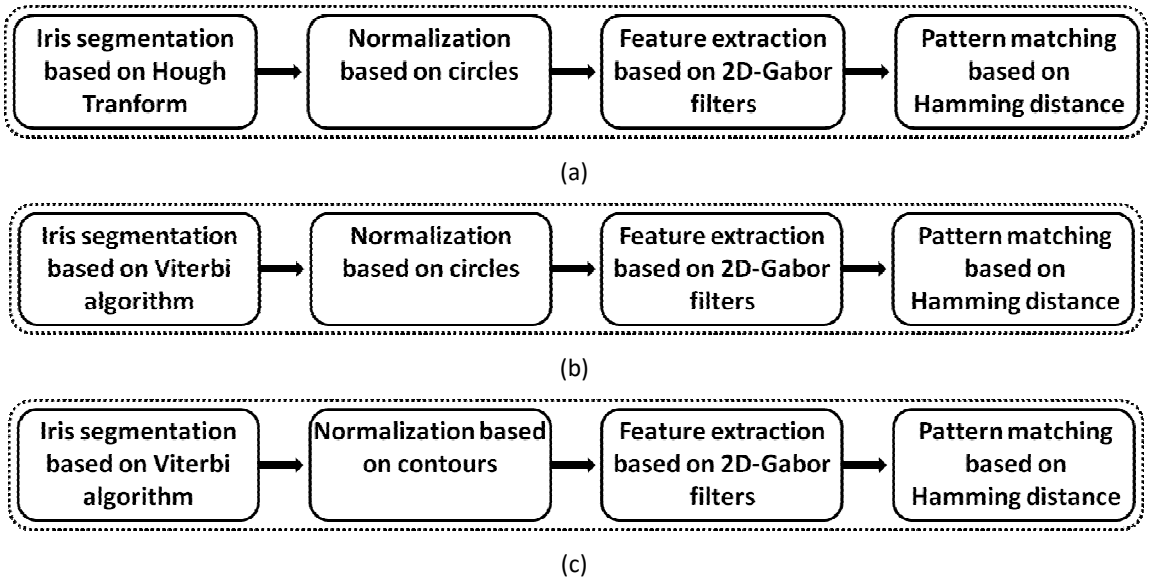

Figure 3-6: Flowchart of: (a) OSIRISV2, (b) OSIRISV4, and (c) OSIRISV4.1 [33].

3.2.1.3. OSIRISV4.1

OSIRISV4.1[2] version is an upgrade of OSIRISV4. The difference between both versions lies in the normalization step. In the previous version V4, the normalization is based on a modelization of the iris borders by circular contours in order to unwrap the texture following the pioneer normalization algorithm in the literature proposed by Daugman [13]. Even in recent works [85] [86] [105], the iris is furthermore modeled by two non-concentric circles. Nevertheless, it is clear that using such a simple parameterization of contours is not optimal to recover the iris zone. Indeed, as contour borders are not an exact circle, any circular model will induce errors. Moreover, Proença and Alexandre [106] have shown that small errors in the estimation of circles' parameters change the resulting normalized image and this can dramatically impact the performance of the overall system.

[2] *http://svnext.it-sudparis.eu/svnview2-eph/ref_syst/Iris_Osiris_v4.1/.*

Two normalized iris images resulting from different acquisitions of the same person may present a high discrepancy and consequently lead to wrong authentication. Therefore, having an accurate description of the iris boundaries is an essential task to avoid significant degradations of performance.

Beyond circles, other types of parametric contours are proposed in the literature to model the shape of the iris such as ellipses [81] [82] [84] and polynomial curves [83]. In another way, parametric contours given by Fourier series are also used to describe the border of the iris in the works of Daugman [73] and Proença [107]. Such parameterization, which does not make an assumption of the contour as a known geometric curve, allows obtaining more flexible and generalized iris contour description. OSIRISV4.1's modelization fits in this category. Actually, the iris boundaries used in the normalization are the coarse contours resulting from the Viterbi optimization of a cumulative gradient function around the center of the pupil. Contrary to [73] and [107], fewer points are used in the noisy areas which correspond to usual locations of the occlusions (close to the eyelids and the eyelashes) than in the clean ones. Therefore, the obtained contour corresponds to a sequence of non-regularly sampled points, as shown in Figure 3-5-b. By this way, the number of possible erroneous contour points is reduced. These coarse contours are finally used in Daugman's rubber-sheet in order to unwrap the iris texture.

We note that outer coarse contours look like a circle even in the superior part where the occlusion occurs (upper eyelids). This is due to the Viterbi algorithm that imposes regularity in the search of the contour points. More precisely, the obtained contour is a series of radii $R(n)$ in polar coordinates, where index n stands for the angle (varying from 1° to 360°). A non-regular sampling of the angles is considered as follows: in "difficult" areas (where occlusions might occur), one contour point is selected every eight pixels, while in other regions, one contour point is selected every two pixels. The Viterbi algorithm is used to find an optimal path through the gradient map. It imposes the search of the radius $R(n+1)$ in the restrained interval $[R(n)-1\ ;\ R(n)+1]$.

In Figure 3-5-b, the upper part of the iris boundary corresponds to the "difficult" area (possible occlusions), where contour points are sparse. Therefore, the radius does not change roughly and the final contour looks like a circle. In this way, the area considered as iris after the normalization step, will be similar for a given person, independently of the presence of occlusions or not in the original image (case of upper eyelid).

Figure 3-7 shows the difference between the components used in the two iris recognition systems OSIRISV4 and OSIRISV4.1.

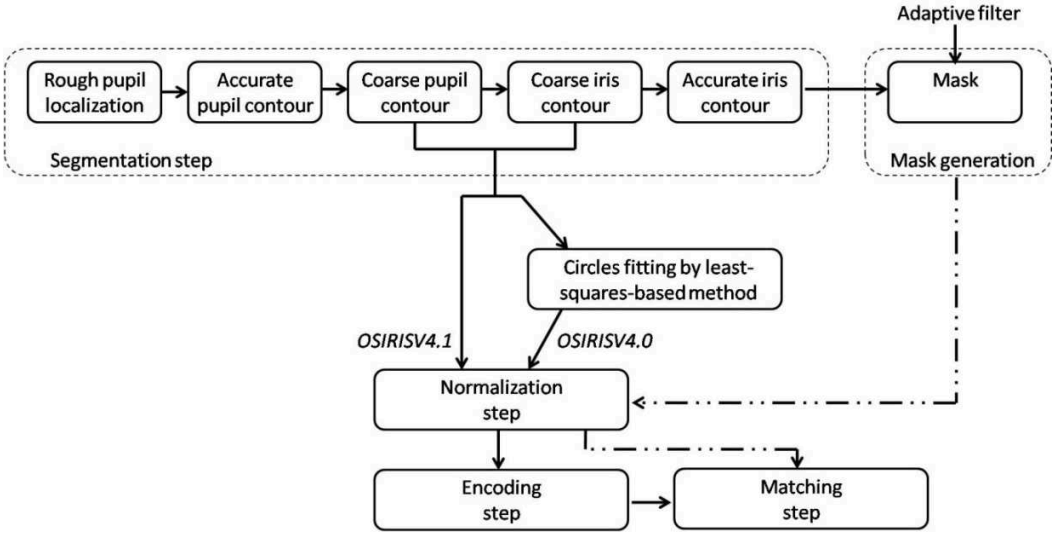

Figure 3-7: The difference between the two iris recognition systems: OSIRISV4 and OSIRISV4.1 [33].

The new normalization follows the following steps. First, let W and H be respectively the width and height of the desired normalized image. Regarding Daugman's approach, we compute a regular sampling of angles θ_k where k ranges from 0 to W, so that $\theta_0 = 0$ and $\theta_w = 2\pi$:

$$\theta_k = \frac{k}{W} 2\pi, \quad k \in [0 \quad W] \qquad (3.8)$$

Let (x_p, y_p, φ_p) and (x_i, y_i, φ_i) be the coordinates of a point of pupil coarse and iris coarse contours respectively where (x, y) are the *x*-coordinate and *y*-coordinate of the radius relatively to the estimated center of each coarse contour and φ the angle of the non-regular sampling. φ follows the non-uniform sampling of the coarse contour as explained above. The next step consists in estimating the new point (X_k^p, Y_k^p) with a sampling as close as possible to θ_k from the coarse pupil contour. To this end, we interpolate the two nearest points of the coarse contour j and $j+1$ to θ_k as follows:

$$X_k^p = (1-\alpha) \cdot x_p^j + \alpha \cdot x_p^{j+1} \qquad (3.9)$$

$$Y_k^p = (1-\alpha) \cdot y_p^j + \alpha \cdot y_p^{j+1} \qquad (3.10)$$

with $\alpha = \dfrac{\theta_k - \varphi_p^j}{\varphi_p^{j+1} - \varphi_p^j}$

This process is illustrated in Figure 3-8. In a similar way, the new points (X_k^i, Y_k^i) of the iris contour are computed.

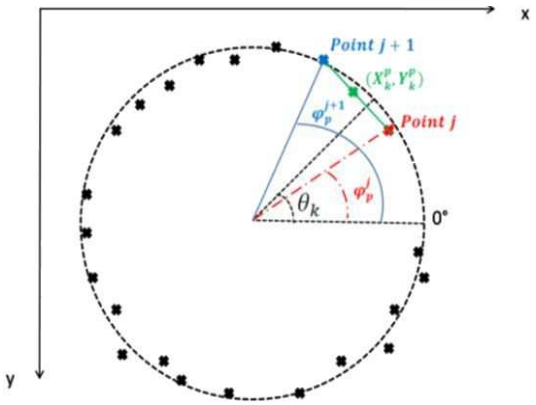

Figure 3-8: How to compute the new coordinates of points (X_k^p, Y_k^p) [33].

The pupil and the iris centers are not necessarily the same. Often the pupil center has a nasal and inferior position relative to the iris center [10]. To cope with this problem, we define a segment S formed by (X_k^p, Y_k^p) and (X_k^i, Y_k^i) as shown in Figure 3-9.

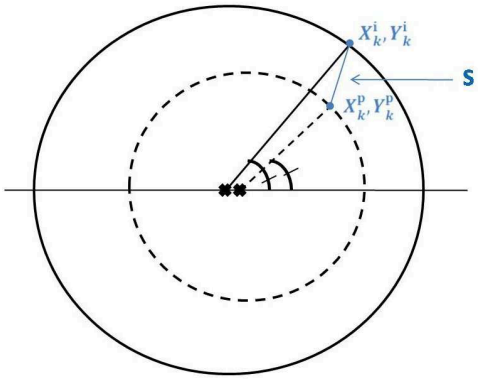

Figure 3-9: Illustration of segment S formed by (X_k^p, Y_k^p) and (X_k^i, Y_k^i). Note: Coarse boundaries are modeled by circles to simplify the figure [33].

S is then rescaled so that it fits with the height H of the normalized image. On the normalized image, the pixel on h^{th} row and k^{th} column will take the same value as the pixel located at $(x_{k,h}, y_{k,h})$ on the original image as follows:

$$x_{k,h} = \left(1 - \frac{h}{H}\right) \cdot X_k^p + \left(\frac{h}{H}\right) \cdot X_k^i \qquad (3.11)$$

$$y_{k,h} = \left(1 - \frac{h}{H}\right) \cdot Y_k^p + \left(\frac{h}{H}\right) \cdot Y_k^i \qquad (3.12)$$

with $h \in [0\ H]$.

Compared to OSIRISV4, in OSIRISV4.1 the borders used for normalization are closer to the real ones in the sclera area and in the lower eyelid part, as illustrated in Figure 3-10. Therefore, the matching points considered in the comparison of two irises are better aligned resulting in increased performance. For instance, on CASIA-IrisV4-Thousand, an improvement of 25.36% is observed at the FRR@FAR=0.001 operating point. More results are reported in [33]. The flowchart of OSIRISV4.1 is resumed in Figure 3-6-c.

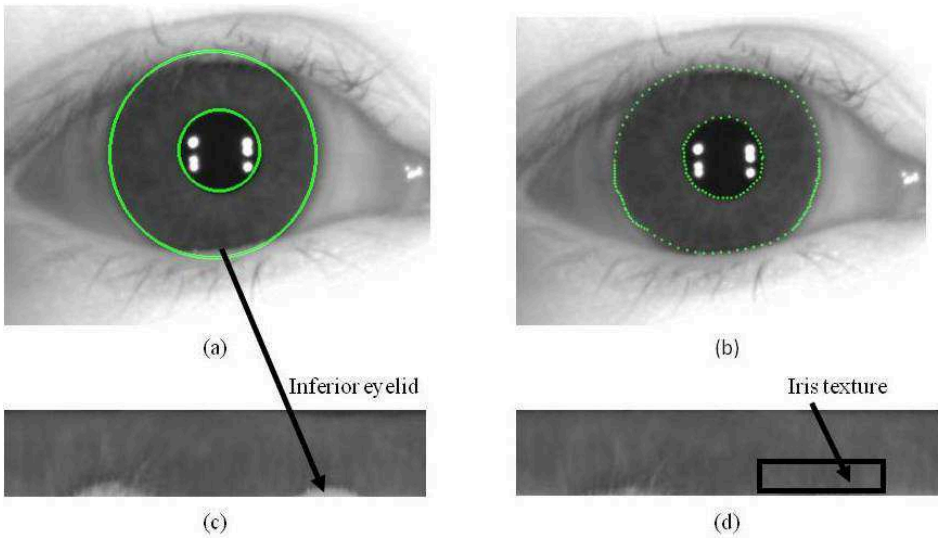

Figure 3-10: (a) Border points used for normalization in OSIRISV4.0, (b) Border points used for normalization in OSIRISV4.1, (c) normalized image by OSIRISV4.0, (d) normalized image by OSIRISV4.1 [33].

3.2.2. OSIRIS's impact in the research community and evaluation performance

OSIRIS reference system has been cited in several papers since 2009, in different topics such as iris segmentation [3] [108] [109] [110] [111] [112], iris aging [113], cryptography [114] [115] [116] and

quality assessment [117]. To our knowledge, OSIRISV2 and OSIRISV4.1 have been respectively used in 14 and 11 works as reported in Table 3-1 (until March 2015).

Table 3-1: OSIRIS citations for each version since 2009.

Year	OSIRISV2	OSIRISV4.1
2009	*2*	*X*
2010	*2*	*X*
2011	*3*	*X*
2012	*3*	*X*
2013	*2*	*X*
2014	*2*	*9*
2015 (until March)	*0*	*2*
Total of papers	*14*	*11*

Table 3-2 lists an overview of the teams that have used OSIRIS reference system in their research. More precisely, we give for each team, the number of papers in which OSIRISV2 and OSIRISV4.1 have been used, with the corresponding field of application. We also cite one example of paper per team. We notice that OSIRIS is used by a large community in different areas of research.

We also note from Table 3-1 and Table 3-2 that the use of OSIRISV2 has decreased in favor of OSIRISV4.1, despite the more recent availability online of the latter. This is due to the improved performance of OSIRISV4.1 compared to that of OSIRISV2 as shown in [33] on two well-known iris databases: ICE2005 [58] and the challenging CASIA-IrisV4-Thousand [37].

In addition, OSIRISV4.1 has been benchmarked on an unpublished subset of CASIA-IrisV4-Thousand database in the context of the first ICB competition on iris Recognition [44]. Eight participants (institutions and companies) from six countries submitted 13 algorithms in total. With an EER of 3.02%, OSIRISV4.1 corresponds to the 2nd best system. The best EER was equal to 2.75% and was obtained by Zhuhai YiSheng from Electronics Technology Co, Ltd.

OSIRISV4.1 gives competitive performance relative to other state-of-the-art iris recognition systems. The efficiency of this version relies on two important ingredients: (i) an implementation of a segmentation algorithm able to determine accurate contours through a gradient optimization implemented by the Viterbi algorithm and (ii) a non geometric and non uniform parameterization of the contour which allows a precise localization and normalization of the iris texture. Therefore,

OSIRISV4.1 can be used with high benefit as an up to date, relevant tool for benchmarking novel iris recognition algorithms, which is publicly available online.

Table 3-2: Summary of works that have used OSIRISV2 and OSIRISV4.1.

OSIRISV2			**OSIRISV4.1**		
Team	**Topic**	**Number of papers**	**Team**	**Topic**	**Number of papers**
Carlos III University of Madrid	*Quality assessment, (Tomeo-Reyes et al., 2011) [117]*	*2*	*Electrical Engineering Department - DEE Federal University of Campina Grande, Brazil*	*Cryptography, (Rodrigues et al., 2014) [115]*	*1*
Department of Computer Sciences, University of Salzburg, Austria	*Iris segmentation, (Rathgeb et al., 2013) [3]*	*5*	*The University of Electro-Communications, Tokyo, Japan*	*Iris segmentation, (Oishi et al., 2015) [110]*	*1*
Department of Computer Science and Engineering, University of Notre Dame, USA	*Iris recognition system, Bit reliability in an irisCode, (Hollingsworth, 2009) [108]*	*4*	*Norwegian Biometric Laboratory, Gjøvik University College,, Norway*	*Iris segmentation for Smartphone applications, light field camera... (Raja et al., 2014) [111]*	*7*
Department of Electronics and Systems Federal University of Pernambuco, Brazil	*Cryptography, (Camara and Rocha, 2010) [114]*	*1*	*Advanced Technologies Application Center, Havana, Cuba*	*Iris segmentation, (Sanchez-Gonzalez et al., 2014) [112]*	*1*
Institute of Control and Computation Engineering, Warsaw University of Technology, Poland.	*Iris aging, (Czajka, 2014) [113]*	*1*	*Faculty of IT, Monash University, Melbourne, Australia*	*Cryptography, (Torres et al., 2014) [116]*	*1*
Oak Ridge National Laboratory, USA, and The University of Tennessee Health Science Center: Hamilton Eye Institute.	*Iris segmentation, (Santos-Villalobos et al., 2012)* [109]	*1*			

3.3. Iris acquisition systems in less constrained environments

Conventional iris systems require restrictive acquisition conditions on the subjects, which can cause inconvenience to the participants. The major limitations for such systems are:

- The proximity of the subject to the camera: Iris caption is actually carried out at close distances (under 50 cm) in comparison with other modality such as face.
- Static participants during the acquisition.
- Slow acquisition time: Such systems require an active cooperation of the participants. Quality checks including feedback to the user are used in order to assist him/her in providing biometric samples free from noise, resulting in slow acquisition time.

To overcome those drawbacks and make iris recognition feasible in more realistic conditions, new imaging systems were proposed rather than conventional cameras. In this section, details on iris recognition systems that function on the move and at a distance will be discussed.

3.3.1. Literature review

Several researchers have concentrated their efforts on designing iris recognition systems in more realistic conditions with acceptable recognition accuracy. To our knowledge, this ambitious objective has been addressed for the first time by Fancourt et al. in 2005 [118]. They proposed two iris recognition systems at 5 and 10 meters. Each one is based on a custom-built telescope connected to a NIR camera. During the acquisition, the participant was seated and his head was fixed by a chin rest with a forehead stabilizer. The experimental results show the successful feasibility of iris recognition at larger distances. Nevertheless, the iris acquisition conditions are still constrained (fixed location of the head, staring at a spot light). Therefore, further research was developed in order to design iris recognition systems under less restrictive conditions imposed on position and movement of the participants.

The Iris-On-the-Move System (IOM) later proposed by Matey et al. [25] in 2006, was the first system able to capture iris images at a distance and on the move with a sufficient quality for recognition. The subject is moderately cooperative: he is asking to walk at a normal speed through a confining portal, looking forward. The camera is positioned at a fixed distance of 3 meters in front of

the participant. The system is designed to produce images with a resolution of approximately 100 pixels across the iris diameter. An illustration of an acquisition by the IOM system is given in Figure 3-11. One limitation of this system consists in the inability of capturing irises for people with different heights (children, tall person) due to the small capture field of view. Another drawback of IOM system lies in the low-resolution of the resulting iris images. Despite the relaxation of the acquisition constraint, the user is still cooperative: he looks forward without any intended behavior to prevent iris acquisition.

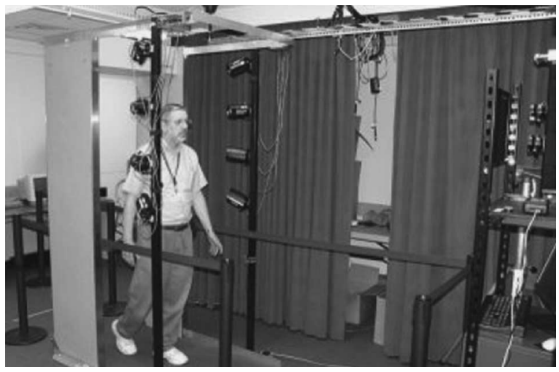

Figure 3-11: An illustration of the concept of IOM system [25]. The camera is visible at the far right of the figure.

In 2007, Yoon et al. [29] proposed to use a pan-tilt-zoom camera to acquire iris images at a distance. For user convenience, the system was designed for providing large operating range which can cover the natural movements of a standing user. The wide height and width of operating range is obtained by the pan-tilt unit and the large depth is achieved by zoom lens. The capture is done in two steps. Firstly the face is detected and secondly it is zoomed to fit the entire image in order to produce a high-resolution iris image (diameter > 150 pixels). Figure 3-12 shows the concept of this system.

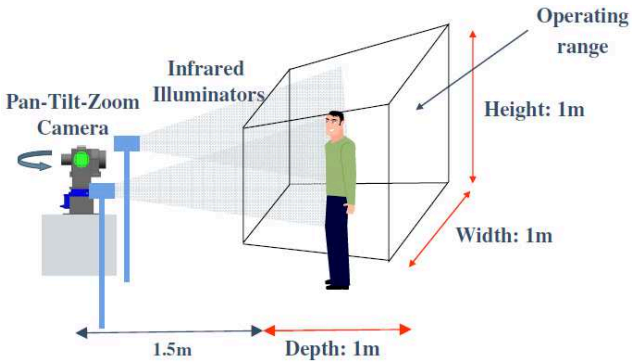

Figure 3-12: Concept of Yoon's system [29].

In the same way as [29], Wheeler et al. [27] proposed a stand-off iris recognition system for access control application at a distance of 1.5 meters but with heavier imposed cooperation from participants. The system is designed for cooperative users of any height who stops, stares, and looks towards the iris camera, with no possibility of natural movement. The difference between [27] and [29] is in the localization of the face. The system is configured in order to acquire iris images at a resolution of approximately 200 pixels across the iris diameter.

Bashir et al. [26] [119] proposed a novel prototype of system called Eagle-Eyes which uses video surveillance techniques to acquire multiple biometrics (face and iris modalities). It is able to recognize a person by their irises at a large stand-off distance of 3 to 6 meters. The system combines multiple cameras with hierarchically ordered field of views, a high pan tilt unit, and a long focal length zoom. The used cameras in the system are: (i) fixed scene camera for human tracking, (ii) face camera for face detection and (iii) NIR iris camera in order to capture iris images. The iris resolution meets the specifications pointed in ISO/IEC 19794-6 [35] (between 100 to 200 pixels across the iris). Similar to Eagle-Eyes system, Dong et al. [28] proposed a stand-off iris recognition system at 3 meters based on a hierarchy of cameras for successive detection of human, face and then eyes. An illustration of iris acquisition is given in Figure 3-13.

Figure 3-13: Iris acquisition at a stand-off distance of 3 meters [28].

Long range iris acquisition and recognition systems have been also developed by Villar et al. in [31] and Venugopalan et al. in [30]. In [31], the system is able to recognize people at a distance of 30 meters. It uses a wide field of view camera to locate the subject via face and eye, and then a narrow field of view camera attached to a telescope is pointed to the detected eye. Iris images of approximately 190 pixels across the diameter are acquired by the system. The subject is stationary, standing in a

corridor. In [30], the iris acquisition system operates at 8 and 12 meters. The system captures both the face and the iris using a single camera of high-resolution. The subject can be stationary or mobile (walking toward the camera). For moving subject, during the course between two check points (for example position A and B in Figure 3-14), the user's speed is estimated in order to finely tune the focus of the system to the subject motion and then a set of high-resolution images are acquired at a desired check point (position C in Figure 3-14). Based on the estimated speed, the focus is continuously adjusted while the subject is approaching the system. The location of this check point depends on the required iris resolution.

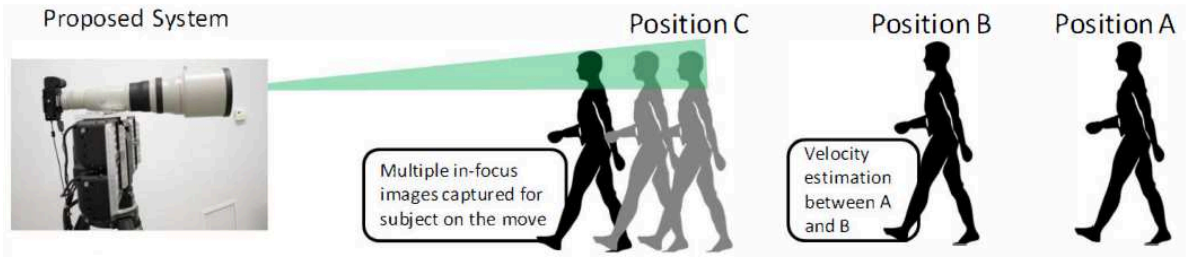

Figure 3-14: Iris acquisition by CyLab System. The subject is walking toward the system. His speed is estimated between position A and B to set the focus of the camera to the position C to acquired in-focus iris images while the subject approaches the system [30].

Recent commercial solutions for iris recognition at a distance are also available. For instance, AOptix Technologies proposed a system, named InSight® [120], able to acquire both irises and face images at a standoff distance range of 1.5 and 2.5 meters. Four seconds are required for dual-iris and face capture, including quality assessments and encoding functionality. More recently, MORPHO (SAFRAN) has developed a stand-off iris recognition system named MORPHO IAD™ [121]. The acquisition of both irises and face is performed under less than 1 second, at a distance range of 0.8 to 1.2 meters. Both systems can be used for enrollment and authentication and they are suitable in border control, aviation security and for securing sensitive sites.

3.3.2. Challenges in iris acquisition systems

Image acquisition plays a crucial role in successful recognition. Dealing with mobile subjects, and acquisition at a distance, the main concern is the quality of the resulted images for recognition purpose. Poor imaging conditions have been shown to affect the genuine score distribution. In fact, the similarity between iris templates belonging to the same subject considerably decreases under less constrained acquisition conditions [122]. However, impostor scores are largely less dependent on

image quality. The quality of the images is basically related to two major factors: the imaging system itself and the environmental conditions during the capture.

Imaging systems must be carefully designed in order to achieve acceptable recognition accuracy. The challenges associated with iris recognition design arise principally from two necessities: (i) enough resolution (number of pixel across the iris diameter) and (ii) enough NIR illumination intensity.

- *Resolution:* According to the iris image data interchange standard released [35] in 2005, an image with 200 pixels across the iris diameter is considered as a high quality iris image. The lower limit of the number of pixel is set to 100. Below this limit, the recognition performance is dramatically degraded.
- *NIR illumination:* The light is emitted from a NIR illumination source, with a wavelength range that emphasizes the iris texture while providing sufficient contrast between the pupillary and limbic boundaries, and covering uniformly the iris surface. The intensity must be sufficient to maximize the signal/noise ratio that is collected by the camera sensor. As high illumination can cause permanent eye damage, the level of illumination must be set carefully. Indeed when working with NIR wavelengths, the human eye does not respond to its natural light protective mechanism such as aversion, blinking and pupil contraction.

Even if these two issues are addressed properly by the hardware design, relaxing the imposed constraints on the participant during the acquisition causes significantly quality variations in the iris images. In fact, the captured images may suffer from blur due to motion and/or out of focus, distortion, strong occlusions, poor resolution, low contrast and so on. These factors have to be handled by software algorithms in order to improve the accuracy of the recognition system.

3.4. Conclusion

In this chapter, we explained basic considerations on iris recognition. In particular, a literature review on pioneer and recent iris recognition algorithms was presented. Existing open source systems for iris recognition were also described. After that, the reference system: OSIRIS that we used throughout this thesis was presented. Several versions have been implemented aiming at improving the accuracy of the recognition. Finally, we related a literature review on iris acquisition systems in less constrained environment. As explained in this chapter, in such condition, the resulting iris images suffer from

diverse degradations. These perturbations dramatically decrease the performance of the overall iris recognition system.

As explained in Chapter 2, quality measurement algorithms (QMAs) are very useful for improving performance of a given iris recognition system. Therefore, disposing of a pertinent quality metric will be especially beneficial for us since in this thesis we address iris recognition in uncontrolled acquisition. Indeed, we want to integrate quality measures in the fusion process in order to remedy to eventual degradations. By this way, we expect to enhance the accuracy of the recognition. Therefore, we will first elaborate a relevant quality metric able to measure locally and globally the quality of the iris images. This new quality measure is presented in the next chapter.

Chapter 4. Design of a quality measurement algorithm for improving iris recognition

As mentioned in Chapter 1, many real-world security applications require less cooperative recognition systems. However, less restrictive conditions during the iris acquisition cause a loss in the quality of the resulting images. In fact, the images suffer from lack of resolution, out-of-focus and motion blur, strong occlusions, low eye contrasts, etc. All these degradations significantly decrease iris recognition performance [34]. Biometric system designers are therefore challenged for the conception of such systems for providing iris images of sufficient quality as explained in Section 3.3. Nevertheless, the recognition performance obtained by such systems is still not satisfactory regarding the high demand of security required by the applications. This fact suggests that the resulting images are of insufficient quality for iris recognition purpose.

The ultimate goal of this thesis is to deal with the degradation of the images quality in order to improve the overall recognition accuracy. Our research activities focus on how to fuse the information available in the sequence in order to improve as much as possible iris recognition. Since the performance of the recognition is strongly related to the quality of the images, we propose to integrate a local quality measure in the proposed fusion scheme for retrieving the most relevant data from the sequence. This local quality and its pertinence will be presented in this chapter independently of the fusion scheme which will be detailed in the next chapter.

In Section 4.1, we first relate a literature review on iris quality measures that have been proposed in the state-of-the-art. From this overview, the quality components that influence mostly recognition will be identified. Moreover, a synthesis is provided to determine all the requirements of a relevant quality measure for iris recognition. This will guide us in defining our quality measurement algorithm (QMA) that can respond to all the identified needs. Section 4.2 presents the proposed local quality measure, as well as the details of its implementation. Finally, extensive experiments are conducted in Section 4.3 in order to prove the effectiveness of the approach. We will also show the possibility of defining a global quality from the proposed local quality and demonstrate that it is well correlated to the performance of the recognition.

4.1. Related works

As shown in the literature [34], iris recognition performance decreases dramatically when the iris image quality drops. Therefore, identifying the quality factors and quantifying their effects on the recognition allows us to design a relevant QMA that can considerably improve the performance of the entire system.

Quality assessment can be used in different ways. It can be useful not only to re-acquire an iris image of poor quality but also to select the best image across multiple enrollments. In the case of video acquisitions in less constrained environment, different weights can be allocated to the images regarding their quality in order to give less importance to poor quality images in order to relevantly fuse the images in an iris sequence as done in [54]. It can also be useful to predict the performance of a given iris system via the quality of the couple of images to be compared. In [52], Li et al. explored the relationship between the matching score and the quality of the pairwise iris images by formulating the mapping as a statistical regression problem. They define the uncertainty interval of matching scores. They demonstrated that by discarding the uncertain match pairs the recognition performance is thus improved. In [53], a nonlinear mapping based on a Feed Forward Neural Network (FFNN) is developed for establishing predictions on quality measures and corresponding matching scores.

As iris recognition is increasingly performed in less constrained environment, the interest of designing effective QMA can only increase too. However, image quality measurements allow improving the accuracy of the performance only if the quality metric is well correlated to the recognition accuracy.

4.1.1. Iris image qualities

In the state-of-the-art, various publications have addressed the problem of iris image quality since several years now. In the first proposed iris recognition system [13], the focus level of the images was already pointed out as being a critical factor in the degradation of the performance. Therefore, Daugman introduced new metrics to measure the energy of the high frequency components in an image in order to assess the level of blur in [13] and [72]. This metric was further improved by Kang and Park [123].

Ma et al. presented in [124] a new scheme to assess image quality. They evaluated three quality factors: defocus, motion and occlusion, by analyzing the distribution of Fourier spectra in two local iris regions. These three quality metrics were also addressed by Wei et al. in [125]. They exploited power-based metrics and statistical features to quantify the quality of the images. Both quality assessment algorithms of [124] and [125] are used for selecting clean images in recorded iris sequences for subsequent recognition. Based on the estimated three quality factors, a Support Vector Machine (SVM) is used to classify the images into clean or noisy images. By discarding the identified noisy images, the overall FRR error is reduced.

In [126], Lu et al. suggested a sequential scheme for image quality assessment by designing different situations of bad quality caused by blur (defocus and motion) and occlusions. By comparing each quality component to a fixed threshold, only the images that have higher qualities are kept for further processing. In another way, a dynamic method was proposed by Dong et al. [127] to adjust the threshold of an iris matching module based on the quality of the input iris image. This way, the poor images are not discarded by a quality threshold fixed globally such as in [126]. This method gives a chance to poor images to be matched under a fixed FAR (false accept rate) based on a look-up table, which establishes the relationship between the quality of the images and the matching score. The studied quality factors are defocus, motion, occlusion, and dilation.

Pupil dilation [80] [128] and contact lenses [80] also represent two quality factors that have negative impacts on the performance. Czajka and Bowyer [129] considered three iris quality factors that can be influenced by the behavior of the subject: un-occluded iris area, motion blur and margin. They analyzed the overall quality of consecutive attempts (three times) in a biometric system to complete a transaction. Each of the estimated quality factors is compared to a threshold that has been fixed a priori regarding the exploited database. Only images with enough qualities are accepted for further processing. Gaze angle also disturbs the performance of the iris recognition as demonstrated in several works. It occurs when the subject does not look straight at the camera. Gaze direction can be estimated and then corrected in order to transform the off-angle iris image into a frontal one as done for example in [130] by Yang et al.

The impact of image compression on iris recognition was also investigated in several works [131] [132] [133]. And in [134], Bergmueller et al. conducted a study on the impact of using pre-compressed data for iris segmentation.

The majority of the above works considered less than three quality components. A broader number of quality metrics and a new fusion scheme were proposed by Kalka et al. [135]. The authors proposed an analysis of various quality factors that influence iris recognition such as defocus blur, motion blur, off-angle, occlusion/specular reflection, lighting and iris resolution. All these quality factors are estimated and then combined using a Dempster–Shafer theory approach to obtain one unique value. The authors showed the negative effect of all these discrete factors on the performance, with mainly degradations in the genuine matching scores. Moreover, by using the fused quality, they were able to classify the images into 3 classes: high, medium and low quality. Thus, they demonstrated that this combined quality is a suitable indicator of their ability to predict iris image quality.

In addition to the quality factors that have been addressed in [135], Zuo and Schmid proposed to assess other elements: segmentation scores, interlacing, eye contrasts, and dilation [136]. All these quality factors are then fused by a simple sum rule to avoid high computational cost.

In [137], Mahadeo et al. proposed a quality assessment scheme for detecting the best frames in iris videos. First, the frames with blinks and off-angles are discarded from the sequence by using averaging and correlation methods. Then, the remaining blurred images are dismissed using the Laplacian operator. Finally, frames with poor illumination are removed by analyzing the distribution of the pixels' intensities.

A brief summary of the quality components that have been studied in the literature and their eventual scheme of combination to obtain one single value are reported in Table 4-1.

From the above academic publications, we note that several iris image properties have been investigated. They differ from a work to another. Results show that they all play a role in the degradation of the performance. However, a legitimate question can arise: What are the iris image properties that most influence the iris recognition performance? In this context, the National Institute of Standards and Technology (NIST) organized in 2011 the first public challenge in iris image quality: Iris Quality Calibration and Evaluation (IQCE) [51], already mentioned in Section 2.4. It aimed at defining and quantifying iris image quality components that have the highest influence on iris recognition accuracy. The proposed quality components, their corresponding definition and the motivation of their investigation are the following:

- *Gray scale spread: Def.* Distribution spread of intensity pixels value.

An image of good quality has a wide and well distributed spread of intensity: Better performance is achieved with high contrast and large dynamic range. In contrast, saturation or poor illumination causes a lack of well-spread distribution.

- *Iris size: Def.* Number of pixels across the iris radius, when the iris boundary is modeled by a circle.

The iris size is determined by the iris acquisition condition and environment which include the spatial sampling rate of the image sensor and the distance between the subject and the camera. Too big or small irises cause recognition failures.

Table 4-1: Overview on quality factors that have been studied in the literature.

Publications	Defocus	Motion	Off-angle	Occlusion	Lighting variation	Resolution	Interlacing	Pixels count	Dilation	Margin	Compress-ion	Fusion rule
Daugman [13][72]	*X*											---
Kang and Park [123]	*X*											---
Ma et al. 2003 [124]	*X*	*X*		*X*								*SVM (classification into clear/noisy images)*
Wei et al. [125]	*X*	*X*		*X*								*SVM (classification into clear/noisy images)*
Lu et al. [126]	*X*	*X*		*X*								*No (3 sequential thresholds)*
Dong et al. [127]	*X*	*X*		*X*					*X*			*Multiplication*
Bowyer et al.[80]									*X*			---
Kalka et al. [135]	*X*	*X*	*X*	*X Specular reflection*	*X*	*X*		*X*				*Dempster-Shafer*
Zuo and Schmid [136]	*X*	*X*	*X*	*X*	*X*		*X*	*X*	*X*			*Sum*
Mahadeo et al. [137]	*X*	*X*	*X*	*X (blinking)*	*X*							*No (sequential thresholds removing)*
Czajka and Bowyer [129]		*X*						*X*		*X*		*No sequential thresholds removing*
Daugman and Downing [131]											*X*	---
Ives et al.[132]											*X*	---
Bergmueller et al. [134]											*X*	---
Rakshit, S., & Monro [133]											*X*	---

- *Dilation: Def.* Ratio of pupil diameter to iris diameter.

High dilation induces low usable iris area, hence a lack of information. However, low dilation indicates constricted pupil which generates error in the localization of the iris.

Usable iris area: Def. Percentage of iris that is not occluded by artifacts such as eyelash, eyelid, or specular reflections possibly caused by sunlight or eye-wear.

Eyelid or eyelash occlusions can stem from subject behavior (blinking or squinting) or/and subject character that are induced by genetic factors (droopy eyelids) and eyes diseases. Such occlusions considerably reduce the amount of usable iris area, leading to lack of information in the description of the iris texture, and consequently poor performance. In particular, occlusions that occur at the pupillary or limbic boundaries are considered as the most severe artifacts for iris recognition. They not only diminish usable iris area, but also lead to complicated iris segmentation task (wrong localization of the true borders).

- *Iris-pupil and iris-sclera contrasts: Def.* Difference in intensity between the pupillary and limbic boundaries.

Different contrasts can be caused by intrinsic properties relative to each person (shadow of eyelash on iris, contact lens), medical conditions (cataract, albinism, etc) or extrinsic factors such as NIR illuminator and other imaging system characteristics. These two quality components mostly affect segmentation accuracy, and hence influence iris recognition performance. In general, the contrast between the iris and the pupil is lower than the one between the iris and the sclera, which makes the localization of the pupillary boundary more difficult than the limbic one.

- *Iris and pupil shapes: Def.* Measure of regularity in the pupillary and limbic boundaries.

The boundaries of an iris are rarely circular or even elliptic. This phenomenon is caused by natural anatomical variation, non frontal gaze or medical condition, rather than by the acquisition device. The detection of accurate pupil-iris border is important as the iris region just around the pupil contains a lot of information. Irregular shape leads to difficult iris segmentation.

- *Sharpness: Def.* Absence of defocus blur.

When the object of interest is outside the depth of field of the camera, the acquired image suffers from blur. This artifact can be solved by a better optical design and user guidance.

- *Gaze angle: Def.* The optical axes of the subject and the camera are not aligned.

Off-angle occurs when the user does not look straight to the camera or when his head is rotated or inclined. It leads to iris deformation thereby complicating the recognition.

- *Interlace: Def.* Artifact between odd and even lines.

This type of artifact reduces twice the vertical resolution of the images. (Note that modern iris capture devices use progressive scan instead of interlacing.)

Other quality components such as motion blur and signal to noise ratio have been proposed in IQCE, however their effects on the performance were non-conclusive.

Overall, nine iris recognition vendors participated to IQCE by submitting their own quality measurement algorithms (QMAs) for those quality components. The effectiveness of these QMAs in predicting iris recognition performance was examined. The investigation of the results of the report leads to the following conclusions. They showed that the usable iris area (UIA) has the highest effect on recognition performance followed by iris-pupil contrast, pupil shape, iris-sclera contrast, gaze angle and finally sharpness. In particular, UIA affects significantly the genuine and impostor distributions. The effect on the impostor distribution is smaller than on the genuine distribution but still significant. Therefore the shift in both impostor and genuine distributions denotes that FNMR and FMR are affected by high occlusions. The same behavior is observed for eye contrasts. However, the experimental results show that the UIA is by far the most influential factor on iris recognition. Sharpness has a large effect on the FNMR and on genuine and imposter scores. But, a difference between the qualities of the pairwise images leads to lower FNMR than UIA and eye contrasts.

Another result presented in the report is the improvement of the FNMR after rejecting 3% of the comparisons on ICE2006 database. The value of the decision threshold (explained in Section 2.1) is set to give an overall FNMR of 0.1. It corresponds to the baseline (no rejection). The highest improvement is achieved when the rejection is based on the UIA quality metric. In that case the FNMR is equals to 0.09011, followed by the iris-pupil contrast metric that enables to achieve a FNMR of 0.09085. Other quality metrics such as iris-sclera contrast and sharpness respectively allow decreasing the FNMR to 0.0940 and 0.0980.

Finally, the participants were asked to propose a unique quality namely scalar quality metric for measuring the overall quality of the image. This metric can combine all the quality components that have been cited above or only some of them. When discarding 3% of the comparison on ICE2006 database, the FNMR is reduced from 0.1 to 0.0892. Higher improvement is thus observed by using this

scalar quality component than exclusively the UIA. From these experimental results, we can conclude that the combination of multiple quality components is more pertinent in order to quantify the quality of a given iris image than the use of one quality metric.

The quality assessment algorithms submitted to IQCE were designed as "black-boxes". No information on their estimations as given. In [138], Alonso-Fernandez and Bigun proposed quality metric solutions to estimate mostly quality factors that have been addressed in IREX-IQCE. They also analyzed their impact on the performance of iris segmentation and recognition. The results show that the recognition and the iris segmentation are not necessarily affected by the same quality components.

It is interesting to note that the quality metric can be measured on the entire image or only on the iris region after the localization of the boundaries (segmented image) as done in the previous literature review. However in other works (but more sparse), the quality of the iris image has been defined in a more local way. Indeed, in a given iris image, some regions can contain local artifacts and other parts can present high quality texture. Consequently, some researchers have concentrated their effort on proposing more local quality metrics to quantify the quality of the different regions in an iris image.

To our knowledge, Chen et al. proposed in [139] the first work in which a local approach was used to evaluate the quality of an iris image. They measured the energy of concentric iris bands obtained from 2D wavelets. These local qualities are then weighted regarding the bands location (high weights are assigned to inner band as they provide more texture and are often less occluded by artifacts) in order to obtain one quality index. The experimental results show that this overall quality is reliable to predict the performance of an iris recognition system.

Further local metrics have been proposed by assigning to each pixel of the segmented image a quality measure. Krichen et al. proposed in [77] a probabilistic local quality measure relying on a Gaussian Mixture Model (GMM) that can quantify levels of defocus blur or occlusion. An extension of this model was developed by Cremer et al. in [140]. The new approach is able to distinguish highly textured regions from poorly textured ones. In [141], Li and Savvides exploited two GMMs to model iris and occlusion distributions separately in order to detect locally occlusions in iris images. The approach presents several differences regarding Krichen's work. In fact, in [77], the model is trained on good quality texture so as the GMM gives a continuous value which can be used to characterize not only occlusions but many other artifacts that can occur in iris images. However in [141] the two

GMMs are trained respectively on good and low quality images in order to achieve a binary classification at the pixel-level into two classes: iris or occlusion.

Moreover, in [141] different experiments are performed to choose the input features for optimizing the resulting classifiers. The best feature set is the combination of image intensity and the response of Gabor filters. All works [77] [140] [141] show that a relevant choice of the input features is an essential task in the design of a GMM to ensure the efficiency of the related system.

4.1.2. Synthesis and conclusion

From the above literature review, we infer that to design an effective quality assessment algorithm, some questions should be concerned with:

1. What are the quality components that should be taken into consideration for iris recognition? And which approach has to be followed to compute them?
2. How to use QMA to improve the performance of the iris recognition?
3. How to efficiently combine several quality measures?

In this sub-section, we will answer these questions.

(1): What are the quality components that should be taken into consideration for iris recognition? And which approach has to be followed to compute them?

Image quality assessment for biometric purpose can be divided into two categories: image-specific qualities (generic, used for many image based applications such as sharpness, contrast, compression artifact) and domain-specific qualities (related to the modality). These quality metrics differ from a biometric modality to another. For example, face geometry, pose eye detect-ability, expression and illumination angles are standard quality components for face recognition (determined by the ISO/IEC 19794-5 [142]). Moreover, as explained in Section 2.2, the visual human quality of a biometric sample (visual inspection) may differ from its quality for matching performance. In particular, for iris recognition purpose, a human can judge a well focused image, without problem of illumination of good quality. However, if the spotlights of the LEDs occur exactly at the pupillary boundaries, the iris segmentation will probably fail. Therefore, QMA should be designed regarding the ultimate goal which is the matching performance and not according to human's statements about sample's quality.

Various iris quality factors have been investigated as summarized in Table 4-1. Different protocols of evaluation and different use of quality assessment algorithms have been proposed, making thus the identification of the most influential quality component on the recognition impossible. However the IREX II - IQCE report has answered this question. The experimental results pointed out that the quality component with the highest impact on recognition performance is the UIA, then iris-pupil contrast, pupil shape, iris-sclera contrast, gaze angle and sharpness. For further improvement in the performance, several quality components should be combined in order to take into consideration various artifacts.

The quality components can be measured on the entire image, or more locally, on the segmented iris image. In the literature, most of the quality metrics are calculated from the segmented image. Moreover, it is shown in [138] that local estimations are better than global ones for evaluating quality metrics but at an additional cost of computation as local measures requires prior segmentation of the iris.

From these observations, we conclude that a QMA has to combine essentially three criteria to be considered as a relevant quality metric:

- *The global quality of the entire image:* without blur and enough iris resolution;
- *The intrinsic iris quality:* well textured in NIR and enough non-occluded iris pixels;
- *Segmentation quality:* Errors in iris localization lead to wrongly normalized iris images. In that case, two normalized iris images resulting from the same eye may present a high discrepancy and consequently are prone to failure in the recognition step. Low eye contrasts and occlusions at the pupillary and limbic boundaries contribute to severe segmentation errors. As these errors affect significantly the overall performance of the system, it is crucial to assess the segmentation quality of the iris images.

(2): How to use QMA to improve the performance of the iris recognition?

Quality assessment may be used in many applications for:

- Predicting matching performance;
- Giving feedback on the quality during the enrollment;
- Providing a weighted scheme for multimodal biometric systems;
- Selecting the best images in a sequence;

- Providing a weighted scheme for fusing a sequence.

As shown before, many quality factors that affect the performance have been identified, with different degrees of influence. Therefore, considering a set of quality metrics for quantifying the level of quality is better than using one single factor. However, this set of qualities, usually expressed as a vector, is not immediately exploitable in many applications as cited previously. Most usage of QMA requires a single quality value which indicates the match-ability of the image (if the iris will be correctly recognized). Therefore, a step of qualities' combination is often required. From this summary quality value, the performance of an overall recognition system can be improved by for example discarding images of low quality for further processing, or quantifying the quality of the images by a continuous value in order to perform a weighted scheme in multimodal systems or even by fusing a sequence by giving less importance to low quality images in the fused image.

(3): How to efficiently combine several quality measures?

In the literature, different ways of using multiple quality components have been proposed. For example in [126] and [137], the decision of discarding low quality images for further processing follows a flowchart scheme. The image has to fulfill all the investigated quality criteria. Each quality measure is compared to a threshold which corresponds to the minimal required quality. In [125] and [124], SVMs are used to classify the images into clear or noisy. The output of these approaches is a binary decision which consists in rejecting or keeping the images regarding one or multiple fixed thresholds. They are set arbitrarily with some a priori on the used database.

In other works, a unique quality measure of the image is obtained by fusing all the individual qualities. The fusing method can be a simple multiplication like in [127], a sum [136] or a more sophisticated method by using the theory of Dempster–Shafer [135]. However, the combination of the quality metrics has to be performed carefully, without losing information. There is not universal fusion scheme to do so and in general some a priori is inserted in the fusion protocol. Moreover, whatever the followed method, the fusion process previously requires a normalization step on the quality values, which is not a trivial task either.

In this doctoral work, we propose a different approach to compute the quality of an iris image which is able to deal with most of the disadvantages mentioned before. The quality measure deals with several quality factors that have been identified in IREX II - IQCE to have a negative impact on the recognition. The method does not require individual estimations of the iris properties and hence no

scheme of combination is needed. Our quality measure is based on local quality estimations and gives an indication on the quality of the segmentation. The approach is explained in detail in the next section.

4.2. Definition of the proposed method for quality assessment

4.2.1. Choice of the model

As mentioned before, the aim of the thesis is to improve the iris recognition accuracy in non ideal situations. One way to try to circumvent this bad situation is to fuse iris images of the same eye in the recorded video sequence. We concentrated our effort in proposing a fusion scheme at the pixel-level. As the degradation of the performance is related to the quality of the images, we improved the approach by integrating QMA in the fusion scheme. We decided to perform QMA on the normalized iris image for two reasons (i) to avoid the alignment problem in the fusion scheme (thanks to the normalization) and (ii) to follow the recommendation of most works in the literature: QMAs are more precise when they are calculated on the segmented image [138].

Moreover, to achieve more precise measurements, we decided to estimate the quality on several local regions of the normalized image. Our intuition is that the quality of the iris image is not similar in different parts of the image. Therefore we would like to assess the amount of quality texture in each sub-region of the normalized iris image. Our objective's statement can be modeled by a classification problem. In fact, we wish to classify different regions of the normalized image according to their corresponding quality. For performing this, we have chosen a model based on supervised classification. Such approaches require labeled samples in order to train the model. There are two categories of learning algorithms for performing such classification: discriminative and generative.

Discriminative learning algorithms try to learn directly the conditional distribution of the class y given the observation x (posteriori probability $p(y/x)$). The learning phase consists in learning the borders between all the classes. Such approach requires labeled samples for each class. Linear regression, SVM and neural networks are examples of such methods. In our context, if we use such type of algorithm to classify iris regions according to their quality, we would need labeled iris regions containing all possible type of artifacts (eyelash and eyelid occlusions, specular reflection, blur, segmentation errors...) and also high quality regions (well-textured). In contrast, generative learning algorithms try to model $p(x/y)$ (and $p(y)$) instead of $p(y/x)$. This approach allows learning each

class individually by using only labeled samples of this class. Gaussian Mixture Model, Naive Bayes and Hidden Markov models belong to this type of models.

As our goal is not to classify iris region according to the nature of the artifacts but only to identify highly textured iris regions, we have chosen a generative model. Indeed, our ultimate aim is to give more importance to such high quality regions in the fusion process and less to the other noisy regions, in order to reconstruct a fused image of better quality. Details on the proposed fusion schemes are provided in the next chapter. By using a learning generative algorithm, we only need to label high textured iris regions to model the probability distribution of one single class, which corresponds to high quality regions. By this way, we avoid explicitly defining all the other possible classes. Indeed, these classes correspond to all the possible types of artifacts that can occur in the iris regions. They are various and diverse as explained in Section 4.1.1. Therefore, learning the separations between all the classes would be a complex task. Moreover by using such algorithm, we define only one single quality measure instead of computing individually each quality factors and then combining them by fusion rule as done in the literature. Consequently, the task of measuring iris image quality becomes simpler.

We have chosen a Gaussian Mixture Model (GMM) for characterizing iris textures of high quality. The use of this model for performing this task is motivated by the capability of Gaussian mixtures to model the probability distribution associated to a class of sub-images as previously shown in [77].

4.2.2. Description of the model

To our knowledge, the first GMM was introduced by Reynolds et al. [143] for speech recognition tasks as a simplified model of classical Hidden Markov Models [144]: GMM provides a probabilistic model without imposing Markovian constraints between the classes.

A Gaussian mixture density of a given class λ consists in a weighted sum of M Gaussian component densities. It can be defined by the following equation:

$$p(x / \lambda) = \sum_{m=1}^{M} w_m \cdot g_m(x) \qquad (4.1)$$

where x is a D-dimensional observation vector, $g_m(x), m = 1, \dots, M$ are the component densities and $w_m, m = 1, \dots, M$ are the mixture weights.

Each component density is a *D*-variate Gaussian function of the form:

$$g_m(x) = \frac{1}{2\pi^{D/2}|\Sigma_m|^{1/2}} \exp\left\{-\frac{1}{2}(x-\mu_m)^T \Sigma_m^{-1}(x-\mu_m)\right\} \qquad (4.2)$$

with mean vector μ_m and covariance matrix Σ_m. The mixture weights satisfy the constraint that $\sum_{m=1}^{M} w_m = 1$.

The model is entirely parameterized by the mean vectors, covariance matrices and mixture weights from all component densities. These parameters are collectively defined by:

$$\lambda = \{w_m, \mu_m, \Sigma_m\} \quad m = 1,...,M \qquad (4.3)$$

The learning phase of the GMM aims at determining these M sets of elements from the training dataset. This is achieved by an iterative process in three steps: initialization of the model λ_0, successive re-estimation of λ_{n+1} from λ_n model and verification of the halt criterion at each n iteration. These steps are explained in the next sub-section.

4.2.3. Implementation of the model

4.2.3.1. Model's input vector for characterizing good iris texture

The GMM is trained on sub-images of high quality as done in [77] and [140]. These sub-images are extracted from the normalized iris images. They contain only high quality textures free from any artifact such as eyelids, eyelashes, shadow, specular spot, etc. For each pixel i of the extracted sub-images, an input vector x_i is associated. This vector is called the observation vector. In the work of Cremer et al. [140] x_i is composed of four local observations, measured in a $5x5$ neighborhood of a given pixel i. The vector contains the intensity of the pixel, the local mean, the local variance and the local contrast. The contrast is defined as the difference between the maximum and minimum of the intensities in the fixed neighborhood.

All these statistical observations correspond to first order descriptors of textures. To improve the model, we enriched the input vector by adding a second order texture measure because of its benefits in characterizing texture patterns. More precisely, it considers the spatial relationship of the pixels. A standard tool for performing this is the Gray Level Co-occurrence Matrix (GLCM) proposed by Haralick in the 1970s [145]. Due to its potential and effectiveness, GLCM is still popular until now

in many fields. In the area of iris recognition, many studies [146] [147] [148] and [149] have aimed at extracting iris features by using these matrices instead of the traditional iris features extracted from 2D Gabor filters as proposed by Daugman. The results of these works show the successful capacity of GLCM for characterizing iris texture. Therefore, we expect a better representation of the iris texture by using this second order descriptor. In particular, we would like to generate a GMM model which is more discriminative against the different level of the texture quality.

GLCM is a square matrix of size VxV, where V is the number of gray levels in the image I. Each element of the matrix represents the joint-probability of a couple of pixels intensities (v_x, v_y) in fixed relative positions (x, y) and $(x + dx, y + dy)$. dx and dy are fixed at various scales d and orientations α. This can be expressed as:

$$GLCM\ (d, \alpha) = \begin{pmatrix} p(1,1) & \cdots & p(1,V) \\ \vdots & \ddots & \vdots \\ p(V,1) & \cdots & p(V,V) \end{pmatrix} \quad (4.4)$$

Each element of the matrix $p(v_x, v_y)$ represents the probability that a pixel with value v_x at coordinate (x, y) is adjacent to a pixel of value v_y at $(x + dx, y + dy)$. Several statistical features have been derived from GLCMs for characterizing the co-occurrence matrix contents such as energy, correlation, contrast, entropy... [150].

For each pixel of image I, one or more GLCM can be calculated on a neighbourhood, defined by a window. Then, several statistical features can be applied on the resulting matrix for describing image properties. These results are associated to the pixel, localized in the center of the window, as depicted in Figure 4-1. Then the window is shifted by one pixel and the procedure is repeated for the entire image.

Due to the possible values of the parameters d and α, a large set of GLCMs is often computed. There are eight possible values for the orientation: 0°, 45°, 90°, 135°, 180°, 225°, 270°, and 315°. The arrows of Figure 4-2 represent the direction from the reference pixel to its neighbor pixel, for each orientation. These eight matrices are thus sensitive to the direction. Therefore, they are usually averaged to obtain a unique rotation invariant matrix as done in [147] and [149]. In [146], the GLCMs are not applied on the images but on pre-processed ones in order to make them invariant to rotation. In practice d is limited to a narrow range of small values for computation time reasons.

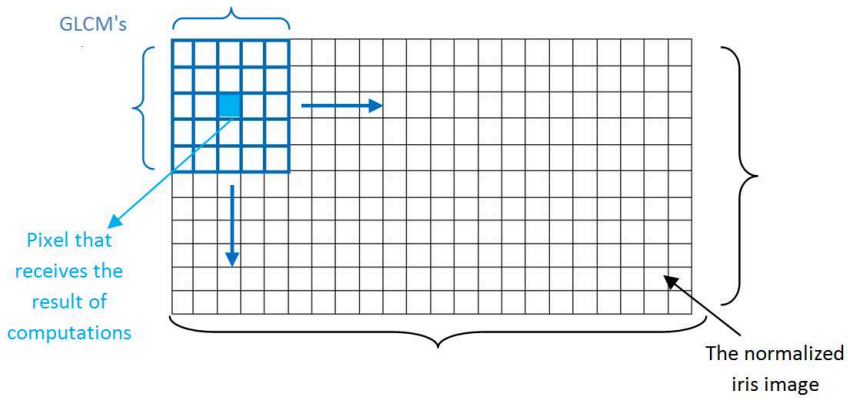

Figure 4-1: How to compute GLCM features from the normalize iris image.

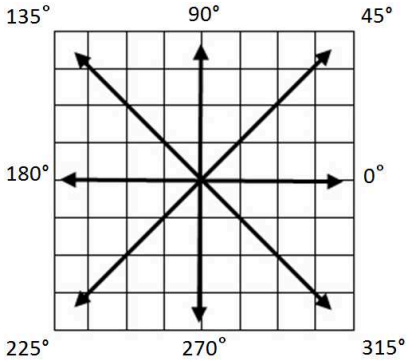

Figure 4-2: GLCM's directions.

In our context, the GLCMs are computed on the iris image with a range of at least 256 gray levels for iris recognition (as recommended in [35]) and thus $V = 256$. The dimension of each matrix is thereby $256x256$. This wide size leads to a large number of computations for an iris image of size $64x512$. In addition, a large size of the GLCM induce sparse matrix [151]. In practice, most of the matrix entries are zeros. Applying feature statistical measurements on them is thus an inefficient procedure. Therefore, it is recommended to reduce this range in order to decrease the complexity and also to be less sensitive to noise. In [150] [151] and [152], the number of gray level is reduced by using simple gray-level quantization techniques. However, the matrices are still sensitive to rotations.

To avoid all these disadvantages, we do not calculate the GLCM on the iris image but on the Local Binary Pattern (LBP) iris image. LBP was introduced in [153] and has been widely used in texture classification because of its efficiency and simplicity. We decided to apply the uniform invariant rotation Local Binary Pattern (uirLBP), detailed in [154] to the normalized iris image. It quantifies the frequency of the individual rotation invariant patterns corresponding to a specific micro-

feature in the image. By considering a neighborhood of size 8 and a radius of 1, the number of gray levels in the iris image is reduced to 10 ($V = 10$). This operation has two benefits for our application. Firstly, it considerably reduces the number of gray level in the image, and thus the size of the GLCM. Secondly, due to its rotation invariant characteristic uirLBP decreases the number of possible orientations. For a given normalized iris image, Figure 4-3 shows energy features (defined in Table 4-2) extracted from the GLCMs in all the directions, with a window of dimension $5x5$ pixels. We note that there is a high similarity between the GLCMs of the first column. The same behavior is observed for the second column. Therefore, the number of possible orientations can be reduced to 2. $GLCM(1, 0°)$ and $GLCM(1, 45°)$ are arbitrary selected for further investigation. We note that the same observation is obtained by using other feature descriptors. To simplify, we only give the results obtained by the energy descriptor.

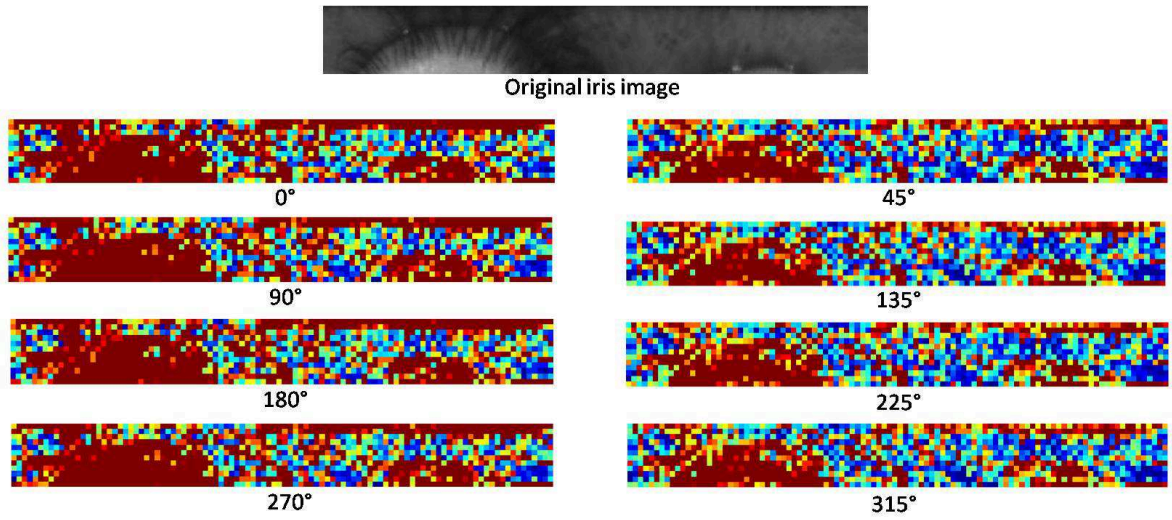

Figure 4-3: Energy features extracted from GLCMs at the eight possible orientations of for a given normalized iris image.

As mentioned before, there are several statistical features that can be applied on the GLCM. According to [150], three fundamental properties can be extracted from the matrices. First, the main diagonal points out the degree of smoothness of the texture. This property can be obtained thanks to several features such as the contrast, the dissimilarity and the inverse difference. Second, the uniformity of the entries of the GLCM can be also studied by using features e.g. energy, the entropy and the maximum probability. Finally, the description of the correlation between the pairwise gray-levels in the image is given by correlation features. For our analysis, we selected one feature per each category: energy, contrast and correlation features. They are defined in Table 4-2.

Table 4-2: GLCM's statistic features. v is number of gray-levels in the image. (μ_x, μ_y) and (σ_x, σ_y) are respectively means and standards deviations of row x and column y.

Features	Formula	Properties
Energy	$\sum_{v_x,v_y=1}^{V} p(v_x,v_y)^2$	*Homogeneity statistics*
Contrast	$\sum_{v_x,v_y=1}^{V} p(v_x,v_y)(v_x-v_y)^2$	*Smoothness statistic*
Correlation	$\sum_{v_x,v_y=1}^{V} \frac{(v_x-\mu_x)(v_y-\mu_y)p(v_x,v_y)}{\sigma_x\sigma_y}$	*Correlation statistic*

The feature extraction procedure is as follows. We first compute the corresponding uirLBP image. Then, we calculated the $GLCM(1,0°)$ and $GLCM(1,45°)$, with a window of dimension $5x5$ pixel. Finally the energy, the contrast and the correlation of the two matrices are computed in order to represent the texture properties. On a given normalized iris image of good quality, the corresponding results are given in Figure 4-4 . We used cold colors (e.g. blue) for high values, warm colors (e.g. red) for small values.

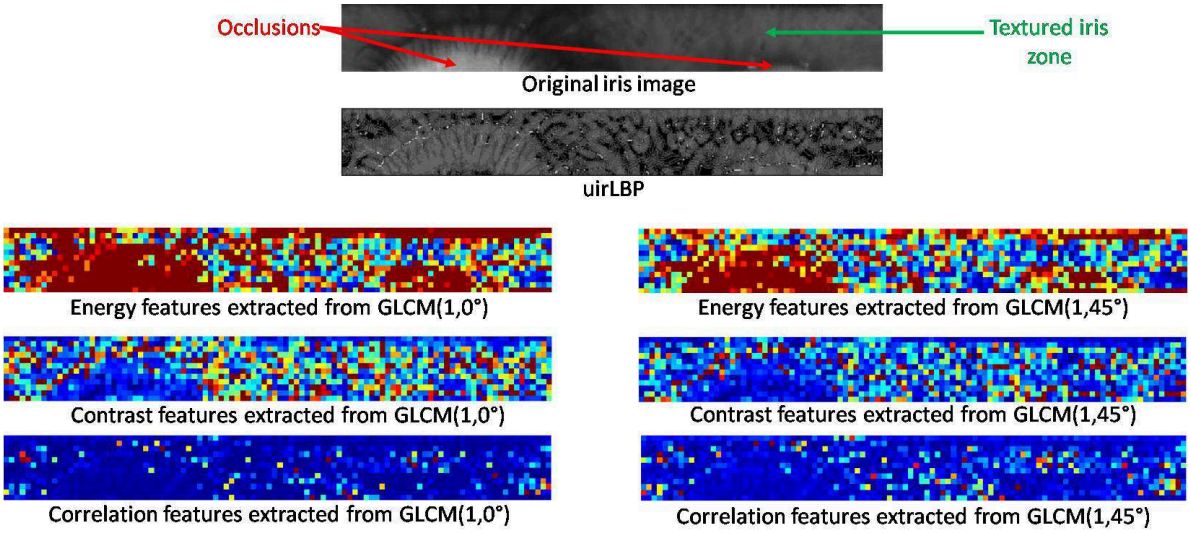

Figure 4-4: Energy, contrast and correlation features extracted from GLCMs. Note that for the values of the features we used cold color for high value, warm color for small value.

As our aim is to characterize iris texture, it is crucial that the used statistical feature is able to distinguish between iris and non iris pixels (artifacts). As displayed in Figure 4-4, the energy is the best

discriminative feature for performing this task. It highly distinguishes well-textured zones (cold colors) from less textured ones (warm colors) which correspond to occlusions such as eyelids, shadows etc. Energy feature is a measure of the image homogeneity since it measures textural uniformity. In other words, it detects pairwise gray repetitions in the image. As the iris image is highly textured, the GLCM will have a large number of small entries and the energy will be small. However, GLCMs that are extracted from less textured zones (homogenous regions) would have fewer entries of large value as few pairs represent the texture. This leads to high energy values. This statistical feature is thus selected.

Due to the similarity of $GLCM(1, 0°)$ and $GLCM(1, 45°)$ and to reduce the complexity, we arbitrarily decide to use only the second one, on which the energy is extracted. This value is added to the input vector x_i of the GMM as the fifth observation.

So, the final dimension of our observation vector is $D = 5$. It contains the intensity of pixel i, the mean, the variance, the contrast and the GLCM's energy, computed on its neighborhood of size $5x5$ pixels.

4.2.3.2. Estimation of the model's parameters

The GMM is learned on small images selected from QFIRE datasets at different distances [38] [39]. We trained the model with 6 Gaussians on 122 sub-images free from occlusions, well focused and highly textured as in [140]. These sub-images are manually extracted from 47 normalized iris images of size $64x512$, taken from different collections of data, namely QFIRE05, QFIRE07 and QFIRE11 (see Section 2.3.3). These normalized iris images constitute the training set and are not subsequently used. The sub-images have different dimensions (an average of 4171 pixels per sub-image).

Several tests have been conducted in order to set these values. By analyzing their influence on the GMM's training, the final values have been determined empirically. They correspond to a trade-off between the accuracy of the model and the computational cost.

Let K and T_k be respectively the number of sub-images of the training set and the number of pixels in the k^{th} sub-image. M is the number of Gaussians. The estimation of the GMM's parameters, $\lambda = \{w_m, \mu_m, \Sigma_m\}, m = 1, \dots, M,$ follows these steps:

- Initialization

The GMM's parameters are initialized by k-mean algorithm [155]. First the means of the Gaussian components are randomly initialized. Then, each observation vector O_t^k ,where $k =$

$1, \ldots, K,\ \ t = 1, \ldots, T_k$, is assigned to a particular Gaussian for which the Euclidean distance between its mean and this observation vector O_t^k is minimal. Then, the mean vectors μ_m and the covariance matrices Σ_m are computed for each of the M equal groups. For each Gaussian m, the associated weight w_m is obtained by computing the portion of the observation vectors in the group.

- Re-estimation of the GMM

The GMM's parameters are iteratively re-estimated by using the Expectation Maximization (EM) algorithm [156]. EM is used to estimate GMM parameters λ that maximize the log-likelihood $\overline{LL}_{train}$ given the training data defined as:

$$\overline{LL}_{train} = \frac{1}{K}\sum_{k=1}^{K}\frac{1}{T_k}\sum_{t=1}^{T_k}\log\left(P\left(O_t^k/\lambda\right)\right) \qquad (4.5)$$

The principle of the EM algorithm consists in beginning with an initial model λ, in order to estimate a new model $\bar{\lambda}$, such that $P\left(O/\bar{\lambda}\right) \geq P\left(O/\lambda\right)$, where O is the set of the K observation vectors. After that, the new model becomes the initial model for the next iteration. The process is repeated and stopped when the following halt criteria is verified:

$$\left|\frac{\exp\left(\overline{LL}_{train}^{before}\right) - \exp\left(\overline{LL}_{train}^{after}\right)}{\exp\left(\overline{LL}_{train}^{before}\right)}\right| < \varepsilon \qquad (4.6)$$

where $\epsilon < 10^{-2}$. The value is set empirically.

4.2.4. Computation of our quality measurement

In this part, we explain how the GMM is exploited to define a local quality measure. As described in the previous sub-section, GMM has been trained on sub-images that are well textured and free from artifacts for characterizing textures of high quality. In the test phase, a likelihood can be assigned by the GMM to each observation vector associated to a given pixel in the image. This likelihood takes its value between 0 and 1. Highest values correspond to the closest tested observation vectors to those used for training the model.

The GMM can be used for categorical or probabilistic classification. In the first case, a threshold should be set on the likelihood to classify the pixels into two classes: high quality or non-high quality pixel. This implies the binarization of the real-value of the likelihood, leading to a loss of

information. Consequently, we have chosen to rather exploit the model for probabilistic classification. In the test, for each sub-image a likelihood that it is of high quality will be assigned. This way, the GMM will characterize good quality iris texture and will therefore give a low probability on the noisy regions, which result from blur or artifacts. The interest of this approach is that there is no need to identify in advance the type of noise present in the images.

In practice, the model is applied to local observations grouped in the input vector x_i for each pixel i of in the sub-image. The local quality measure (LQ) associated to a sub-image ω is given by the formula:

$$LQ(\omega) = \exp\left(-\frac{1}{d} \sum_{i=1}^{d} \left| \log(p(x_i / \lambda)) - \overline{LL}_{train} \right| \right) \qquad (4.7)$$

where d is the size of the sub-image ω, x_i is the observation vector of the GMM, $p(x_i/\lambda)$ is the likelihood given by the GMM λ to the input vector x_i, and $\overline{LL}_{train}$ is the mean log-likelihood on the training set as defined in formula 4.5. We recall that x_i is composed of five elements: the intensity of pixel i, the mean, the variance, the contrast and the GLCM's energy, computed on its neighborhood of size 5x5 pixels.

To normalize the log-likelihood with respect to the training set, we take the absolute value of the difference between the log-likelihood given by the GMM to the test vector *x* and the log-likelihood of the training set. This result can be seen as a distance: the lower the value is, the closest the test vector *x* is to the training dataset. The mean of these distances are computed for all the *d* pixels belonging to the sub-image ω. A negative exponential is then used to obtain a value between 0 and 1. The closer the LQ value is to 1, the higher is the quality of the sub-image ω, namely being free from occlusion and highly textured.

Note that even if this quality measure was trained on specific collections of databases, it can be used for characterizing any iris images, with the same illumination, coming from other sources. In fact, the model is only sensitive to the global variation of the pixels' intensities. To overcome this eventual issue, a simple preprocessing can be done on the sub-images on the training set as well as the test images on which the GMM will be applied. For example in [140], all the images are pre-processed such that their mean gray-level would be close to a constant value.

Each normalized iris image of dimension $64x512$ is divided in sub-images of size $4x8$ without overlap as displayed in Figure 4-5. On each sub-region ω, the local quality measure is computed as follows:

For each pixel i of the sub-image ω:

On its neighborhood of size $5x5$, we :

- ✓ Compute:
  - m: the mean of the pixels intensities,
  - v: the variance of the pixels intensities,
  - c: the contrast: Difference between the maximum and minimum of the intensities,
  - e: the energy of the GLCM applied to the uirLBP iris image
- ✓ Assign its corresponding input vector x_i which contains the gray level of pixel i and the values: m, v, c and e
- ✓ Compute $p(x_i/\lambda)$: the likelihood given by the GMM λ to the input vector x_i

Finally, the local quality of the sub-image ω given the GMM model is computed as defined in Formula 4.7.

At the end, we obtain a matrix of local qualities of 1024 values.

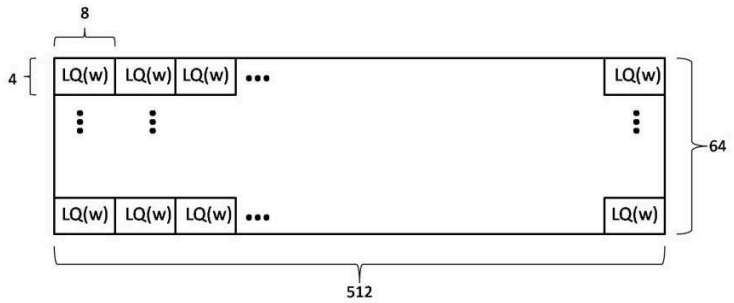

Figure 4-5: Computation of the local qualities on sub-images of a normalized iris image.

Examples of matrices of local qualities:

As mentioned in Section 4.2.3.1, we enriched the proposed model of Cremer et al. [140] by adding a descriptor of texture of second order to the observation vector. This element takes into account the spatial relationship between the pixels. Figure 4-6 and Figure 4-7 show the difference between the GMM used in [140] (namely GMM4obs) and the new one (namely GMM5obs) on two examples of iris images: one of good quality and the other of low quality. Dark colors (resp. light) correspond to pixels of low (resp. high) quality.

We notice that the GMM5obs detects occlusion zones better than the GMM4obs, especially the eyelashes of the iris image in Figure 4-6. Moreover, iris blurred zones of the iris image in Figure 4-7 are not distinguished by the GMM4obs contrary to what occurs with GMM5obs which is more sensitive to the blur.

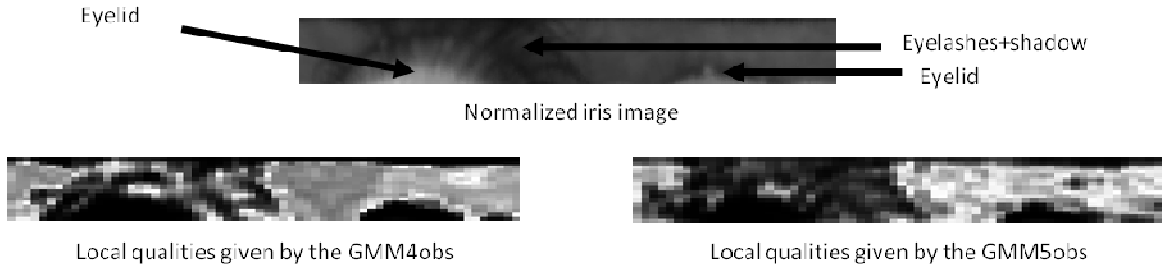

Figure 4-6: Normalized iris image of good quality with their corresponding local qualities given by the 2 GMMs: GMM4obs and GMM5obs.

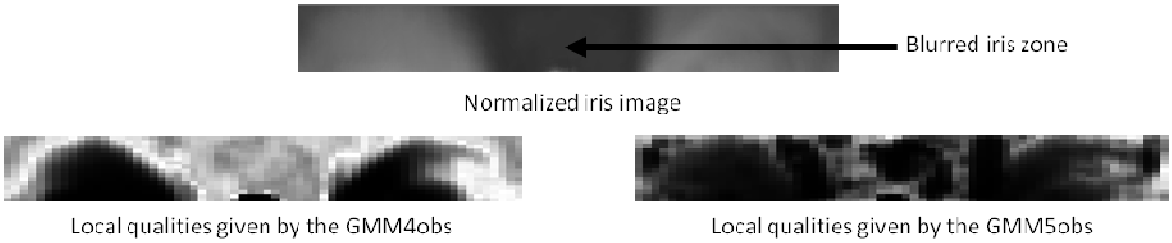

Figure 4-7: Normalized iris image of poor quality with their corresponding local qualities given by the 2 GMMs: GMM4obs and GMM5obs.

Global quality measure:

The local measure presented in formula 4.7 can also be employed to define a global measure of the quality of the entire image by averaging the probabilities given by the GMM of each sub-image as follows:

$$GQ = \frac{1}{N}\sum_{n} LQ(\omega_n) \qquad (4.8)$$

where N is the number of sub-images and $LQ(\omega_n)$ is the local quality given by the GMM on the n^{th} sub-image.

4.3. Evaluation of our quality metric

The objective of this section is to show the effectiveness of the proposed QMA. To this end, we have exploited our local quality measure to compute a global quality such as defined in Formula 4.8. We wish to demonstrate that this global quality is well correlated to the performance of the recognition. As explained in Section 2.2, a pertinent QMA should be linked to the recognition rate.

First, we will show the improvement brought by the enriched model. Therefore, we will compare the two models GMM4obs and GMM5obs for classifying iris images according to their quality. We believe that the added fifth element to the observation vector of the GMM is promising to improve the effectiveness of our quality measure.

As explained in the literature, the quality of the iris texture and the usable iris area (area free from occlusions) represent the two quality factors with the greatest impact on the iris recognition [51]. Therefore, we would like to assess how our GMM-based quality measure defined in Section 4.2 is related to those two criteria.

Throughout this section, the reference system OSIRISV4.1 that is described in Section 3.2.1 is used to perform the recognition. The experiments are carried out on 5400 images randomly taken from the QFIRE07 dataset (see Section 2.3.3). We have chosen this distance as a compromise between small (QFIRE05) and long (QFIRE11) distances.

4.3.1. Validation of the improved GMM-based quality: GMM5obs

In this part, we would like to prove that our GMM-based quality obtained by the GMM5obs achieves better characterization of the iris texture than the GMM4obs, developed in [140]. To establish a comparative evaluation between these two QMAs, we used ranked-DETs tool as done in the IREX II - IQCE report [51] of NIST. The more the distance between the DETs is high, the more the QMA is effective.

To compute the performance, we have considered all the images as independent ones and we have followed a 1 to 1 matching scheme. For each QMA, a global quality (GQ) is computed for each normalized iris image as defined in Formula 4.8. The number of genuine and impostor comparisons are respectively 41,650 and 7,315,114.

The pairwise quality of the two images to be compared can be obtained by several manners from the quality of the two images as explained in Section 2.2. However, the difference in the achieved

results is not significant as shown in [34]. In our case, we decided to take the minimum between the qualities of the two images. We selected the minimum as only one of the two images of the couple having a low quality is sufficient to degrade the performance. According to this pairwise quality, we partition the comparison scores into three groups: low, medium, and high. The set of lowest (resp. highest) quality contains a matching score with pairwise qualities in the lowest (resp. highest) 15 percentile. The rest of the matching scores constitutes the medium quality set. For each QMA, we generate three ranked-DETs, one for each set above as shown in Figure 4-8.

We notice that the ranked DETs of Figure 4-8-b are better separated that those of Figure 4-8-a. In fact, the distances between the ranked DETs (connection lines) are higher when the images are classified according to the GQ given by the GMM5obs model. Consequently, we deduce that our QMA based on GMM5obs achieves better performance ranking than the QMA based on GMM4obs. In particular, when we observe the achieved performance of the highest quality sets, we note that lower FNMR and FMR are obtained for higher quality images, based on the GMM5obs than the GMM4obs. Therefore, our intuition which consists in claiming that the GMM5obs model characterizes the high quality texture better than GMM4obs is confirmed.

The remaining experiences are carried out with the best model: GMM5obs.

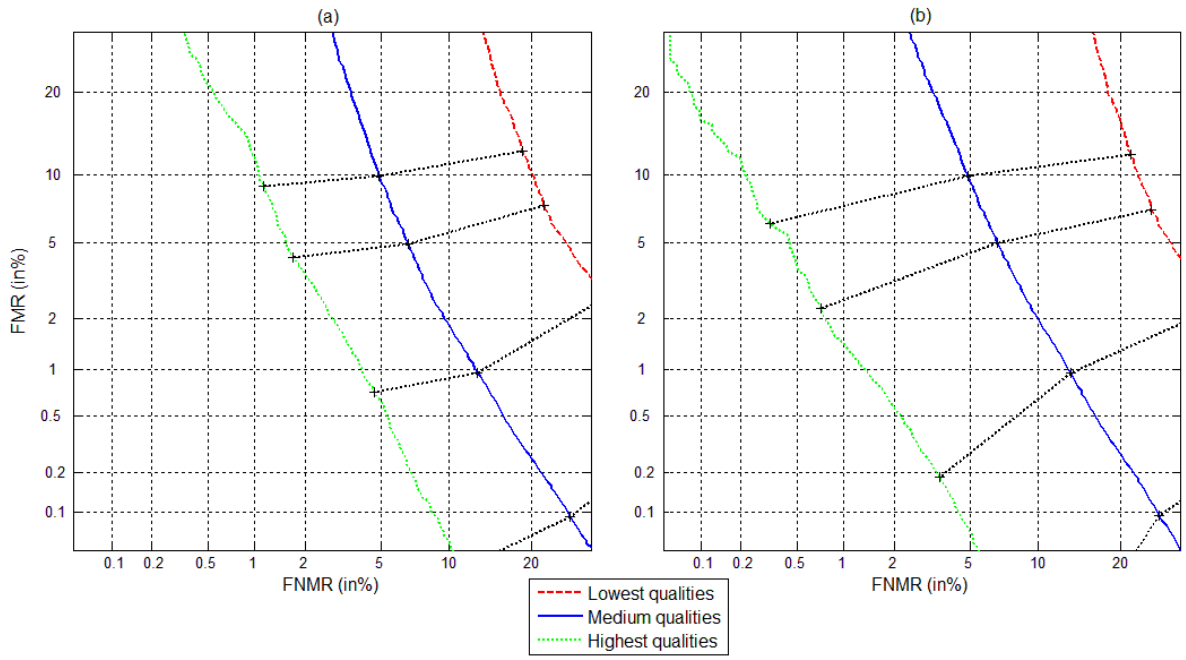

Figure 4-8: Ranked-DETs based on the GQ given by the model: (a) GMM4obs, (b) GMM5obs.

4.3.2. Assessment of the improved GMM-based quality: GMM5obs

4.3.2.1. Relationship between the GMM-based quality and the quality of the texture

In this part, we analyzed how the GMM-based quality is related to the amount of texture present in the normalized iris image. The poor texture can be caused by iris pigmentation characteristics (for instance, heavily pigmented irises are less textured even in NIR) and/or by blur introduced by the out of focus of the camera or the subject moving.

As shown in [157], there is a strong correlation between the quality of the texture and the accuracy of the recognition and as outlined in [51], low sharpness significantly affects the performance of the iris system by increasing both FNMR and FMR. Therefore, we expect to show a strong correlation between the GMM-based quality and the texture quality, and thus the recognition performance.

To better assess the quality of the iris texture, we have to mask all the occlusions of the normalized iris image before computing GQ, as done in [157]. To this end, we used the mask given by OSIRISV4.1. We call GQM (Global Quality of the Masked normalized image) the global quality computed only on regions free from occlusions and we compared it to the approach of [157] based on a classical iris texture-quality measure. Indeed in [157], Gong et al used a $5x5$ convolution matrix method proposed by Kang et al. [158] which is an improved version of the Daugman filter to extract the amount of texture. Convolution matrix methods are based on optical defocus models. This quality measure is called "Quality Assurance of Texture" (QAoT).

We use scatter plots in order to investigate the relationship between GQM and QAoT. To avoid the over-plotting of data points in the large dataset, we grouped the data into 13 equal count bins by abscissa (GQM) and then we plotted the average and the standard deviation for each bin. Figure 4-9 shows the link between the amount of texture QAoT and GQM.

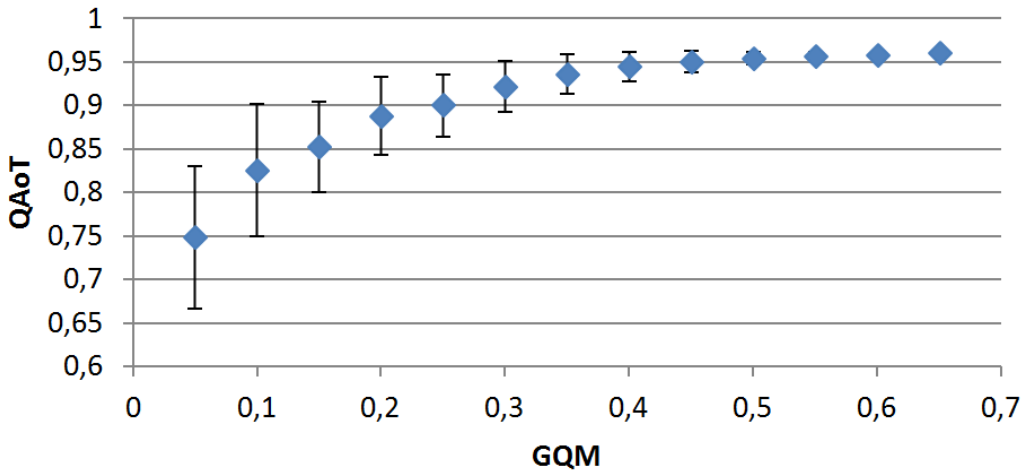

Figure 4-9: Relationship between GQM and QAoT.

As expected, our quality measure increases with the amount of texture. These results show that GQM is able to quantify the quality of iris texture and therefore to discriminate highly textured regions from poorly textured ones.

4.3.2.2. Relationship between the GMM-based quality and the usable iris area

As underlined in [51], among all quality components, the usable iris area has the greatest influence on performance. This quality measures the proportion of iris pixels non-occluded in the normalized image. For each image, we compute the following measures:

- *UIA:* It measures the usable iris area which corresponds to the number of pixels non-occluded according to the mask of OSIRISV4.1.
- *GQ:* It represents the average of the local qualities given by the GMM5obs on the sub-parts of the entire normalized image without any detection of occlusion.
- *GQM:* It is the average of the local qualities given by the GMM5obs only on the sub-parts of the normalized image free from occlusions. The occlusions are detected by the mask of OSIRISV4.1 such as in UIA measure.

To achieve a comparative evaluation between the quality metrics cited above, we calculate the recognition performance according to the quality of the images. Indeed, relevant quality metrics should be strongly linked to the recognition performance: the higher the quality according to this metric, the

higher the performance should be. We use ranked-DETs curves to evaluate the efficiency of these quality measures. To this end, we have followed the same scheme as in Section 4.3.1. We have used 7,315,114 inter-class and 41,650 intra-class comparisons and for each comparison, the minimum the between the qualities of the two images represents the quality of the pairwise. The partition of the comparison scores is also performed in a similar way: we have considered 3 categories of quality: low, medium, and high. The lowest (resp. highest) quality set is composed of comparisons with pairwise quality in the lowest (resp. highest) 15 percentile. The remaining comparisons which represent 70% of the entire matching scores are assigned to the middle quality set. For each quality metric, three ranked-DETs are generated, one for each set above as displayed in Figure 4-10.

We observe that the ranked-DET curves are well separated for all the measures. Consequently, these qualities are effective criteria for predicting the performance. An appropriate behavior is observed: lower FNMR and FMR are observed as the quality increases. As expected, the highest performance is noticed for the images with the fewest occlusions and the lowest performance for the images with a high degree of occlusion.

In addition, we observe that the GQ and the GQM allow the higher separation among the three curves. The difference is higher than one order of magnitude. This fact indicates that GQ and GQM are more pertinent quality measures than UIA for sorting the images according to their quality. In particular at the EER, the improvement between the high and the low ranked-DETs by the GQM is higher than UIA (from 19.64% to 1.13%, vs from 15.57% to 3.21%). Therefore, we conclude that our quality measures are relevant for classifying the image into low, medium, and high quality.

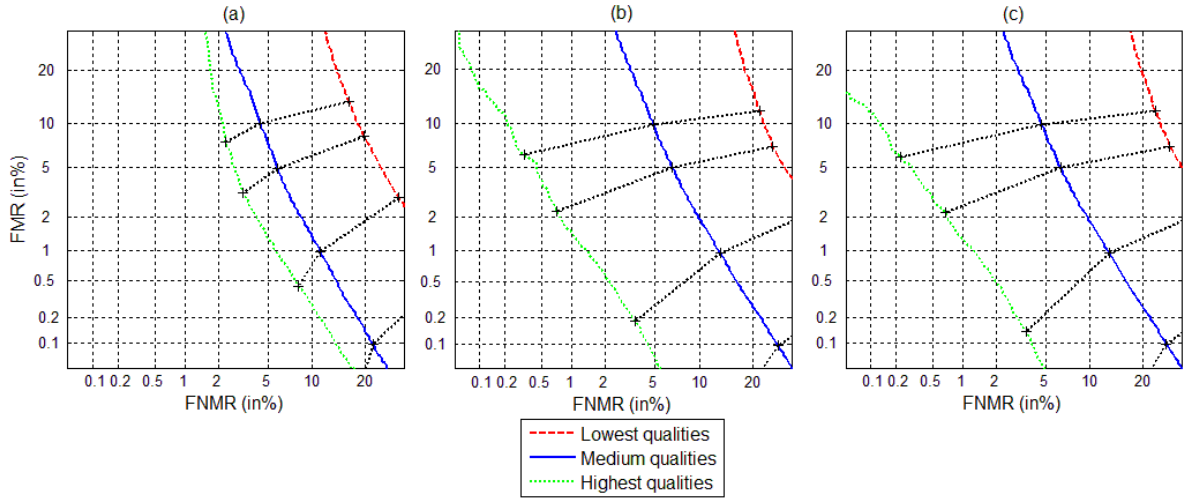

Figure 4-10: Ranked-DETs based on (a) UIA, (b) GQ, and (c) GQM.

One other metric for the comparative evaluation of quality measures is the error versus reject curves. These curves are used to demonstrate how efficiently the rejection of low quality images results in improving the performance as introduced in the IREX II - IQCE report. To this end, we compute the average of the image False Non Match Rate (iFNMR) and the FNMR at FMR equals to 0.001 (FNMR@FMR=0.001) at diverse fractions of comparisons rejected. The iFNMR is calculated at a FMR equals to 0.001 corresponding to a threshold where false match errors actually occur as suggested by Tabassi in [50]. Figure 4-11 shows error versus reject curves for each quality measure.

We notice that all the quality measures are effective. The iFNMR and FNMR@FMR=0.001 improve as more as low-quality pairwises are discarded. The curves decrease quickly with the fraction of comparison rejected but not with the same slope, which allows the metrics to be compared as the higher the slope, the higher the pertinence of the quality metric.

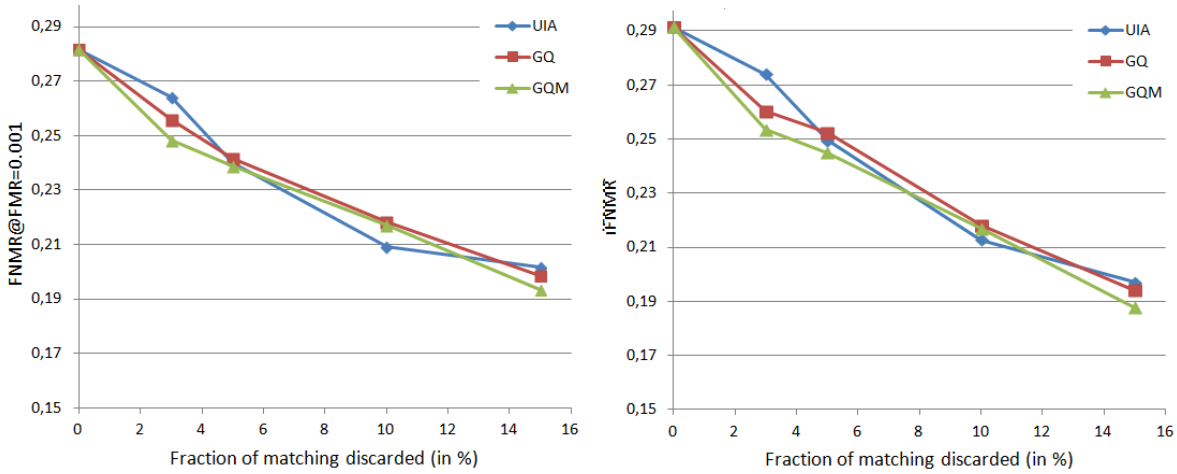

Figure 4-11: Error versus Reject curves based on UIA, GQ and GQM.

We also observe that GQM generally outperforms the two other quality metrics mostly at a 3% rejection threshold. In fact, GQM quality reduces the FNMR@FMR=0.001 by almost 11.85% and the iFNMR by 12.96%. Table 4-3 sums up the improvement of the performances at 3% rejection threshold for all the quality measures. As shown in Table 4-3, GQM outperforms UIA. In fact, UIA calculates only the number of non-occluded pixels without taking in account their quality. However, the GQM gives a weight to each pixel according to the local quality of the region given by the GMM5obs. Therefore, GQM contains more information than UIA. It represents the quality of the usable iris area and not only the percentage of occlusions.

Table 4-3: Improvement of the FNMR@FMR=0.001 and the IFNMR at a 3% rejection of comparisons based on UIA, GQ, AND GQM on QFIRE database.

Metrics	UIA	GQ	GQM
FNMR@FMR=0.001's improvement	*6.27%*	*9.22%*	*11.85%*
iFNMR's improvement	*5.96%*	*10.72%*	*12.96%*

On the other hand, by observing Figure 4-11 and Table 4-3, we can see that GQ is slightly worse than GQM. In fact, GQ is computed by using all the sub-regions of the images. We expected that GQ would be able to give a very small weight to the occluded pixels and therefore that it would play the role of a mask. Nevertheless regarding the error versus reject curves, GQ seems to be less discriminative than the mask of OSIRISV4.1 which is used by UIA and GQM. In fact, the mask allows us not to take into account the occlusion in the quality measure, while GQ considers them even if the associated value is low. For this reason, we decide to use both the mask of OSIRISV4.1 and our quality in the fusion schemes in the next chapter.

In IREX II - IQCE report, the improvements of the FNMR regarding several quality criteria estimated by the best contestant's QMA were also given. For example, on ICE2006 database, a rejection of 3% according to UIA criteria brought an improvement of 9.89%. In the case of the scalar quality component (which includes all the quality factors such as our global quality measure), the FNMR is improved by 10.8%. Due to the fact that the evaluation was done on two different databases (for IREX II - IQCE on ICE2006 and for us on QFIRE07), it is difficult to perform an exact comparison between these improvements and ours (UIA: 6.27% and GQM: 11.85%). However, the two used datasets present some quality similarities as the images of ICE2006 approximately have the same resolution as QFIRE07 (> 200 pixels). They also contain occlusions and blur as in QFIRE07.

4.4. Conclusion

In this chapter, we presented a relevant approach to quantify the quality iris images. The measure is based on a GMM, trained on samples of high quality. We showed the capability of the quality measure in detecting regions of good quality as well as regions with artifacts such as eyelids, eyelashes, shadows, specular spot... Moreover, our quality measure is able to distinguish highly iris texture from lower ones.

The strong point of the approach consists in identifying locally several quality factors that have an impact of the performance, i.e. usable iris area and sharpness as reported in the evaluation of IREX

II - IQCE. Moreover the quality is a unique measure, estimated on the segmented image, without need of identifying a priori the type of the degradation(s). Therefore, no individual estimation of each quality factors is required and no step of qualities combination is hence needed.

We have conducted comparative evaluations between two GMMs, based on different input features. The difference in the results shows that the choice of these input vectors is a crucial task in the design of a GMM to ensure the efficiency of the related system.

Through several experiments, we assessed the correlation between the proposed quality measure and the amount of texture and the usable iris area. The results show a strong link between them. Consequently, the developed QMA can be considered as a relevant tool for estimating iris quality.

In the next chapter, we will present the proposed schemes of fusion for improving iris recognition in degraded sequences, as well as the integration of the quality in the fusion process.

Chapter 5. Fusion approaches for iris recognition in sequences

As explained before, the excellent performance of iris recognition systems are obtained by controlling the quality of the captured images, by both imposing certain constraints on users, such as standing at a close fixed distance from the camera, and using algorithmic measurements of image quality, such as contrast, illumination and textural richness controls. However, in many recent security applications, many of these constraints become impossible to impose especially for scenarios of iris recognition at long distance and/or on the move. The usual NIR sensors are not optimized for such acquisition and therefore the resulting images present a lack of resolution, leading to blur and low contrast between the different boundaries of the iris. All these degradations significantly decrease iris recognition performance.

One way to try to circumvent this bad situation is to use some redundancy arising from the availability of several images of the same eye in the recorded sequence. In the literature, researchers have concentrated their efforts on proposing several approaches based on fusion schemes to exploit the entire sequence rather than using one single image, selected as the best image in term of quality. State-of-the-art on fusion approaches for iris recognition in sequences under less constrained acquisition is related in Section 5.1.

We will see that the literature agrees on the fact that the quality of the iris images that are used in the fusion scheme plays a crucial role in its success. Therefore, we will introduce our quality measure presented in the previous Chapter 4 in the fusion process. Details on the proposed fusion processes and how we have integrated our quality measure in these approaches are given in Section 5.2.

Finally, the proposed fusion processes are benchmarked on several public iris databases. The experimental results are given in Section 5.3. Different acquisition scenarios are investigated: iris recognition on the move, multiple images shot with intra-variability, and recognition at a distance.

5.1. Related works

5.1.1. Signal fusion of iris sequences

The idea of exploiting multiple still images or video sequences has been previously proposed for face recognition. For instance, one challenge of the Face Recognition Grand Challenge [159], organized by NIST, has addressed this issue. It is reported that exploiting multiple still images can significantly improve the accuracy of face recognition. Promptly researchers assumed that employing

same approaches in the field of iris recognition would also lead to enhancement in the recognition performance.

Taking benefit of having at disposal multiple still images in iris databases, researches have started to propose approaches based on the combination of matching scores across multiple comparisons. In [92], Ma et al. proposed to use three templates of a given iris in the enrollment database and took the average of three Hamming distances as the final matching score. Krichen et al. [160] performed a similar approach. The authors used the minimum matching score instead of the average. In [161], Schmid et al. presented two methods for fusing Hamming distance scores: they demonstrated that fusing the scores using log likelihood ratio gave superior performance when compared to average Hamming distance. All these approaches use multiple images available in the gallery dataset (also called reference dataset).

Two main drawbacks stem from using still iris image instead of iris video (or sequence) as input of the recognizer:

- Artifacts such as occlusions, specular spots and blur reduce the amount of high quality texture contained in a still image. However in the case of a sequence video, due to several factors, this quantity of iris texture can vary between the frames, (e.g. eyelash occlusions not constant, absence/presence of spots, image well focused or out of focus...). Therefore, it is possible to reconstruct a better template by using various frames than one single image.
- Illumination variation between two still images to be compared causes degradation in the matching score. However, this difference can be reduced by fusing several frames of a video sequence in order to built one final template, used in the comparison instead of a single still image.

Recent works shifted toward proposing new approaches based on signal-fusion rather than score-fusion frameworks, aiming at improving the performance of iris recognition in less restrictive acquisition. Taken advantage of temporal continuity in videos, a possible direction is to fuse the frames of the videos at the pixel-level, exploiting this way the redundancy of the iris texture at an early stage. The feature extraction and matching steps are then performed on the resulting fused images, reducing drastically the complexity. At this level of study, the question arising is how to perform this fusion stage so that the performance can be improved compared to 1 to 1 matching (baseline) or score-fusion schemes. In [162], Hollingsworth et al. proposed performing a simple averaging of the normalized iris images extracted from the video in order to match NIR iris videos against NIR iris videos from MBGC

database. Ten images with the highest qualities are selected from the video for averaging the signal. The experimental results showed that a registration of the images is not necessarily for this dataset. The signal fusion scheme reduces the FRR@FAR=0.001 from 3.32% to 1.1% (compared to the baseline: no fusion). The proposed method is also compared to score-fusion approaches: it outperforms [92] (Hamming distances' average) and [160] (the minimum of the Hamming distances) methods and achieves comparable performance to [161] (log likelihood method). The authors proposed also a new approach based on a score-fusion, namely Multi-Gallery Multi-Probe (MGMP). It considers independently the N frames in the reference video and the M ones of the test video, and hence computes NxM matching scores. Then, these scores are fused by the min operator in order to get a unique score per video. When compared to signal-fusion methods, the results are slightly better but with a very higher computational cost.

Jillela et al. in [163] explored the fusion in the feature domain using Principal Components Transform (PCT). Their approach uses the availability of multiple images of the same iris to extract discriminatory information. NIR iris videos of MBGC database are used to benchmark the method. Only six images of good quality are manually selected for the assessment stage. The authors performed the following scheme: low-resolution probes images (also called test images) are compared to high-resolution images gallery. The probe images are generated by artificially degrading high-resolution images (down-sampled). The authors claim that the proposed method avoid registration requirement. The approach leads to an EER of 1.48%.

Another way is to use super-resolution (SR) approaches to build a high-resolution template from successive iris images of low-resolution. Indeed, SR techniques are a well-known solution for fusing and exploiting the information arising in a sequence of poor quality. In general, SR approaches can be achieved in the pixel or feature domain. To our knowledge, the first paper that considered the problem of fusing images of low quality in iris videos for improving recognition performance via SR is from Fahmy [164]. He proposed a super-resolution technique based on an auto-regressive signature model in the pixel domain for obtaining high-resolution images from successive low-resolution ones, captured at a long distance. However, his approach uses the whole eye image for registration (based on cross correlation model), which potentially prone to errors, especially in less constrained recognition applications. He shows that the resulting images are valuable only if the initial low-resolution images are free of blur and focused, stressing already the bad influence of low quality images in the fusion.

In the same way, Nguyen et al. proposed fusing different irises coming from NIR face videos at a pixel-level after an interpolation step [54] [165]. The authors use a quality factor in their fusion scheme, which allows them to give less importance to images of bad quality in the fusion. The interpolation procedure as well as the quality weighting is shown very efficient for improving recognition performance. The experiences are conducted on the challenging dataset: MBGC portal. NIR face videos are compared against NIR high-quality still iris images. An EER of 2.1% is achieved by their approach in [54] . In particular, the proposed method outperforms classical scheme based on best quality frame selection [32] and other existing approaches: MPMG score-fusion (10,1%) and signal-fusion methods (2.6%) [162].

In a more recent work [166], Nguyen et al. explored feature-domain SR for iris recognition using eigeniris as the features. A different protocol is adopted in this work: two images are selected from the NIR high-quality iris still images of MBGC database. One is devoted to the gallery, while the other is artificially degraded to create a series of low-quality images. The proposed method leads to better performance than their previous work [54] with this new protocol. The EER is approximately reduced from 10% to 5%. However, it is shown that 2D Gabor wavelets are more discriminate features for iris recognition than eigeniris features. Therefore, in [167] feature-level SR approach is directly conducted on the Gabor filtered images.

A super-resolution scheme based on an improved iterated back projection algorithm is also proposed by Ren et al. in [168]. A high-resolution image is reconstructed from multiple still iris images, taken from CASIA-Iris-Lamp. The images are also artificially down-sampled. Lower EER is obtained by the SR method.

In another direction, Liu et al. [41] proposed a fusion scheme based on a modified Markov network at the bit-level to obtain a high-resolution irisCode from a sequence of low-resolution ones. Heterogeneous comparisons are performed between high and low resolution videos, coming from QFIRE05 and QFIRE11 respectively. Only images free from noise and successfully segmented are used. They also proposed measuring the reliability of each bit in the enhanced irisCode in order to improve iris recognition performance.

Mahadeo et al. [169] proposed a method that reconstructs an optimized irisCode from several frames of an iris video. The method selects the best rows and columns in different irisCodes coming from the sequence. The best row (resp. column) corresponds to the raw (resp. column) that achieves the lowest mean of the Hamming distances with the corresponding rows (resp. column) in the remaining

irisCodes of the sequence. The optimal irisCode is obtained by performing an AND operator between the best rows and columns. A mask is also generated: it corresponds to the bits that disagree between these two best entities. NIR iris videos of MBGC are used to assess the approach. Only frames with high quality are used. The proposed bit-fusion scheme is compared to other score-fusion ones: it outperforms [92] (the average of the Hamming distances) and [160] (the minimum value of the Hamming distances). More precisely, the obtained EER by the proposed method, [92] and [160] are respectively 0.018%, 0.1022% and 0.1041%.

5.1.2. Synthesis and choice of the fusion approach

All the related works of the above literature review agree on the fact that the quality of the used images in the fusion process is a very important factor for its success, and hence for obtaining an improvement in the recognition performance.

Except [54] [165], in all the works only images of high quality are used to perform the fusion. They are selected either manually [163] [164] [166] [168] or according to quality assessment algorithms [162] [167] [169]. The images are well focused, with a reasonable percentage of visible iris area in the frame. After that, the quality of the segmentation is also examined. Images poorly segmented are discarded [41] or corrected [162] for assessing their proposed approaches. Moreover, in [163] the images are fully segmented manually. The selected database for benchmarking most of these related works is the NIR iris video dataset of MBGC which is from relatively high quality. This is due to the controlled acquisition mode (close acquisition distance, static subject...).

Other works proposed to estimate the image quality in the sequence to give to this image less or more weight in the fusion process according to its quality [54] [165]. Super-resolution technique is performed to improve the resolution of the images. The assessment of the proposed approaches is conducted on the MBGC portal challenge dataset. Compared to the NIR iris video dataset, less constrained conditions during the acquisition are imposed in the portal scenario which corresponds to more realistic applications (long distance, iris on the move). The resulting images are thereby of lower quality.

As explained before, the context addressed in this doctoral work is iris recognition in videos under less constrained acquisition. As in [165] we propose to fuse the different frames of the sequence at the pixel-level. This fusion is based on a basic super-resolution approach, allowing image resolution enhancement. When dealing with videos, contrary to [165], we consider a video vs. video scenario,

more adapted to the re-identification context, meaning that we will use several frames in both low quality videos to address the person recognition task.

We note that the above state-of-the-art review dealing with super-resolution in particular [165] [54] [164] [168] has stressed the importance of choosing adequately the images involved in the fusion process. Integration of low quality images leads to a decrease in performance producing a rather counterproductive effect. Indeed, in general iris videos taken at a distance or on the move suffer from blur and low contrast between the pupillary and limbic boundaries. Moreover strong occlusions can occur on iris regions. These degradations may lead to wrong iris localization, which particularly influences the precision of the iris segmentation and consequently the quality of the normalized iris texture. In this case, two normalized iris images resulting from different acquisitions of the same person, present a high discrepancy and consequently one must be very careful in fusing such images. Therefore, it is important to consider accurately the quality of the images in the fusion process in order to increase the recognition performance.

Following these considerations, we therefore concentrate our efforts on proposing a novel and relevant way of measuring and integrating quality measures in the image fusion scheme. More precisely, our first contribution is the proposition of a global quality measure of normalized iris images that we will use in two ways: as a selection tool and as a weighting factor in the same way as proposed in [165]. More precisely, we propose to use our quality assessment algorithm previously described in Chapter 4. We recall that our measure exploits a local Gaussian Mixture Model based characterization of the iris texture. The interest of our quality measure compared to [165] is its simplicity and the fact that its computation does not require identifying in advance the type of degradations that can occur in the iris images. Bad quality normalized iris images are therefore images containing a large part of non-highly textured zones, resulting from blur or occlusions.

Taking advantage of this local measure, we propose as a second novel contribution to perform a local weighting in the image fusion scheme, allowing us to take into account the fact that degradations can be different in diverse parts of the iris image. This means that regions free from occlusions will contribute more in the reconstruction of the fused image than regions with artefacts. Thus, we believe that the quality of the reconstructed image will be optimized and we expect this scheme to lead to a significant improvement in the recognition performance. To our knowledge, this is the first work in which a local quality is proposed for fusing iris sequences instead of a global one as done in the literature.

We have chosen to fuse the images of the sequences at the pixel-level. Our motivation lies in the fact that our local quality is estimated on the normalized images for each pixel. However, we will see in the next chapter that it is also possible to exploit this local quality at the bit-level.

5.2. Proposed approaches for fusing iris sequences

The aim of this section is to present our strategy for fusing iris images, aiming at improving iris recognition in less constrained environment. We first describe the implemented super-resolution process allowing interpolation and fusion of images of a given iris video. After that, we will explain how we have integrated our quality measures presented in Chapter 4 in the fusion process. Finally, we summarize the overall architecture of the system that we propose for person recognition from a sequence of iris images, using frames fusion with local and global quality measures.

5.2.1. Fusion process

5.2.1.1. Super-resolution implementation

Super-resolution (SR) is a set of image processing techniques that generate a higher-resolution image from multiple lower-resolution images of the same scene. SR aims at building details finer than the sampling grid of a given imaging device by increasing the number of pixels per region in an image [105]. Indeed, the high-resolution image contains a high pixels density and hence more details on the original scene. As we are working with sequences acquired by biometric systems in less constrained environment, e.g. at a distance or/and on the move, the resulting images may suffer from poor resolution. In the current state-of-the-art, it is shown that a lack of resolution leads to significant degradation in iris recognition performance. SR technique can remedy to this lack of resolution by producing an enhanced restored image from multiples images.

SR techniques in general:

SR techniques involve the three following principles: image observation model, registration and reconstruction.

i. Image observation model:

SR problem is usually modeled as an inverse problem where "the source (High-resolution (HR) image) has to be estimated from the observed data (Low-resolution (LR) images)" [170]. In order to

solve this inverse problem, an observation model is first defined. In our context, the observation model which consists in relating the HR image *h* to the observed LR images *l*, and can be expressed as [171]:

$$l_i = DB_iM_ih + n_i \quad for\, 1 \le i \le F \quad (5.1)$$

where *D*, *B* and *M* respectively denote the sub-sampling, blur and warp matrix. *n* represents the additive Gaussian noise and *F* is the number of frames in the video.

ii. Image registration:

This process ensures the correct alignment of the multiple images coming from the same scene at distinct times. Image registration is a fundamental image processing problem. This task becomes more difficult especially when the observations are degraded: low-resolution images with strong artifacts in our case.

As well known, image registration accuracy decreases when the resolution of the observations diminishes [172]. Indeed, the boundaries are more blurred in the images of low-resolution. This fact can introduce severe registration errors. Therefore, the quality of the reconstructed high-resolution image depends on the performance of the registration.

Registering images can be expressed as a mapping or a transformation of the pixels from the observation to the reference image (rotation, translation...). This stage can be global i.e. performing the same transformation on the whole image, or local i.e. addressing differently the sub-regions of the image [126]. Global transformations are generally used when the observed scene is rigid. Adversely, when the scene is not rigid, local transformations are more suitable.

iii. Image reconstruction:

SR techniques can be categorized into three main classes: interpolation, frequency and regularized based algorithms. Major principles of those methods and some of the most popular methods are given below. More details can be found in the technical review [171].

- Interpolation-based algorithms:

It consists in recovering the HR image by projecting all the LR images to a reference image. After that, all the LR images are fused. This is justified by the fact that, each one of them can bring an additional amount of information about the scene. A deblurring procedure is then applied to the obtained fused image in order to obtain the final HR image. Non-uniform interpolation can be

performed as in [173] [174]. The interpolation can also be iteratively conducted by e.g. back-projection algorithm [175], or projection onto convex sets algorithm [176].

- Frequency-based algorithms:

Such approaches exploit the aliasing effect that exits in each LR image to restore the HR image. Indeed, this effect is easily modeled in the frequency-domain. The first algorithm was proposed by Huang and Tsai [177] and followed these principles: (i) shifting properties of Fourier Transform, (ii) the aliasing relationship between Discrete Fourier Transform coefficients (DFT) of the LR images and the continuous Fourier Transform of the original HR image, and (iii) the original HR image is band-limited. In [178], Discrete Cosine Transform (DCT) has been proposed instead of DFT. An iterative EM algorithm [179] was also used for performing registration, de-convolution and interpolations processes. The use of wavelets has been also investigated for recovering the high-frequency information in many works [180] [181] [182].

The major limitation of these techniques lies in the fact that the registration can only be performed globally. However, such approaches have a low complexity cost.

- Regularized-based algorithms:

Due to insufficient number of LR images or ill-conditioned blur operators, various regularized-based approaches have been implemented to "stabilize" the inverse problem, by decreasing the number of possible solutions. Some prior knowledge of the source HR image is incorporated to solve the problem. Such methods can be classified into deterministic or stochastic approaches.

In deterministic SR reconstruction methods, the observation model given in Formula 5.1 can be entirely specified: prior information about the solution is exploited to make the problem well posed. A typical method can be used for performing this: the constrained least squares. Stochastic approaches rely on the possibility that the posteriori probability density function of the original HR image can be established, by using information on both observed LR images and prior knowledge on the HR image. Bayesian-based SR approaches belong to this type of category. One of the most popular Bayesian-based SR approaches is the Maximum a Posteriori (MAP) estimation approach [183].

SR in the field of iris recognition:

In the literature, SR techniques have been used for fusing iris sequences of low quality in order to reconstruct a highest resolution iris image as related in Section 5.1.1 in several works [54] [164] [165] [168]. We give below more details on the SR approaches.

In [164], Fahmy presented an SR approach based on an auto-regressive signature to construct a higher resolution iris image from a video sequence. First a set of 9 un-blurred frames are selected from the video, and registered with the first frame by using cross correlation model. No criterion of selection is mentioned in the paper. Then, auto-regressive signatures are calculated between the reference frame and the remaining frames in 3 directions: vertical, horizontal and diagonal. For each direction, the frame that gives the highest value is selected. These three images and the reference image are then interleaved to create a 4 times higher resolution image. This process can be repeated to build a 16 times higher resolution frame to the original iris frame. Experimental results show recognition enhancement for the HR images compared to original ones (LR).

A reconstruction-based SR approach that incorporates quality criteria was proposed by Nguyen et al. in [54] [165] to improve iris recognition accuracy. The approach is based on a bilinear interpolation. In [54] the registration is as follows: for each interpolated iris image, the corresponding irisCode is calculated and then shifted to compute several Hamming distances with the reference image. The shift that produces the smallest value is used to register the interpolated image. In [165] a phase correlation patch-based registration is used for registering the images. In both works, the interpolated and registered images are then averaged by using quality criteria. The HR image is then restored by applying a deblurring Wiener filter.

Ren et al. [168] proposed a robust SR algorithm to construct a HR image from several distinct and proper LR images (well-focused and without strong occlusions). The images are first segmented and normalized. Then, the normalized iris images are registered to the reference image by using translation and rotation transforms. In the Fourier domain, the slope of the phase difference is calculated to provide the translation shift in the pixel domain while the rotation angle corresponds to the value that provides maximum correlation between the Fourier transform of the reference image and the normalized iris image to be registered. Finally, the reconstruction phase relies on two stages: (i) the nearest interpolation of the reference image (first image of the sequence) to get a HR image and (ii) the total square error between the reference and the remaining registered images is iteratively calculated. Iterations are done with the sum of the images and the gradient of the total square error. The process is stopped when the error reaches a fixed threshold value. The method is compared to other SR algorithms such as robust mean averaging algorithm [184]. The proposed method gives lower EER.

SR approaches have also been performed to build a HR iris image from a single LR image instead of various LR images, aiming at improving the recognition. For example, in [185] Kwang et al.

explored a learning-based SR algorithm based on multiple Multi-Layer Perceptrons (MLPs) to enhance the resolution of the images. By using bilinear interpolation based on the output pixels of the trained multiple MLPs, a HR iris image is produced. To this end, the MLP is trained with back propagation algorithm only on clean pixels (free from occlusions). The LR image is divided into small blocks and each of them is classified into one of the 3 following classes: vertical, horizontal and non-edge depending on the edge direction of the iris patterns. These 3 types of blocks are fed into 3 corresponding MLP neural networks to estimate the new pixels. The resulting blocks contain the old and the new pixels. These blocks are then combined in order to get a HR iris image. Pixels without values are restored by using bilinear interpolation. Experimental results of the proposed approach on Casia-IrisV3-Interval database show lower EER than conventional bilinear interpolation.

Another learning-based approach based on Circular Symmetric Filter (CDF) [186] was proposed by Huang et al. in [187]. Prior probability relations between the information of different frequency bands of iris features extracted by CDFs and used for the recognition are learned and then incorporated in the SR to enhance the visual effect. Local spatial relationships between LR and HR patches are modeled by using a Markov Network [188]. Better recognition accuracy are obtained by performing this feature-domain approach compared to the traditional interpolation SR algorithm of Freeman [189] operating in the pixel domain.

Adopted super-resolution in the doctoral work:

Among the various ways used to reconstruct the HR image, we chose a simple interpolation-based SR technique in the pixel-domain, similar to that exploited in [165] resulting in a double resolution image. We will show on several iris databases that this simple SR technique is sufficient to improve the performance of the recognition. We presume that more sophisticated algorithms could lead to further improvement as learning-based approaches but with a higher complexity cost. However, the choice of the SR algorithm should be done carefully, as it is reported in the literature [165] [187] that learning-based methods fully learned on pixel intensity to model the relationship between HR and LR images introduce some fake high frequencies in the reconstructed HR image in order to produce good visual effect. These biased data can lead to possible performance degradations.

As highlighted before, a process of registration has to be performed on the images before the pixel-fusion to ensure that the pixels are correctly aligned with each other in the sequence. Therefore, each iris image of the sequence is first segmented and then normalized. Indeed, the process of normalization performs a scaling of the iris zone dealing with pupil dilation, and thus allowing an

alignment of the pixels. This method is sufficient for the registration due to the fact that the images of the selected databases for benchmarking are frontal images. However, a different method of alignment would be necessary for iris videos with head rotation or eye movement (off-angle).

After that, each normalized image of the sequence is bi-linearly interpolated and then averaged to obtain one high-resolution image. Bilinear interpolation consists in assigning to each unknown pixel a value which corresponds to the weighted average of the pixels' intensities in the nearest 2-by-2 neighborhood. Finally, the Wiener deconvolution filter [190] is then applied on this fused image for enhancing its quality (deblurring stage). However, the obtained performances on the selected databases show similar recognition accuracy results with or without this filter. Therefore, we decided to remove the filter to reduce the complexity of the method.

5.2.1.2. Integration of quality assessments

We explored specifically two possible fusion schemes, depending on how the quality has been exploited:

i. Global quality-based fusion process

As done in [165], we weight the value of each pixel of each normalized iris image by the same factor but for this we use our empirical global quality measure (GQ) as defined in Formula 4.8 in the previous chapter. GQ allows us to estimate one unique quality measure per image avoiding a fusion phase of various quality measures, which requires identifying a priori the type of each degradation. We recall that the GQ is the mean of the local qualities, estimated on sub-regions of the normalized iris image as illustrated in Figure 4-5 of Section 4.2.4 of the previous chapter. More precisely, the normalized iris image of size $64x512$ is divided in $4x8$ non overlapping regions, leading in 1024 quality measures. These values are then averaged to obtain a single value: the global quality GQ.

ii. Local quality-based fusion process

We also propose a novel scheme using the local quality measure (LQ) defined in Formula 4.7. Our aim is therefore to take into account the fact that degradations can be different in diverse parts of the iris image. This means that regions free from occlusions will contribute more in the reconstruction of the fused image than regions with artifacts. In this case, we compute the quality measures of all the sub-images as in the global quality-based fusion process but they are differently exploited. Instead of averaging the qualities, we let them in the matrix form. This matrix is then bi-linearly interpolated in the same way as the normalized iris image to create two entities of equal size. Finally, we weight the

value of each pixel of each interpolated image by its corresponding value in the interpolated quality matrix (same location).

We have used bilinear interpolation instead of nearest neighbor algorithm to avoid blocky appearance in the weighted quality-based fused image. Figure 5-1 illustrates the weighted local quality-based fusion process. More details are given on the next sub-section.

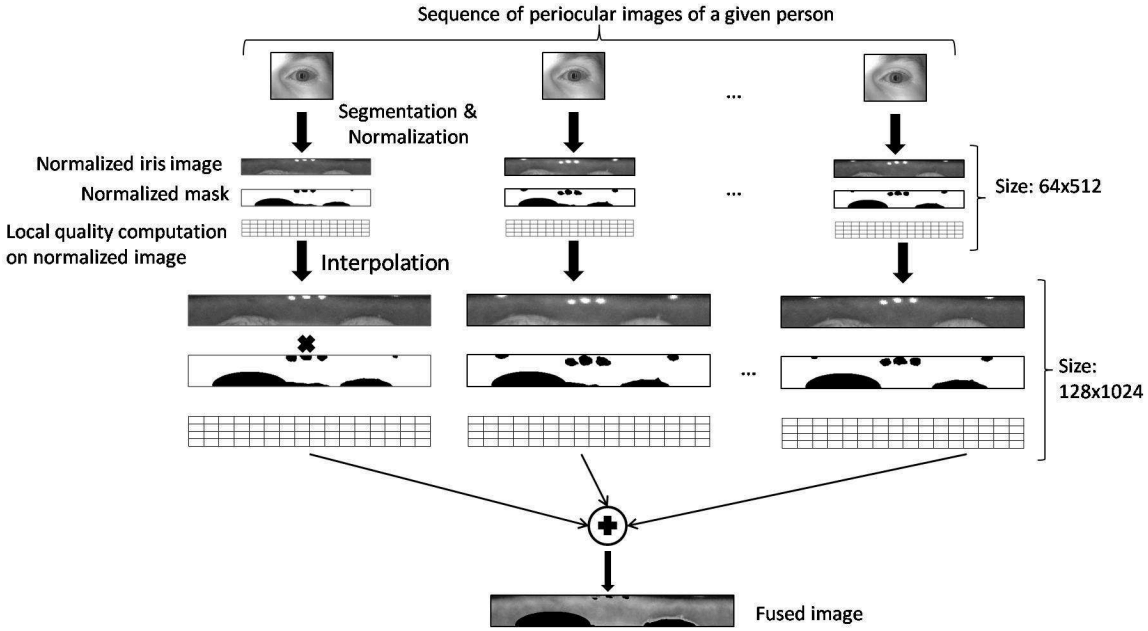

Figure 5-1: Fusion process of the proposed local quality-based method

5.2.2. Overall architecture of the quality-based system

The steps carried out in the quality-based system including the fusion process are summarized in this sub-section. The proposed system takes as input, sequences of periocular images. The main stages of the quality-based system are described as follows:

For each frame, we:

- ✓ Segment the iris: Search of the pupillary and limbic boundaries;
- ✓ Generate the iris mask: Search of the possible occlusions occurring on the iris regions;
- ✓ Normalize the segmented iris and the iris mask;

- ✓ Measure the local quality on the normalized image using the GMM already learned given in formula 4.7,
- ✓ Interpolate the normalized iris image and its local quality matrix to a double resolution using the bilinear interpolation. The normalized mask is also interpolated by performing nearest neighborhood algorithm instead of bilinear interpolation to avoid real values in the mask.

Then, for all the frames, we generate the fused image as follows:

i. In the case of the global quality-based fusion process, the reconstructed HR image is obtained as follows:

$$I(x,y)_{fused} = \frac{\sum_{i=1}^{F} I^i(x,y) \cdot M^i(x,y) \cdot Q^i}{\sum_{i=1}^{F} M^i(x,y) \cdot Q^i} \quad (5.3)$$

where F is the total number of frames, $I^i(x,y)$ and $M^i(x,y)$ are the values of the pixel in position (x,y) of, respectively, the i^{th} interpolated normalized image and mask. Q^i is a scalar which represents the global quality of the i^{th} image. I_{fused} corresponds to the weighted average of non-occluded pixels. Each weight corresponds to the global quality of the iris image.

ii. In the case of the local quality-based fusion process, the reconstructed HR image is obtained by the following formula:

$$I(x,y)_{fused} = \frac{\sum_{i=1}^{F} I^i(x,y) \cdot M^i(x,y) \cdot Q^i(x,y)}{\sum_{i=1}^{F} M^i(x,y) \cdot Q^i(x,y)} \quad (5.2)$$

where F is the total number of frames, $I^i(x,y)$ and $M^i(x,y)$ are the values of the pixel in position (x,y) of, respectively, the i^{th} interpolated normalized image and mask. $Q^i(x,y)$ is the value in the location (x,y) of the i^{th} interpolated local quality matrix. I_{fused} corresponds to the weighted average of non-occluded pixels. Each weight corresponds to the local quality of the pixel.

The last steps of the recognition process, namely feature extraction and matching, are performed on the fused image. Note that from one video of F frames, we get only one image

performing this way an important and efficient compression of the information. Figure 5-2 shows the architecture of the proposed quality-based super-resolution scheme.

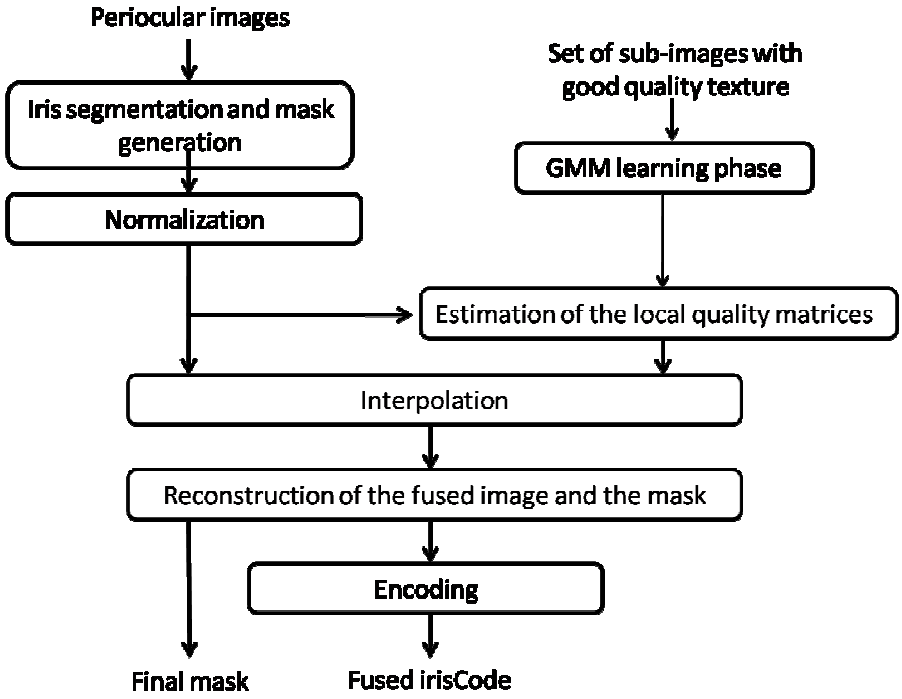

Figure 5-2: Diagram of the quality-based super-resolution scheme for video-based iris recognition.

5.3. Assessment of the proposed fusion processes

In this sub-section, we will evaluate the proposed fusion approaches on several iris databases: the portal challenge of MBGC, Casia IrisV4-Thousand, QFIRE05, QFIRE07 and QFIRE11. We divided this sub-section into two main partitions: the experimental results of our preliminary works are given in Section 5.3.1 while the results of the final proposed strategy for the fusion are given in Section 5.3.2. Indeed, during the doctoral work, the proposed fusion approaches have been improved. At the beginning, the fusion approach was performed on images that have been manually segmented (images of the portal challenge of MBGC). And, the local quality was estimated by the GMM4obs, explained in Section 4.2.3.1, on the images of the portal challenge of MBGC and Casia IrisV4-Thousand. For the remaining databases e.g. QFIRE05, QFIRE07 and QFIRE11, the fusion process is entirely automatic and the local quality is given by the GMM5obs.

For all the databases, our test protocol rely on the comparison of a sequence against a sequence, like in the first popular work on signal-fusion in iris recognition [162].

5.3.1. Preliminary works

In the first experiments performed during this thesis, the proposed fusion schemes have been evaluated on two challenging databases: the portal challenge of MBGC and Casia IrisV4-Thousand. The images of the first one suffer from poor resolution and blur. The images of the second database are better in terms of quality but they are considered as difficult to segment due to the spots on the boundaries of the pupil and the iris and the presence of eyeglasses. In this way, we can show the interest of our fusion scheme for two distinct problems for iris recognition, which are the very low quality of the images resulting from an acquisition at a distance and on the move, and the wrong segmentation of the iris.

5.3.1.1. Multiple biometric Grand Challenge: Portal dataset

At the beginning of our doctoral research, we have addressed the problem of iris recognition at a distance and on the move. To benchmark the proposed fusion schemes, we have chosen the portal challenge of MBGC database. As presented in Chapter 2, the database contains NIR face videos of subjects, walking towards a portal. However, as described in the previous sub-section, our quality-based system has as input a sequence of periocular images. Therefore, we first have to detect and track the eyes in the video sequence. In general, the tracking is guided by the presence of spots that are located around the eyes.

After that, highly blurred frames from the sequence were removed by using wavelet's transformation. Once this stage has been completed, the fusion process requires the usual iris segmentation and normalization of the images as seen in Section 5.2.2.

Iris segmentation on this database is considered to be a challenging task for many reasons. One of the difficulties present in the images lies in the fact that light spots often occlude the pupillary boundary. Consequently, the shape of the iris becomes irregular which disturbs segmentations based on a detection of a specific parametric shape such as circles or ellipses. The other difficulty consists in the change of illumination between the different frames in the same sequence, resulting in dark and bright iris images. Consequently, the images suffer from low contrast, and thus the segmentation becomes very tricky.

All these factors appear during the acquisition in non ideal conditions. However, the iris recognition systems that have been presented in Chapter 3 namely OSIRISV2 and OSIRISV4.1 have been developed in the context of still images, taken from static subjects in restrictive conditions of acquisition. More precisely, their parameters have been defined and set up according to ICE2005 database in order to work well on it. Consequently, their performance cannot be optimal on other databases, acquired in a different scenario (sensor, environment...).

As pointed in Chapter 1, our goal is to propose a fusion scheme, aiming at reducing the high error rate of the overall performance system in less constrained acquisition, caused by the degradations of the images, whether the segmentation is accurate or not. However, the quality of MBGC images is so poor that no version of OSIRIS was able to perform at least one acceptable segmentation per video. The fact that several aberrant segmentations occur in a sequence is critical for the further processing steps, making those images of the sequence not exploitable whatever the fusion process used. Indeed the segmentation task aims at providing a model of the iris boundaries, used to achieve the normalization step. The normalized images of the sequence are then used as input to perform the fusion procedure. If that input is completely aberrant, there is no chance to improve the performance. Figure 5-3 illustrates an example of correct and aberrant segmentations and the corresponding normalized images for a given iris.

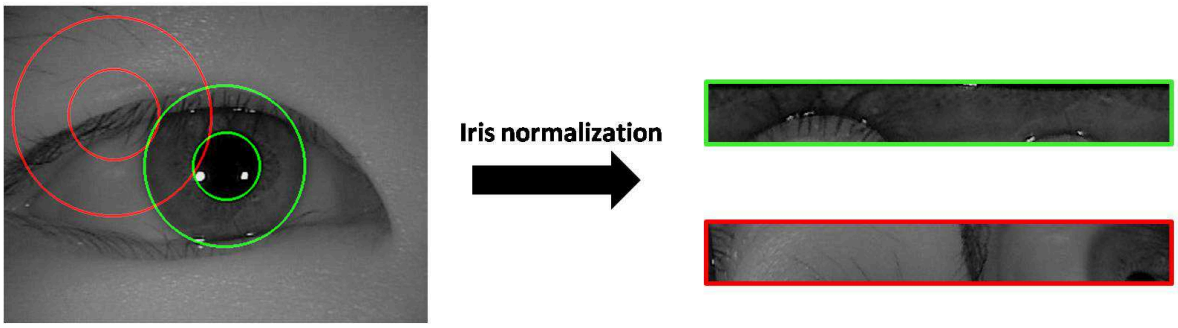

Figure 5-3: Illustration of correct (in green) and aberrant (in red) segmentations and the corresponding normalized images for a given iris.

Since none of the segmentation modules of the different OSIRIS versions satisfies this requirement on the portal challenge of MBGC database, we performed a manual segmentation of the iris boundaries. Those borders are modeled by two circles, which fit at best the pupillary and limbic boundaries, manually determined. According to these circles, the normalized image is obtained with the Daugman rubber sheet, coded in the normalization module of OSIRISV4.1. The possible

occlusions are detected through an adaptive filter applied on the normalized images [104]. The further steps namely feature extraction and template matching are also performed by OSIRISV4.1.

After all these pre-processings, the database was composed of 108 subjects and each one possesses 2 sequences with at least 4 frames per sequence. For each person, we used the first sequence as a target and the second one as a query.

Experimental results and discussions:

The proposed approach is first compared to other fusion score methods such as Multi-Gallery Simple-Probe (MGSP), Multi-Gallery Multi-Probe (MGMP) and then to fusion signal methods as simple averaging of images [162] and finally weighted super-resolution as done in [54].

i. Fusion at the score level:

As a first step, we performed different score-fusion methods:

- *Matching 1 to 1:* All the frames in the video of a person are considered as independent images and used for performing inter-class and intra-class comparisons. This system was used as a baseline system to compare the other methods.
- *Matching N to 1: Multi-Gallery, Simple-Probe (MGSP):* In this case, the different images in the video are considered dependent as they represent the same person. If the number of samples in the gallery and the probe are respectively *N* and 1 per person, we get N Hamming distance scores which can be combined by making a simple average [92] or the minimum of all the scores [160].
- *Matching N to M, Multi-Gallery, Multi-Probe (MGMP):* In this case, we consider *M* images in the probe and *N* images in the gallery. We thus get NxM scores per person and combine them by taking the average or the minimum.

The performances of these score-fusion schemes on the portal of MBGC are reported in Table 5-1.

The best score's fusion scheme reduces the Equal Error Rate (EER) from 14.32% to 4.66%. This indicates that recognition performance can be further improved by the redundancy brought by the video. However, the corresponding matching time considerably increases when the recognition score is calculated for NxM comparisons.

Table 5-1: Equal error rate on the portal challenge of MBGC for different score's fusion schemes.

Methods	EER (in %)	
Baseline: 1 to 1	*14.32*	
	Minimum	*Average*
MGSP	*9.30*	*10.27*
MGMP	*4.66*	*5.65*

ii. Fusion at the signal level:

- Without a quality measure:

At first, the fusion of images is done without using the quality measure. For each sequence, we create a single image by averaging the pixels intensities of the different frames of such a sequence. We experimented two cases: without and with interpolated images (SR). In the first case, we wish to demonstrate the eventual improvement brought by a simple fusion scheme. This scheme of fusion is called "SA". The second one allows us to quantify the impact of the super-resolution on the results. We named this fusion scheme "SR-NoQ". The EERs of these two methods are reported in Table 5-2.

The results shows that the fusion method based on the interpolation of images before averaging the pixel intensities, outperforms the simple average method with a relative improvement of 25.30% at the EER functioning point. This result is coherent with Nguyen's results which states that super-resolution greatly improves recognition performance [54].

Table 5-2: Equal error rate on the portal challenge of MBGC for different image's fusion methods without using quality.

Strategy of signal fusion	EER (in %)
SA	*4.90*
SR-NoQ	*3.66*

By observing Table 5-1 and Table 5-2, we see that the MGMP-min method is slightly better than the simple average (4.66% vs 4.9%). These results are coherent with those obtained by Hollingsworth et al in [162]. However, as explained in their work, the required processing time is much lower for image's fusion than score's fusion (17.09 seconds vs. 1008.9 seconds).

- With a quality measure: Global or local

Given the considerable improvement brought by the interpolation, we decided to perform our further experiments only on SR images. We introduce in the fusion, the global quality (GQ) and local quality (LQ) fusion schemes, as described in Section 5.2.1.2. These two signal fusion methods are respectively called "SR-GQ" and "SR-LQ". The Equal Error Rate of all methods is shown in Table 5-3 and the DET-curves of these methods are shown in Figure 5-4.

As reported in Table 5-3, introducing our global quality criterion in the fusion gives a high relative recognition improvement (25.95% at the EER) compared to when no quality is considered. Our method is in agreement with Nguyen's result [165] who obtains an improvement of 11.5% by introducing his quality measure (but with another evaluation protocol). Compared to his method, our quality is simpler to implement. Indeed, the metric employed by Nguyen for estimating the quality of a given frame includes four independent factors: focus, off-angle, illumination variation and motion blur. After calculating individually each of these quality scores, a single score is obtained with the Dempster-Shafer theory [165]. Our quality measure has the advantage of not requiring an extra strategy of combinations neither knowing in advance the possible nature of the degradation.

Table 5-3: Equal error rate on the portal challenge of MBGC for different image's fusion methods with and without quality measures.

Strategy of signal fusion	EER (in %)
SR-NoQ	*3.66*
SR-GQ	*2.71*
SR-LQ	*2.58*

By incorporating our GQ measure in the fusion process, the contribution of each frame in the fused image will be correlated to its quality, this way more weight is given to the high quality images.

Table 5-3 also shows that LQ-based fusion method outperforms the GQ-based fusion method with a relative improvement of 4.79% at the EER. This is due to the fact that the quality in an iris image is not globally identical as we expected. Indeed, due for example to motion blur, a region in an iris image can be more textured than another one. Moreover, our LQ measure can detect eventual errors of masks and assign them a low value. The LQ-based fusion scheme allows therefore a more accurate weighting of the pixels in the fusion scheme than the GQ-based method.

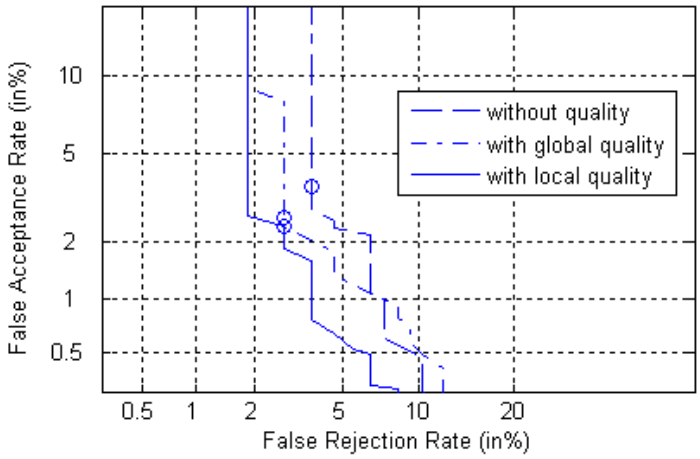

Figure 5-4: DET-curves of the three image's fusion approaches for MBGC portal videos.

Conclusions

We have proposed two novel contributions for implementing image fusion of frames extracted from videos of moving persons with the aim of improving the performance in iris recognition. Our main novelty compared to the literature is the introduction in the fusion scheme, at the pixel-level, of a local quality (LQ) measure relying on a GMM estimation of the distribution of a clean iris texture. This LQ measure can also be used for giving a global quality (GQ) measure of the normalized iris image. We have shown on the MBGC database that the LQ-based fusion allows a high improvement in performance compared to other fusion schemes (at the score or image level) and to our GQ-based fusion. We therefore conclude that the quality in an iris image is not globally identical: indeed, due for example to motion blur, a region in an iris image can be more textured than another one. Our intuition is that LQ measure can detect eventual errors of masks and assign them a low value. The SR-LQ based fusion scheme allows therefore a more accurate weighting of the pixels in the fusion scheme than the SR-GQ method.

As the segmentation was done manually, the segmented images do not contain errors of segmentation. However, if this procedure is replaced by an automatic one, we expect a large number of errors of segmentation, caused by less constrained acquisition. Our intuition is that our local quality measure should be able to detect those errors and that our system will therefore be able to discard those bad-segmented pixels from the fusion procedure. If this is the case our fusion procedure should not suffer too much from segmentation errors. Our future works will tend to validate this hypothesis by using a bigger iris database: Casia IrisV4-Thousand on which segmentation errors will be present.

After this preliminary work, we note that we did not re-benchmark the approaches on MBGC portal with an improved automatic segmentation algorithm as the interest for this database by research community has considerably decreased over the time. Therefore, we preferred to use more recent iris datasets.

5.3.1.2. CASIA-IrisV4-Thousand

In complement to the work developed on MBGC, we have studied the impact of possible inaccurate segmentations in the proposed fusion process. This aspect cannot be previously studied due to the manual segmentation. Casia IrisV4-Thousand includes 20000 iris images from 2000 eyes of 1000 persons. Thus, each subject has 10 instances of both left and right eye. We have selected randomly 600 subjects. The resolution of the images is higher than in MBGC portal. The main sources of variations in this database are eyeglasses, specular reflections and dilation (see Chapter 2), which make the iris segmentation particularly difficult. For each person, several images are taken under different conditions, but there are at least some images of "good quality". This way, the automatic segmentation is not aberrant for all the images in a given sequence. Even if errors may occur, possible improvement can be obtained by the fusion approaches.

To perform the segmentation step, we used the OSIRISV2 reference system described in Section 3.2.1. As mentioned, the segmentation is based on Hough transform and active contour. This version has been improved in the latest version but, as our purpose is to show the impact of using a local quality measure in the fusion process when the segmentation of the iris fails, we decided to use the second version, which leads to more cases of wrong segmentation. For instance, Figure 5-5 illustrates two examples of segmentation: a good (Figure 5-5-a) and a wrong (Figure 5-5-b) and their corresponding normalized image and local quality matrix.

On Figure 5-5-b, we can see a part of the sclera on the normalized iris image. This is due to the wrong localization of the boundary between the iris and the sclera. When fusing the iris images, this zone which does not correspond to iris texture will degrade the results. Therefore, we should give to this zone less importance in the process of fusion. To do this, we will fuse the normalized iris images using their local quality matrices. This way, dark areas of this matrix, which correspond to low quality zones (zones not belonging to the iris region), will therefore contribute less in the fusion than bright ones. Therefore, the local quality can be considered as a real valued mask.

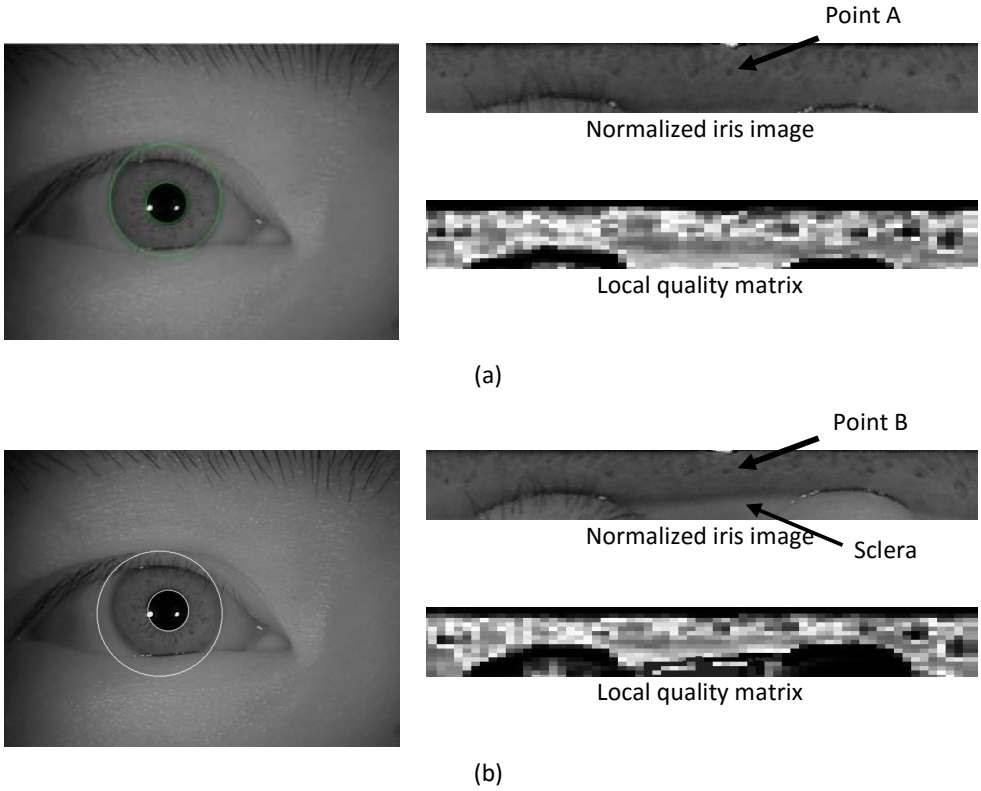

Figure 5-5: Examples of two different segmentations on the same eye: (a) Good segmentation and corresponding normalization, (b) Wrong segmentation, and their corresponding normalized iris image and local quality matrix.

Apart from this undesirable effect, a bad localization of the borders of the irises also introduces some disparities in the normalized iris images and therefore two images from the same eye can lead to two normalized images in which two points with the same coordinates do not correspond to the same texture. This effect is illustrated in Figure 5-5. The two points A and B correspond to the same part of the observed iris. However, due to the wrong segmentation, they are not well aligned (Point A is below Point B). Our proposed quality-based fusion process does not take this effect into account.

For each subject, we divided arbitrary the ten instances into two equal parts: we used five images as a target sequence (references) and the rest as a query sequence (test).

Experimental results and discussions:

As done on MBGC portal, several experiments have been conducted on Casia IrisV4-Thousand database. We performed both score-fusion and signal-fusion methods.

i. Fusion at the score level:

We first analyzed the impact of score-fusion methods on recognition performance following the three previously defined protocols: Matching 1 to 1 (baseline: 1 to 1), Matching *N* to 1 (MGSP), and Matching *M* to *N* (MGMP). In this case, *N* and *M* are equal to 5. The recognition performance at the EER is given in Table 5-4.

Table 5-4: Equal error rate on CASIA-IrisV4-Thousand for different score's fusion schemes.

Methods	EER (in %)
Baseline: 1 to 1	*23.82*
MGSP	*9.98*
MGMP	*6.29*

ii. Fusion at the signal level:

We also analyzed the impact of image fusion methods considering only the case of interpolated images (SR-NoQ). Recognition performance is computed by comparing the obtained fused test image to the obtained fused reference image. This protocol is close to the MGMP one: in both scenarios, we assume dependency between the reference images and the test images. Recognition performance results are reported in Table 5-5 and the DETs are given in Figure 5-6.

We first observe, as expected, that the results are highly improved thanks to the fusion of the scores. A relative improvement of 56.16% is observed considering the scenario 5-1 (MGSP) and of 73.56% considering the scenario 5-5 (MGMP), compared to the scenario 1-1.

Table 5-5: Equal error rate on the CASIA-IrisV4-Thousand for different image‘s fusion methods

Strategy of signal fusion	EER (in %)
SR-NoQ	*5.48*
SR-GQ	*4.86*
SR-LQ	*5.54*

When comparing the results reported in Table 5-4 and Table 5-5, we notice that all the images fusion methods outperform the best obtained score-fusion (EER= 6.29%). This interesting result points

out the contribution of the fusion at the image level compared to the fusion at the score level that is high time consuming.

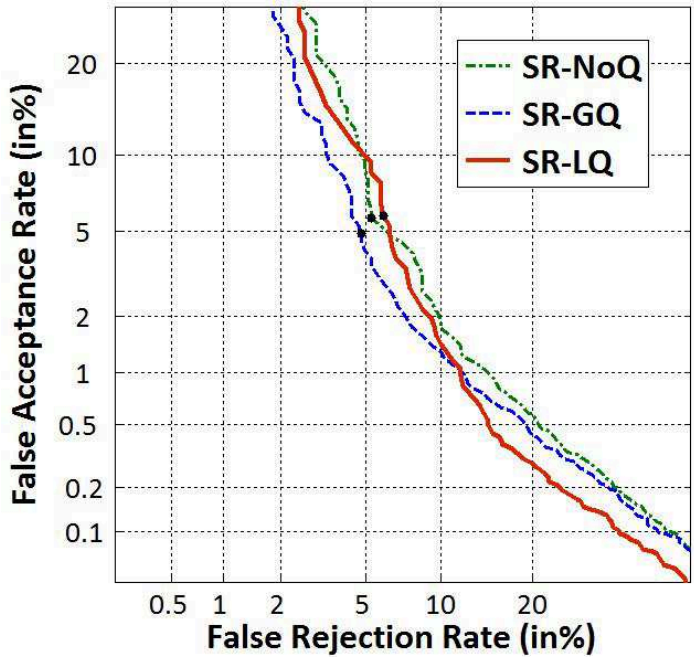

Figure 5-6: DET-curves of the three image's fusion approaches for CASIA-IrisV4-Thousand

We also notice in Table 5-5 that the best performance is obtained when the global quality is considered in the images fusion (SR-GQ, EER=4.86%), while the result at the EER functioning point with the local quality (SR-LQ) is the worst one. To refine this analysis, we plotted in Figure 5-7 the DET curves of the different image fusion methods at low FAR. We observe that at FAR values lower than 1%, the local quality-based system leads to a significant improvement in terms of recognition performance compared to the global quality-based system and to the case when no quality is considered. Indeed at FAR= 0.1%, FRR=33.3% with the local quality measure while FRR=39.5% with the global quality measure and FRR=41.2% when no quality is considered. This is an interesting result, as low FAR values are often considered in the iris recognition framework, when high security is demanded.

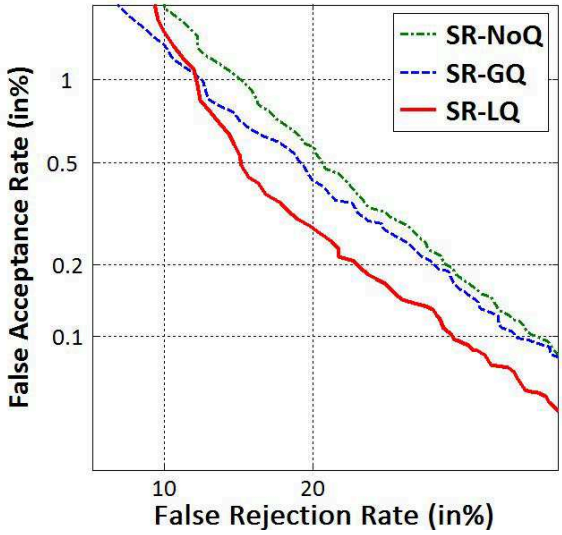

Figure 5-7: DET-curves (at low FAR) of the three image‘s fusion approaches for CASIA-IrisV4-Thousand.

Conclusions:

As was the case with MBGC portal, the experimental results on Casia IrisV4-Thousand database also show a big improvement thanks to the use of image fusion for the references and test sets. While the LQ-based image fusion does not bring any improvement at the EER functioning point compared to the global quality schemes, it is very efficient at low FAR values. Despite the wrong segmentations (obtained by OSIRISV2), the local quality was able to improve the recognition accuracy. These results confirm our intuition that the LQ is able to detect segmentation errors in the normalized images. By assigning small values to those regions (pixel badly segmented), the reconstructed HR image is of better quality.

The good results that we obtained by performing the local quality-based fusion of sequences of multiple still images from Casia IrisV4-Thousand (which present intra-variability and therefore segmentation defaults) and videos of very low quality from MBGC portal (manually segmented, hence no segmentation errors) make us optimistic in the overall performance of an automatic system in the context iris recognition in less constrained environment.

5.3.2. Final model tested on QFIRE databases

Subsequently during the thesis, we wanted to investigate the behaviour of our fusion approaches in the context of a scenario where the acquisition is performed at different distances. Meanwhile, a new

collection of datasets was available: QFIRE databases (see Section 2.3.3). One of the main interests of this database for us is that the iris videos are captured at various distances i.e. 5, 7 and 11 feet, allowing the resolution of the iris images to be quantified. This variability in the distance was introduced to produce high, medium and low resolution iris images as depicted in Figure 5-8.

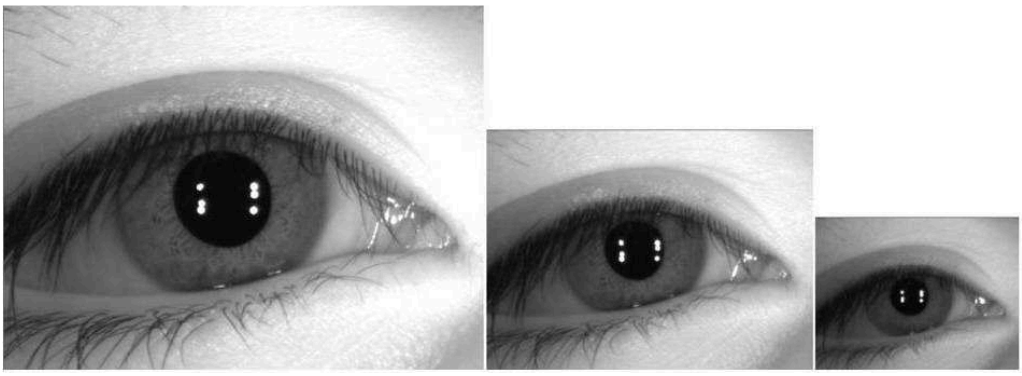

Figure 5-8: Example of extracted eye region from frames of QFIRE database at a distance of (a) 5 feet, (b) 7 feet and (c) 11 feet.

We have conducted several experiments on QFIRE05, QFIRE07 and QFIRE11. To study the contribution of our fusion approaches, we benchmarked them on all the available distances by comparing videos against videos as protocol (at least 10 frames per video). For all these databases, the iris recognition system OSIRISV4.1 was used to perform iris segmentation, normalization, feature extraction and template matching, leading to an entirely automatic system. Consequently, the segmentation of the images in a given sequence can be accurate as well as inaccurate, even aberrant, even if OSIRISV4.1 can already be considered as an efficient reference system [33]. By this way, we show the effectiveness as well as the limitation of the proposed fusion methods.

As in the previous Section 5.3.1, we have considered four fusion schemes: SA, SR-NoQ, SR-GQ and SR-LQ to create one single fused image. We recall their definition:

- Average of the pixels' intensities of the different frames: SA;
- Average of the pixels' intensities of the different frames, with interpolation: SR-NoQ;
- Weighted average of the pixels' intensities by GQ of the corresponding interpolated frame: SR-GQ;

- Weighted average of the pixels' intensities by their corresponding values in the interpolated quality matrix LQ of the corresponding interpolated frame: SR-LQ.

For each fusion scheme, instead of presenting only the estimated FRR@FAR=0.001, we also give the 90% confidence interval. This allows better assessment and comparisons between the fusion methods. The confidence interval is based on a bootstrap methodology, which consists in sampling randomly the individual of the database with replacement such as explaining in [191].

The experiences are organized as follows. First, we propose to show the contribution of the fusion (SA) compared to other schemes, which do not apply fusion (Section 5.3.2.1). Second, we propose to study the contribution of the super-resolution without introducing any quality in the fusion process (Section 5.3.2.2). Finally, we evaluate the impact of quality by implementing SR-GQ and SR-LQ fusion processes. GQ quality can also be used to select the best images of a sequence. A comparison between these two cases (selection and fusion) was also conducted to determine the best strategy of fusion (Section 5.3.2.3) according to the resolution of the images.

5.3.2.1. No fusion vs. simple average fusion

In this section, we first want to give an estimation of the improvement that can be brought by fusion as compared to 1 to 1 matching schemes. Contrary to what we did in our preliminary works (Section 5.3.1), we did not implement any score-fusion algorithms, as they are computationally costly. We will compare the simple fusion scheme SA to the following basic schemes, which consider only the matching of two images of the video at a time:

- *Matching 1 to 1:* All the frames in the video of a person are considered as independent images and used for performing inter-class and intra-class comparisons. This system was used as a baseline system to compare the other methods.
- *Matching Best to Best:* For each video, only the image with the highest quality is considered for performing inter-class and intra-class comparisons. The quality is computed by the global quality given by GMM5obs previously explained in Chapter 4. There is no fusion in this case.

We compare these methods to the simplest fusion scheme without introducing image quality: SA. We note that all the frames of the sequence are used in the fusion scheme (ten frames). The performance results of these methods are reported in Table 5-6.

Table 5-6: FRR@FAR=0.001 on QFIRE databases for 1 to 1, Best to best, and SA.

Methods	QFIRE05	QFIRE07	QFIRE11
Baseline: 1 to 1	*24.3%*	*34.12%*	*52.65%*
Best to Best	*8.0%*	*15.0%*	*16.38%*
SA	*4.18% [4.04-4.20]*	*10.0% [9.71-10.06]*	*12.62% [11.03-12.75]*

As shown in Table 5-6, the SA fusion scheme reduces the FRR@FAR=0.001 for all the databases. This indicates that recognition performance can be further improved by the redundancy brought by the videos. Moreover, SA scheme outperforms the Best to Best scheme: SA reduces the FRR@FAR=0.001 by 47.72%, 33.33% and 22.92% respectively for the datasets QFIRE05, QFIRE07, and QFIRE11.

5.3.2.2. Impact of the acquisition distance on the super-resolution improvement

In this part, we would like to analyze the contribution of the super-resolution without introducing any quality measures (SR-NoQ). For each sub-set QFIRE05, QFIRE07 and QFIRE11, we perform the SA and SR-NoQ schemes on the same datasets of the previous section. We report in Table 5-7 the recognition performance at FRR@FAR=0.001.

Table 5-7: FRR@FAR=0.001 on QFIRE databases for the fusion schemes: SA, and SR-NoQ.

Signal fusions	QFIRE05	QFIRE07	QFIRE11
SA	*4.18% [4.04-4.20]*	*10.0% [9.71-10.06]*	*12.62% [11.03-12.75]*
SR-NoQ	*2.24% [2.24-2.25]*	*5.93% [5.91-5.97]*	*10.23% [9.62-10.34]*

Table 5-7 shows that the fusion method based on the interpolation of images before averaging the pixel intensities outperforms the simple average method with a relative improvement of 46.42%, 40.62%, and 18.91% at the FRR@FAR=0.001 point for resp. QFIRE05, QFIRE07, and QFIRE11. As expected, the improvement due to the super-resolution decreases when the distance between the camera and the subject increases. We note that for the dataset QFIRE11, the improvement significantly drops. This may be explained by the fact that the iris videos are taken at a very long distance, therefore

the images suffer more from blur at this distance as shown in Figure 5-8 and it is well known that the super-resolution performs less well with blurred iris images [164].

Moreover, we notice that this sub-set QFIRE11 contains more segmentation errors than QFIRE05 and QFIRE07. These segmentation errors are dramatic for the super-resolution for the reason that they induce registration problems. Better performances could be expected for this dataset by performing more accurate registration methods as usually employed in SR methods (i.e. phase correlation).

5.3.2.3. Assessment of the global and local quality in the fusion scheme

In this part, we investigate the contribution of the quality in the fusion process. The GQ can be used in 2 ways for:

- ✓ Selecting the best images of the sequence. We call this scenario: "BestIm";
- ✓ Weighting the different frames of the sequence. This scenario is called "AllIm".

In the following, below we compare the performance of a scheme where we first select the optimal number of good quality images, which are afterwards averaged, to a scheme where all the frames in the sequence (ten frames) are fused according to the global quality. Secondly, we also assess the interest of a local fusion in both scenarios.

- BestIm scenario:

In "BestIm", we compare the SR-NoQ, and SR-LQ fusion schemes for various numbers of frames ranked by their global quality GQ. Figure 5-9 shows the recognition performance at FRR@FAR=0.001 of these fusion methods for each dataset QFIRE05, QFIRE07 and QFIRE11. We have also plotted the SA scheme as the baseline fusion system.

We note that for QFIRE05, the FRR@FAR=0.001 tends to stabilize at 6 frames, without degradation by adding frames of lower quality. However this is not the case of QFIRE07 and QFIRE11: the FRR@FAR=0.001 decreases respectively until 4 and 6 frames and then increases drastically by adding frames of lower quality. This fact confirms the well-known paradigm that fusing images of bad quality degrades the performance in SR (SR-NoQ scheme). Moreover, these results

indicate that there are more images of good quality in QFIRE05 than in QFIRE07 and than in QFIRE11. From Figure 5-9, we notice that despite the ranking of the images according to their global quality GQ, using the local quality LQ in the fusion allows an improvement in the performance, especially when the number of frames exceeds the value 6 and this is true for all the databases.

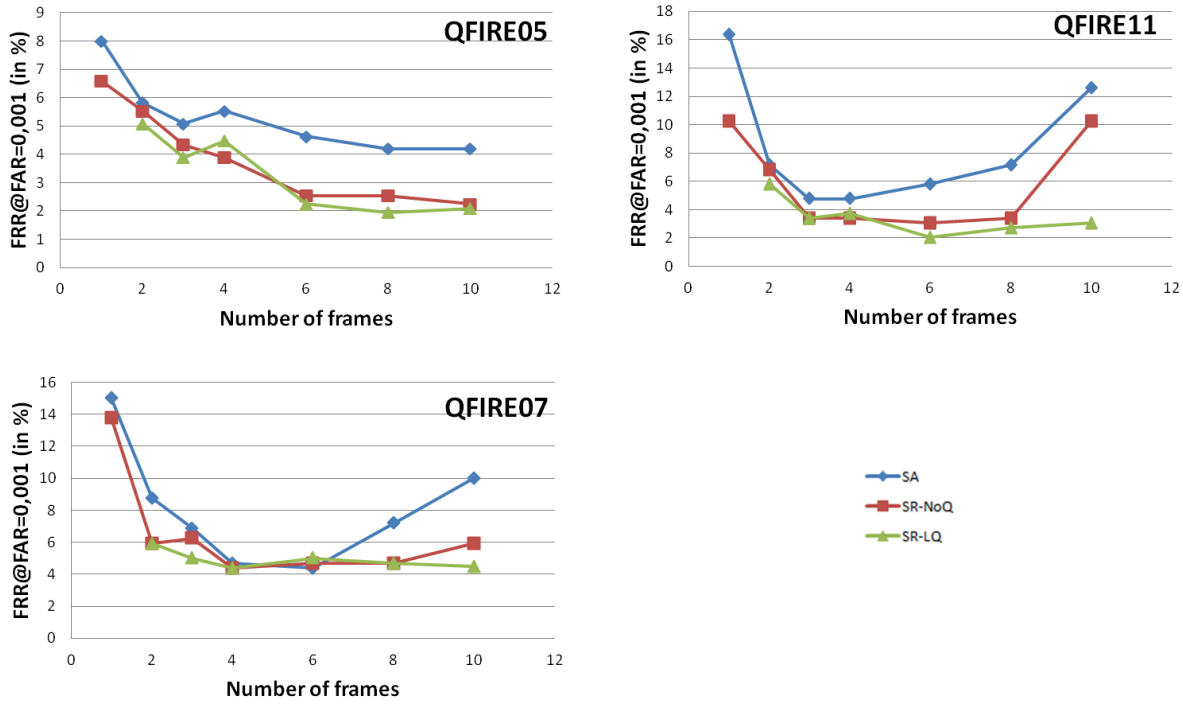

Figure 5-9: FRR@FAR=0.001 for various numbers of best frames for SA, SR-NoQ, and SR-LQ fusion schemes for each QFIRE dataset.

- AllIm scenario:

In AllIm scenario, we perform two weighted fusion schemes of all the frames by the GQ and the LQ which correspond respectively to the SR-GQ and SR-LQ schemes.

To compare this scenario with BestIm one, we report in Table 5-8 the best performances of the SR-NoQ of "BestIm" and the SR-GQ of "AllIm". In addition, the FRR@FAR=0.001 of the corresponding SR-LQ schemes is given in Table 5-8 for both scenarios.

Table 5-8: FRR@FAR=0.001 on QFIRE databases for the fusion schemes SR-NoQ of scenario BestIm and SR-GQ for scenario AllIm.

	QFIRE05		QFIRE07		QFIRE11	
Scenario	**BestIm**	**AllIm**	**BestIm**	**AllIm**	**BestIm**	**AllIm**
Number of frames	*6*	*10*	*4*	*10*	*6*	*10*
Use of the global quality	*2.54% [2.39-2.55]*	*2.09% [2.09-2.25]*	*4.37% [4.09-4.40]*	*4.68% [4.57-4.71]*	*3.07% [2.73-3.10]*	*7.5% [6.55-7.58]*
Use of the local quality	*2.24% [2.24-2.25]*	*2.09% [2.08-2.10]*	*4.37% [4.08-4.40]*	*4.48% [4.19-4.51]*	*2.04% [2.05-2.06]*	*3.07% [2.73-3.10]*

By comparing Table 5-7 and Table 5-8, we can see that introducing the global quality GQ criterion in the fusion gives a relative recognition improvement of 6.7%, 21.08%, and 26.69% at the FRR@FAR=0.001 point for resp. QFIRE05, QFIRE07, and QFIRE11, in the scenario AllIm. The improvement due to GQ is higher for QFIRE07 and QFIRE11 than for QFIRE05. This is due to the fact that these two datasets contain images of poorer quality. By incorporating our GQ measure into the fusion process, the contribution of each frame in the fused image will be correlated to its quality and in this way more weight is given to the high quality images. This result is in agreement with the outcomes of Table 5-3 and Table 5-5. Indeed, we obtained a significant improvement by introducing the GQ quality in the fusion for MBGC portal and Casia IrisV4-Thousand databases.

From Table 5-8, we notice that for QFIRE05, the use of the GQ in the fusion method (SR-GQ scheme of scenario AllIm) slightly outperforms the SR-NoQ of scenario BestIm. We conclude that when dealing with good images of equal quality in the sequence, there is no important difference in the performances between using the global quality inside the scheme for weighting all the images or selecting only the best images for performing the fusion process. However, for QFIRE11, the performances are better with a selection of the best images for the fusion than with a weighted fusion scheme of all the images (3.07% with BestIm compared to 7.5% with AllIm at the FRR@FAR=0.001). We deduce that low quality images, even if weighted by a low value, degrade the performance.

Concerning the use of the local quality as shown in Table 5-8,we observe that LQ does not allow us to increase significantly the performance for QFIRE05 and QFIRE07 neither for BestIm nor for AllIm. However, considering QFIRE11, we note an improvement with BestIm of 33.55% and an even larger one of 59.07% for AllIm. This is due to the fact that the iris images are more difficult to segment at this distance. Indeed, we assume that the LQ measure detects eventual errors of masks and

segmentation and assigns them a low value. The LQ-based fusion scheme allows therefore a more accurate weighting of the pixels in the fusion scheme than the GQ method.

In all cases, it is therefore interesting to use LQ in the fusion process, particularly since its use doesn't introduce extra complexity cost. In fact, we have to calculate the LQ to obtain the GQ (mean of the LQ values) and GQ must be computed on the 10 frames in both BestIm and AllIm scenarios. Moreover, the only difference between all the fusion schemes is in the weighting of the frames by either 1, LQ or GQ values. Therefore all the schemes have a similar complexity.

Conclusion:

We have shown the efficiency of the proposed system through extensive experiments performed on the challenging database QFIRE, which possesses videos acquired at various distances (5, 7 and 11 feet). Our approach is based on simple SR techniques applied on the different frames of a video, improved by taking into account some quality criteria.

We have tested two ways to use the GQ measure in the fusion process, one for weighting the fusion schemes such as done in Section 5.3.1 and one for selecting the best images.

Firstly, we have shown that super-resolution improves significantly the performance of iris recognition only when the images are of good quality. This is the case, when the fusion involves: (i) images taken from short distances or (ii) only best images coming from long distances. We assume that, thanks to the good quality of the images, there are fewer segmentation errors, and hence our image registration scheme in the SR is appropriate.

Secondly, we have noticed that the proposed method based on the introduction of a local quality in the super-resolution (SR-LQ approach) enhances the performance mostly when the quality of the images decreases. For the short distances, we assume that, as the images are well segmented and present no artifact on the iris area, introducing a local quality measure is not really necessary. For the long distances, on the contrary, the SR-LQ fusion allows a high improvement in the performance. Our explanation is that, at such distances, where many bad segmentations occur, the local quality measure is able to detect the bad-segmented pixels and to discard them from the fusion procedure. This way, the LQ weighted fusion procedure does not suffer too much from segmentation errors.

5.4. Conclusion

In this chapter, we have proposed several novel contributions to the problem of iris performance decrease due to degradations of the iris image, occurring when the acquisition is less restrictive. Our approach is based on simple SR techniques applied on the different frames of a sequence, improved by taking into account some quality criteria. Our main novelty is the introduction in the fusion scheme, at the pixel-level, of a local quality LQ measure relying on a GMM estimation of the distribution of a clean iris texture. This LQ measure can also be used to compute a global quality GQ measure of the normalized iris image.

We have tackled two different situations, namely video sequences of low-resolution resulting from an acquisition on the move (MBGC portal database) and sequences of multi-shot still images, presenting variability and therefore segmentation defaults (Casia IrisV4-Thousand database). We have also addressed the problem of video-based iris recognition at a distance (QFIRE databases).

To remedy to the degradation of the performance in such situations, we have proposed two quality-based super-resolution fusion approaches. Extensive experiments on all the databases show that the SR considerably reduces error rates. In addition, big improvement is obtained by the use of the global quality. Moreover, the local quality-based fusion scheme further increases the performance due to its ability to locally consider the different parts of the image and therefore to discard occluded and/or poorly segmented pixels in the fusion process.

In the next chapter, we will test other fusion schemes at the bit-level (quantized feature) and study the interest of quality criteria in this context.

Chapter 6. Quality assessment at the bit-level

As seen in the literature review of the previous chapter, fusion schemes can be performed at different levels. Recent approaches tend towards proposing approaches based on irisCodes [41] [169]. A particular attention has been devoted to the reliability of the bits in the irisCodes. Indeed, since several years, state-of-the-art has shown that sub-parts in these binary codes are more stable than others. This phenomenon is called consistent/inconsistent bits, also known under the name of fragile bits. A bit is fragile if its values changes across different acquisitions of the same iris. Therefore, integrating quality measures at this level in order to individually consider the reliability of each bit can be useful in the fusion scheme to enhance the performance of the recognition.

In Chapter 5, we have demonstrated the effectiveness of our local quality-based fusion scheme at the pixel-level on several challenging databases. However, at this point, a legitimate question can arise: Is it the best level to incorporate quality measures in a given fusion process? Moreover, can we perform a fusion scheme at the bit-level like recent works tend to, and obtain the same level of performance as what we obtained at the pixel-level? In this chapter, we will try to investigate these issues by conducting a simple comparative study between diverse fusion schemes. We will see the advantages and limitation of these approaches.

To understand the existence of fragile bits that appears in sub-parts of the irisCode, a literature review is related in Section 6.1. We will see several manners to exploit the consistence of the bits for improving recognition rate. Section 6.2 describes the proposed method that integrates a local quality measure, relying on a GMM model as presented in Chapter 4, at the bit-level. Finally, this proposed method and other fusion schemes implemented in the state-of-the-art are benchmarked on the challenging collections of QFIRE database, in order to answer these two questions:

- At which level quality assessment should be inserted?
- At which level the fusion should be performed in order to achieve best performance?

The results are given in Section 6.3.

6.1. Existence of consistent/inconsistent bits in the irisCodes

6.1.1. Related works

The existence of "fragile" bits was first formalized by Bolle et al. [192]. The authors noted that the empirical FRR was notably better than predicted by their theoretical model. They deduced that bits in a

given irisCode are not equally predisposed to flip (0 to 1 or 1 to 0) across different acquisitions of the same iris.

This was further investigated by Hollingsworth et al. in the well-know work [108] in 2009. Indeed, a bit in an irisCode is considered as fragile (or inconsistent) if there is significant probability of it ending up to 0 for some images of the iris and 1 for other images of the same iris. The existence of fragile bits was empirically shown on a subset of ICE database. A careful procedure has been followed to select the images of this subset: they are mostly un-occluded by eyelids and eyelashes. Moreover, only images with correct segmentation are kept. This process was done according to visual inspection. Several images for a given iris are selected: they represent the intra-class images. For each class, the corresponding irisCodes are created by using both 1D log-Gabor and multiple sizes of 2D Gabor filters. Then, the irisCodes are correctly aligned to an arbitrary one. All these considerations are carried out in order to conduct a study on irisCodes with less imperfection as possible. We recall that irisCodes are obtained by a coarse quantization of the complex number's phase in one of the four quadrants (see Figure 3-2). Several conclusions were derived from the experimental results:

- ✓ The middle bands of the iris contain more consistent bits that inner bands contrary to previous investigations that had been conducted in the literature [76] [193].
- ✓ The existence of fragile bits appears for both genders and with different type of filters for encoding the irisCode. Fragile bits come from the filter responses near quantization boundaries. Indeed, small changes in the complex number near the axes can induce quadrant switch. The authors noticed that larger filters lead to fewer fragile bits than smaller ones. Therefore, the fragility of a bit totally depends on the encoding algorithm.
- ✓ Fragile bits are invariant to blur noise in the iris images. This result is coherent with Bolle's work [192].
- ✓ Outlier values of complex numbers correspond to specular reflections in the original iris image.
- ✓ Masking fragile bits can reduce the FRR in a given iris recognition system.

Extended experiments have been carried out in [194] on their intern iris database. A new metric called Fragile Bit Distance (FBD) has been defined to improve the accuracy of the matching. It measures how well two fragile bit patterns are aligned. To identify the fragile bits, the real parts of the

complex number are first sorted. Then, according to Daugman's suggestion[3], the lowest quartile of values is considered as inconsistent bits (25%). The same procedure is done for the smallest imaginary values. Only un-occluded bits are taken into consideration. In fact, this method is not sufficient to detect bits coming from occlusions regions. Therefore, the mask given by the segmentation is still used. Given two irisCodes *A* and *B*, the FBD is computed as follows:

$$FBD = \frac{\left\| m_A \cap m_B \cap NOT(f_A \cap f_B) \right\|}{\left\| m_A \cap m_B \right\|} \quad (6.1)$$

where $\cap$ is the AND operators. $f_A \cap f_B$ represents a matrix containing the masked bits for fragility, while $m_A \cap m_B$ is a matrix that is composed of occluded bits. The result of the formula is a scalar value and represents the ratio of un-occluded bits masked for fragility in the comparison.

The results show that when this FBD measure is combined to the standard Hamming distance by multiplication, better performance are achieved than using solely Hamming distance. The EER is significantly reduced from 0.87 % to 0.79%.

In another way, the concept of reliable bits was used to reduce the number of bits needed for iris recognition. In [195], Dozier and al. proposed to reduce the number of irisCodes' bits by a factor of 30% without degrading the accuracy of the recognition (without increasing the FRR). The proposed method is jointly based on a genetic search and bits inconsistency in order to only select the most reliable bits of the irisCode. Ten intra-class irisCodes are used in the training stage for generating their corresponding fragile bit masks. The method was tested on a subset of ICE2006 database. Iris boundaries are automatically detected by two circles, while the eyelids and eyelashes were manually segmented in order to obtain good segmentations at the end.

In [196], Rathgeb et al. suggested a selective bits method for iris recognition. The approach is able to extract the most discriminative bits coming from two irisCodes that have been created by two different algorithms. The resulting irisCode is smaller than both individual templates. The selection is based on a reliability mask that provides the stability of each bit with respect to genuine and impostor comparisons for a given algorithm. The reliability at each bit position is defined as:

[3] Personal communication between the authors and John Daugman. No reference is provided in the paper.

$$R(i) = P_{genuine}(i) + (1 - P_{impostor}(i))/2 \quad (6.2)$$

where is P is the probability of a bit-pair of being 0-0 or 1-1.

According to this mask, an ideal permutation of bit positions is extracted for each encoding algorithm and applied to sort the bits of the irisCodes: first bits are considered as more reliable than last ones. Based on this information, for each algorithm the last half bits of each irisCode is removed. The new template is thereby the result of the concatenation of the two best half parts of bits of the two algorithms. The experimental results show an improvement of 0.37% at the EER operating point compared to the concatenation of the two initial irisCodes. The proposed method provides a trade-off between accuracy and processing time for recognition purpose. The approach was learned and tested on a subset of good quality taken from CASIA-V3-Interval dataset.

Based on this reliability mask, in [197] Rathged et al. proposed this time an incremental method to iris recognition (identification mode) by rejecting in an early stage unlikely matches. More precisely, partial bit comparisons of the probe with each gallery are performed for a given window size. Most reliable bits are first compared thanks to the reliability mask. All the partial Hamming distances are combined with the corresponding obtained Hamming distances from the previous windows. For each iteration, templates of the gallery set with high combined Hamming distances are rejected (dissimilarity score). The other ones are kept: they have better chance for belonging to the correct claimed identity. The approach is benchmarked on the same good quality images as in [196]. For a same portion of bits compared between the probe and gallery, the proposed incremental approach achieves a better identification rate than just comparing sorted irisCodes.

Gentile et al. [198] also suggested reducing the length of irisCodes by extracting highly discriminatory regions. To this end, two analyses have been investigated on a training subset:

- ✓ An analysis based on the Kolmogorov-Smirnov criterion is carried out to identify the rows of the irisCodes that contain most discriminative information. It consists in determining the capacity of each row in separating the genuine and impostor score distributions. The middle band of the iris was found to contain higher information than the inner and outer bands as shown in [108].
- ✓ By estimating the correlation between the rows, high local correlations between nearby irisCode rows have been pointed out. This phenomenon confirms Daugman's

observation in [13]: “Iris patterns such as furrow or ciliary tend to spread across a significant radial distance in the iris, leading to radial correlations”.

These two facts were taken into consideration in order to reduce the size of the irisCode compared to the initial one, without significant degradation in the performance. The approach was validated on images of MMU dataset [199] that have been well segmented (visual verification). The results show slight performance degradation between full length irisCodes (FLICs) and short length irisCodes (SLICs). But, the overall recognition system operates faster with less required memory.

SLICs have been also used in [200] to accelerate the iris recognition process. First, based on bits comparison between SLICs of the whole gallery and the probe, a short list of the top 10 candidates from the gallery is proposed. Then, Hamming distances are calculated between FLICs of the probe and of the short list instead of the entire gallery. Compared to Rathged's work [197], the inconvenient of this approach arises when the correct identity to claim is not included in the short list and this cannot be fixed in the later stage. This limits the true positive rate to approximately 93%.

Dong et al. [201] suggested a personalized iris-matching approach using a class-specific weight map learned from the training images of the same iris class. The personalized weight map of class A denoted W_A contains different weights. These values reflect the reliability of each bit in the iris matching step. The stability of a bit i is computed as follows:

$$w_i = 2 \cdot \frac{m_1^2 + m_0^2}{(m_1 + m_0)^2} - 1, with \quad m_1 + m_0 = n \quad (6.3)$$

where, n is the number of templates in the same class, m_1 and m_0 are respectively the number of time that the bit i is equal to 1 and 0.

The robustness of the personalized weight map depends on the number of intra-class training samples. To obtain an effective map, a large number of training images per class is required, which increases the computational cost.

For each class, a weight map is associated to the corresponding template in the gallery. It has the following properties:

- ✓ High values indicate more stable iris matching results than low values.
- ✓ The weight map cannot replace the binary mask given by the segmentation. The weights are not equal to zero in occluded regions.

- ✓ A general weight map can be derived by averaging all personalized weight map. It reflects the reliability of the matching results on different regions, statistically learned by all iris classes of the database.

The proposed matching score strategy improves the traditional Hamming distance by introducing the weighted map in the matching procedure. For instance, the matching score between a probe *B* and a gallery *A* is obtained as follows:

$$HD_A = \frac{\left\| (IrisCode_A \oplus IrisCode_B) \cdot W_A \right\|}{\left\| W_A \right\|} \quad (6.4)$$

where $\oplus$ is the XOR operator, W_A is the personalized weight map of the iris class A.

This concept is similar to the "fragile bits" work of Hollingsworth [108]. Extensive experiments on several databases have shown the improvement brought by the proposed matching scheme compared to the traditional Hamming distance, especially in the case of poor-quality iris images.

In [139], Chen et al. proposed a wavelet-based local quality metric that estimates the energy in a given concentric band of the iris. Then, this local quality measure was incorporated in the Hamming distance as follows:

$$HD_{Weighted} = \frac{1}{L} \cdot \frac{\sum_{i=1}^{L} \sqrt{E^A_{g(i)} \times E^B_{g(i)}} \cdot \left(IrisCode_{A_i} \oplus IrisCode_{B_i} \right)}{\sum_{i=1}^{L} \sqrt{E^A_{g(i)} \times E^B_{g(i)}}} \quad (6.5)$$

where $IrisCode_{A_i}$ and $IrisCode_{B_i}$ represent the i^{th} bit in the irisCode A and irisCode B respectively, of length *L*. $g(i)$ is the index of the band that contains the i^{th} bit of the irisCodes. $E^A_{g(i)}$ and $E^B_{g(i)}$ are the associated local quality measures of the $g(i)^{th}$ band in iris images *A* and *B* respectively. According to formula 6.5, regions with high quality in both irisCodes contribute more in the computation of the Hamming distance than regions of poorer quality. This weighted scheme is very similar to Dong et al. and Hollingsworth et al. approaches.

The notion of fragile bits has been also observed in irisCodes computed from iris taken in visible wavelength as shown in a more recent work [202].

6.1.2. Synthesis and conclusion

The concept of consistent/inconsistent bits has been addressed in several works of the literature as cited before and the phenomenon was observed on several iris databases. In most works, the authors ensure that the selected images are of good quality [108] [196] [197]. Moreover, the segmentation is verified by visual inspection in order to keep only good segmented irises for benchmarking the proposed method [108] [195] [198] [200]. In most of the works, a training phase is carried out to identify the fragile bits by using intra-class variability [192] [198] [201] [200] or by considering both intra and inter class data [196] [197] [202]. Several images per iris class are required to assess the reliability of the bits. Extensive experiments in [108] and [201] have shown that the stability of the bits depends on the encoding algorithm.

Those approaches can be categorized into 3 classes according to the strategy that was employed to handle the inconsistent bits:

- ✓ Creation of a binary quality mask [194].
- ✓ Creation of a weighted quality mask [139] [201].
- ✓ Reduction of the number of bits in the irisCodes by keeping the most discriminative ones [195] [196] [197] [198] [200].

Only in the work of Dong et al. [201], the weighted Hamming strategy was tested on an iris database that has been captured under less constrained conditions. However, the estimation of the personalized weighted map requires a large number of images (20 images) for every iris class in the gallery.

We note that all the cited works in the previous sub-section are evaluated by performing a matching between two still iris images (matching: 1 to 1). Major approaches are tested on images on good quality. These two facts are in disagreement with the video based recognition context that has been addressed in this thesis.

However, this existence of consistent/inconsistent bits has inspired some researchers in developing fusion approaches that integrate the reliability of the bits. Indeed, in recent works, some authors proposed to fuse iris sequences at the bit-level (irisCode) [41] [169]. The reliability of each bit in the irisCodes is taken into consideration in the fusion procedure in order to extract the most relevant information. This idea is motivated by the concept that not all the bits are equally consistent as proven in previous related works. For instance in [169], the proposed iris fusion is based on the reconstruction

of an optimized irisCode with a high number of reliable bits and a low number of inconsistent bits. In another way, in [41], a weight mask which can measure the reliability of each bit in the reconstructed irisCode, is used to compute weighted Hamming distances in the matching stage. Both works are benchmarked only on high quality images, carefully selected by a quality assessment algorithm [169] or manually checked [41].

In this chapter, we propose to introduce our previous local quality at the bit-level. We believe that our measure is able to identify consistent bits in the irisCodes and hence able to enhance recognition performance. Contrary to [41] and [169], we propose to use all the frames of the sequence and not only high quality images. Indeed, as our main interest is to improve iris recognition in less restrictive environment of acquisition, we decided to keep all the frames, including this way possible low-quality images with eventual segmentation errors, corresponding to more realistic situations.

6.2. Integration of the local quality at the bit-level in the fusion process

One way of integrating our local quality metric in the fusion process is to create a quality mask that measures the reliability of each bit in an irisCode. There are two ways for exploiting this quality mask.

The first one consists in defining empirically a threshold for binarizing the real values of the quality measures in order to generate a binary mask. Regions with lower qualities than the fixed threshold would be masked. This mask is then combined to the mask that is obtained in the segmentation stage. This final binary mask is incorporated in the computation of the Hamming distance as was done by Hollingsworth et al. [194] as well as in Krichen's thesis [203].

The second case consists in introducing a weighted quality mask in the estimation of the Hamming distance as performed in Krichen's thesis [203], as well as Chen et al. in [139] and Dong et al. in [201]. Compared to a binary strategy, the weighted scheme has the advantage of taking into consideration real values of local quality measures. In that way, the higher the quality of the region is, the higher the contribution in the computation of the Hamming distance will be. There is no loss of information compared to the binary strategy. Therefore, we decided to use this weighted scheme since our goal is not to classify regions into iris and non-iris but to quantify the reliability of the bits.

If we consider a matching scenario based on a comparison between two single iris images A and B, the weighted Hamming distance is computed as follows:

$$HD = \frac{\sum_{i=1}^{L} \left\| \left(IrisCode_{A_i} \oplus IrisCode_{B_i} \right) \cap \left(M_{A_i} \cap M_{B_i} \right) \times LQ_{A_i,B_i} \right\|}{\sum_{i=1}^{L} \left\| \left(M_{A_i} \cap M_{B_i} \right) \times LQ_{A_i,B_i} \right\|} \quad (6.6)$$

$$with \begin{cases} LQ_{A_i,B_i} = LQBin_{A_i} \cap LQBin_{B_i}, & if \quad binary \quad strategy \\ LQ_{A_i,B_i} = \min\left(LQ_{A_i}, LQ_{B_i}\right), & if \quad weighted \quad strategy \end{cases}$$

where $IrisCode_A$ and $IrisCode_B$ are the binary codes resulting from the feature extraction of the normalized iris images A and B, M_A and M_B are the binary masks given by the segmentation stage of iris A and B, and $LQ_{A,B}$ is the local quality associated to the couple (A, B). L is the length of each irisCode.

However as we deal with iris sequences and not single images, the Hamming distance given in Formula 6.6 is not directly exploitable. Some modifications should be introduced to carry out a matching based on a comparison between two iris sequences instead of two still images.

Proposed technique:

One way to perform a fusion scheme at the bit-level is to perform a weighted average by multiplying the bits of each irisCode by their corresponding value from the local quality matrix. To this end, we first have to segment and normalize each frame of the sequence. The iris features are then extracted from each normalized iris image. Thereby, we obtain a series of different irisCodes. Then, a weighted average is computed by multiplying each irisCode by its corresponding value from the local quality matrix that is computed from the normalized iris image. A "fuzzy" irisCode with real values is thus obtained. To establish a dissimilarly score based on the Hamming distance, we have to binarize the values of this fused irisCode. To this end, a threshold should be fixed.

After several tested thresholds, the results of this fusion scheme were not promising. In addition to that, this method has several drawbacks. The binarization of the fused irisCode requires a certain threshold as explained before. This value is empirically fixed after several tests in order to optimize the recognition rate. The threshold depends on the database. Moreover, this scheme demands several additional operations compared to the fusion schemes we developed in the previous chapter at the pixel-level: each normalized images coming from the sequence has to be encoded instead of only encoding the fused normalized image.

As the biometric decision is based on the comparison scores given by the Hamming distance in our case, we believe that it is more judicious to directly exploit the local quality in the computation of this value as an indicator on the reliability of the result of the comparison instead of performing this scheme. Therefore we have proposed an alternative solution which is quite similar to the local quality-based fusion (namely SR-LQ) that has been illustrated in Figure 5-2. To better understand the differences between these two schemes, we give the architecture of the proposed fusion scheme at the bit-level in Figure 6-1.

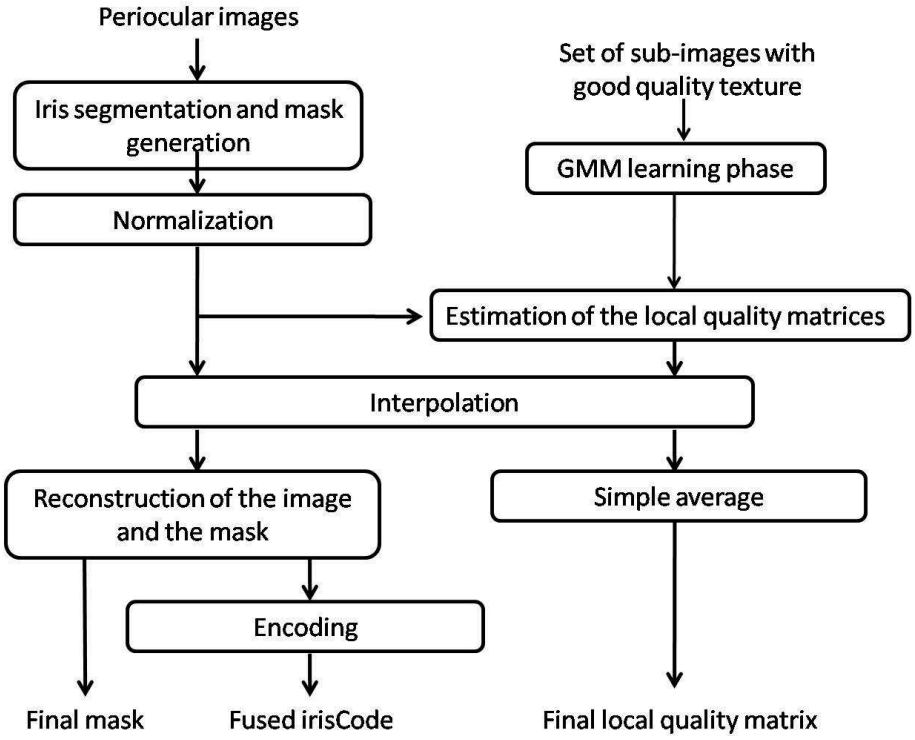

Figure 6-1: How to obtain the fused irisCode, mask and local quality matrix for performing template matching.

For each frame of the sequence, the iris is first segmented. Then, the iris texture is unwrapped to obtain a normalized iris image which is then bi-linearly interpolated. The resulting images are then averaged to get one unique HR image which is encoded using 2D Gabor filters. Three filters of different sizes are used. To generate the irisCode, the real and imaginary parts of the phase response are quantized in a pair of bits according to their position in the quadrant. OSIRISV4.1 is used to perform all these steps. For more details, see Section 3.2.1. In parallel, the normalized masks are also interpolated in the same way as the normalized iris images. We specify that the fused irisCode and the

final mask correspond to the results given by the SR-NoQ fusion scheme as no quality is used to reconstruct the fused irisCode. (SR-NoQ is previously presented in Chapter 5).

As in SR-LQ, on each normalized iris image of size $64x512$, we applied the GMM5obs model to non-overlapped sub-parts of dimension $4x8$ as illustrated in Figure 4-5. As a result, we obtain a matrix of 1024 local quality measures. Then, these local quality matrices resulting from all the iris images of the sequence are bi-linearly interpolated and then averaged. Finally, we get a local quality matrix of the same size of the reconstructed image and the final mask.

At the end, for a given sequence, we obtain at final a single irisCode, a binary mask and a local quality matrix as illustrated in Figure 6-1. We recall that our ultimate goal is to compare the performance between a quality-based scheme at the pixel and at the bit-level. This comparison would allow us to determine at which level the quality should be introduced. As our best quality-based fusion scheme is SR-LQ, we decided to perform the same interpolation step in this new proposed fusion scheme in order to achieve a fair comparison.

Finally, to get a matching score between two sequences of irises *A* and *B*, we compute the weighted Hamming distance according to formula 6.7 in which $\overline{IrisCode_A}$ and $\overline{IrisCode_B}$ represent the fused irisCodes of irises of classes *A* and *B* respectively, $\overline{M_A}$ and $\overline{M_B}$ are the fused masks that are used to mask the occlusions of the reconstructed image. $\overline{LQ_{A,B}}$ contains the minimum values between the final local quality matrices associated to the couple *A* and *B*. *N* is the number of application points. The procedure is depicted in Figure 6-2.

$$HD = \frac{\sum_{i=1}^{L} \left\| \left(\overline{IrisCode}_{A_i} \oplus \overline{IrisCode}_{B_i} \right) \cap \left(\overline{M}_{A_i} \cap \overline{M}_{B_i} \right) \times \overline{LQ}_{A_i,B_i} \right\|}{\sum_{i=1}^{L} \left\| \left(\overline{M}_{A_i} \cap \overline{M}_{B_i} \right) \times \overline{LQ}_{A_i,B_i} \right\|} \quad (6.7)$$

The Hamming distance map of Figure 6-2 represents the results of the comparisons between each pair of bits of the irisCode at the application points. It contains binary values: 0 if the two bits are equal (represented in green), otherwise 1 (shown in red). This map is multiplied by a binary mask and a local quality map to get a weighted Hamming distance map. More precisely, for each couple of non-occluded bits, a real-valued local quality measure is associated to the result of the bit-pair comparison. We believe that this association is able to measure the reliability of the pair-bit comparison.

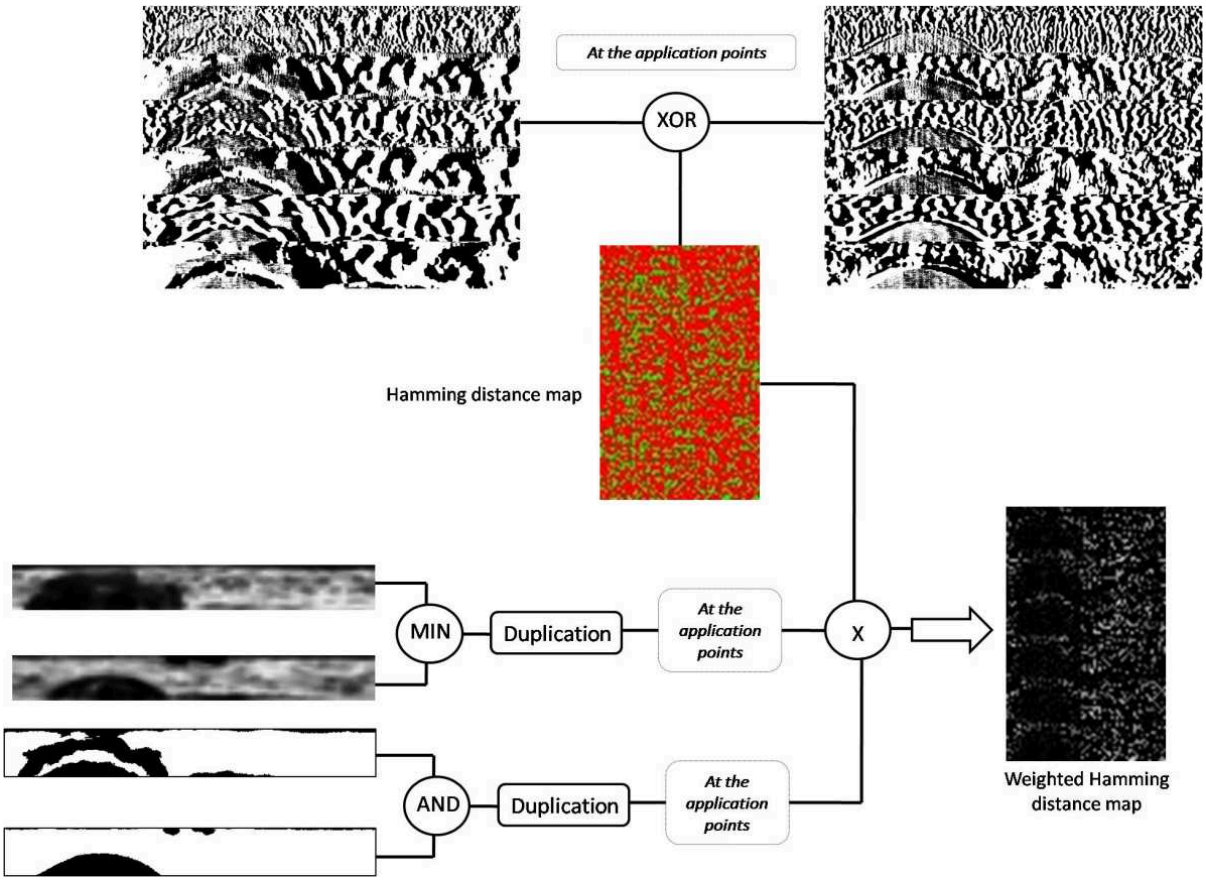

Figure 6-2: Creation of the weighted Hamming distance map.

To generate the local quality map, we have chosen to take the minimum value between the two local quality matrices associated to *A* and *B*. As shown in Chapter 4, these resulting values are well correlated to the performance of the recognition. As explained before, there is no consensus on how to combine two quality measures. Multiplication or simple average could also be performed.

We note that the procedure of weighted Hamming distance computation that is illustrated in Figure 6-2 is repeated several times, with different values of shift that are applied on the fused irisCodes, masks and local quality matrices. Only the minimum value of all comparisons is retained to represent the matching score. We called this quality-based fusion scheme at the bit-level: "SR-HDxLQ".

6.3. Comparative evaluations

6.3.1. Experiments and results

In this sub-section, we will first conduct a comparative evaluation between the best fusion scheme at the pixel-level validated in the previous chapter namely the local quality-based scheme (SR-LQ) and the proposed method at the bit-level described above (SR-HDxLQ). This comparison will allow us to determine which weighted local quality strategy leads to best performance. We note that in both schemes, the same reference system OSIRISV4.1 is used for the segmentation, the normalization and the feature extraction stages. Besides, the same quality assessment algorithm (GMM5obs model) is used to measure the local qualities, leading to the same local quality matrices.

The evaluation is conducted on QFIRE05, QFIRE07 and QFIRE11 as in Section 5.3.2. All the frames of the sequences are used in the fusion schemes. Note that no global quality is used to sort the images. This protocol corresponds to the AllIm scenario described in Section 5.3.2.3. We performed the same genuine and impostor comparisons. To assess the performance of each method, we report the FRR at FAR=0.001 in Table 6-1.

Table 6-1: FRR@FAR=0.001 on QFIRE databases for the fusion schemes: SR-LQ and SR-HDxLQ.

	QFIRE05	QFIRE07	QFIRE11
SR-LQ	*2.09%*	*4.48%*	*3.07%*
SR-HDxLQ	*2.84%*	*5.62%*	*4.77%*

For all the QFIRE databases, we can see that the quality weighted scheme at the pixel-level achieves better performance than the bit-level. More precisely, we note that performance degradation increases as the quality of the images of the database become worse. A significant increase of 0.75%, 1.14%, and 1.70% is respectively observed at the FRR@FAR=0.001 for QFIRE05, QFIRE07, and QFIRE11. Consequently, we can conclude that the best method, out of the two tested quality-based fusion schemes, is SR-LQ whatever the database.

This is not the results we expected. Indeed, as explained in Section 6.1.1, several works have demonstrated the effectiveness of combining a reliability map to the standard Hamming distance in order to estimate a matching score between two still iris images such as proposed by Hollingsworth et

al. in their popular work [194], which inspired latter various works in the literature. The reliability map has also proven its effectiveness in enhancing the performance in the case of matching iris sequences instead of single images as done in a more recent work [41]. Moreover in [169], Mahadeo et al. have shown that irisCodes' fusion achieves better performance that images' fusion with masking fragile bits. However as pointed out in Section 6.1.2, these proposed methods [41] [169] [194] are benchmarked only on images of good quality contrary to our tested iris database.

To better understand our results, we decided to implement the two following approaches:

- Signal fusion + masking fragile bits: *SR-HDxFB*

This fusion scheme is done at the signal level as proposed by Hollingsworth in [162]. This scheme corresponds to the SA approach described in Chapter 5. It consists in averaging the frames of the sequence to create a single image. After that, as suggested in [108] [194] by the same authors, the fragile bits are identified in order to create a binary mask. These bits are coming from complex coefficients which lie near to the real and imaginary axes. Indeed, these bits might end up as a 0 or a 1 across different irisCodes of the same iris image. The un-occluded bits corresponding to the 25% imaginary and real lowest values are considered as fragile and hence masked. We call this mask: *fragile bit map*. Fewer bits will contribute in the computation of the Hamming distance but each of them is more consistent. To establish a fair comparison with our proposed method, we performed an interpolation step before averaging the images. This method will allow us to evaluate our local quality map in the detection of the inconsistent bits compared to this fragile bit approach. In other words, the Hamming distance is computed according to formula 6.7, but this time the LQ_{A_i,B_i} is as follows:

$$LQ_{A_i,B_i} = FB_{A_i} \cap FB_{B_i} \qquad (6.8)$$

where FB_{A_i} and FB_{B_i} are respectively the fragile bit maps of iris *A* and *B*.

Figure 6-3 depicts an example of fragile bits map for a given irisCode resulting from the feature extraction module of OSIRISV4.1. The locations of the fragile bits are coherent with those in [108]: smaller Gabor filters have fewer consistent bits than larger ones.

- IrisCodes' fusion approach: *SR-OptimizedIC*

We have also implemented the approach of Mahadeo et al. in [169], already explained in Section 5.1.1. Only one modification was done in order to achieve fair comparison with our approach. Indeed, instead of computing the irisCodes from the normalized iris images of the sequence, we have

performed a prior step of interpolation on the images as in our scheme. Therefore the resulting optimized irisCode is of double size compared to [169]. We call this approach: SR-OptimizedIC.

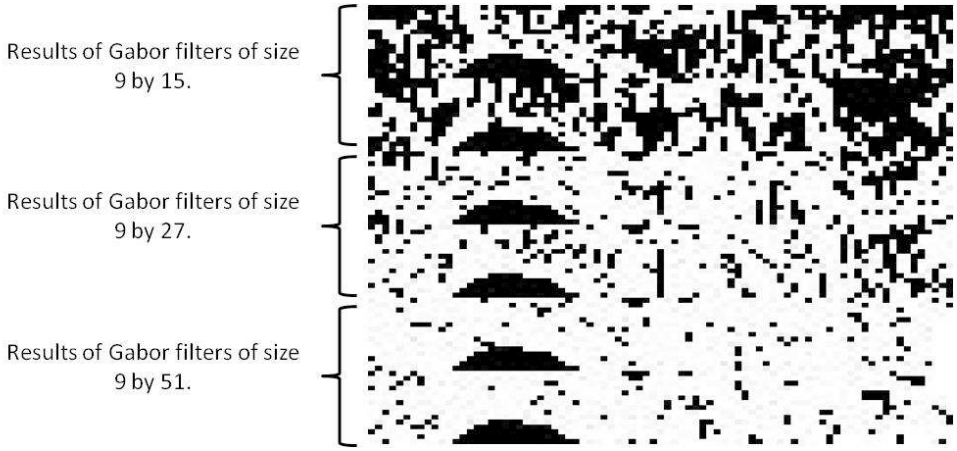

Figure 6-3: An illustration of a fragile bit map of a given irisCode. Fragile bits are represented by black pixels.

The same protocol is used to benchmark these two methods on the three QFIRE databases. To conduct a comparative study between all the algorithms, the FRR at FAR=0.001 on the QFIRE databases are tabulated in Table 6-2.

Table 6-2: FRR@FAR=0.001 on QFIRE databases for the fusion schemes: SR-HDxFB and SR-OptimizedIC.

	QFIRE05	QFIRE07	QFIRE11
SR-HDxFB	*2.82%*	*8.75%*	*12.28%*
SR-OptimizedIC	*5.53%*	*10.01%*	*9.55%*

i. Validation of the reliability map:

From Table 6-1 and Table 6-2, we observe that SR-HDxLQ and SR-HDxFB methods give similar performance on QFIRE05: 2.84% vs 2.82%. This is not the case on QFIRE07 and QFIRE11, for which the SR-HDxLQ scheme outperforms the SR-HDxFB approach. Moreover, performance degradation increases as the acquisition distance increases too. More precisely, the FRR@FAR=0.001 respectively increases by a value of 3.13% and 7.51% on QFIRE07 and QFIRE11.

The well-known method SR-HDxFB had proven its effectiveness in detecting the fragile bits in [108] [194]. However, the method was benchmarked only on images of good quality. The fact that QFIRE05 contains images with better quality than the other database, can explain the comparable performance of our SR-HDxLQ scheme and the SR-HDxFB method on this database. We deduced that our method is also relevant to identify the fragile bits. In the case of lower quality images (QFIRE07 and QIRE11) our method gives better results.

ii. Comparison with an IrisCodes fusion approach:

We note from Table 6-2 that the approach based on the fusion of irisCodes (SR-OptimizedIC) leads to higher errors at the FRR@FAR=0.001 than SR-HDxFB whatever the tested iris database. This is in contradiction to the results in [169]. We believe that the fact that they only select the best frames of the sequence is the reason of this disagreement. Indeed in [169], an automatic quality assessment algorithm is performed in order to identify high quality frames in a sequence. After that, only best frames are used to perform the fusion.

The bad performance may be also caused by the number of irisCodes used in order to generate the optimized irisCode. Indeed, the authors have tested several cases in order to retain the number that maximizes the recognition rate on a specific database. These two reasons can explain the ineffectiveness of detecting consistent/inconsistent bits on our tested databases.

iii. Comparison with our local quality-based fusion:

We can see from Table 6-1 and Table 6-2 that the algorithm which achieves the best performance is the SR-LQ whatever the tested database.

6.3.2. Discussion and conclusions

The comparative study between the different implementations shows the following statements:

- ✓ Better performance is obtained by the local quality-based scheme at the pixel-level (SR-LQ) than the bit-level (SR-HDxLQ).
- ✓ The standard fragile bits method proposed by Hollingsworth et al. [194] is not suitable for images of low quality resulting from less restrictive condition during the acquisition.
- ✓ Approach based on irisCodes' fusion [169] is not appropriate when the images are not of high quality.

The results show that the SR-LQ scheme outperforms the SR-HDxLQ method for all the databases. It is better to perform a local quality weighted scheme at an early stage in the fusion process.

This fact points out that it is better to try to reconstruct a normalized iris image of the best quality as possible that will be used for the further steps i.e. encoding and template matching, than reconstructing a normalized iris image with latent artifacts, then performing encoding stage and only after that, using a quality measure at the last stage i.e. in template matching. Therefore, we believe that artifacts should be handled before quantizing the features into pairs of bits i.e. before degrading the signal. In fact, quantization of the features leads to a loss of information that our local quality is not able to compensate.

The key of successful schemes of fusion relies on the quality of the images that are used in the fusion process. Indeed, in both works [169] [194], the fusion at the bit-level is compared to an approach at the pixel-level on images that have been carefully selected according to their quality. Their results show best performance for the bit-level approach. However, we have shown that such fusion schemes are relevant only thanks to the high quality of the images. These related results combined with those obtained in this chapter, make us saying that approaches based on bits are more sensitive to the quality of the initial iris images. However, they lead to best performance only when one deals with images of high quality.

6.4. Conclusion

We have demonstrated in this chapter that the local quality developed in Chapter 4, also used in Chapter 5 as a local weighted tool in the fusion process, is relevant to assess the reliability of a bit-pair comparisons. However, on the challenging QFIRE databases, our local quality-based fusion scheme at the pixel-level achieves better performance than the proposed bit-level fusion scheme. In less restrictive acquisition, our investigations have shown that quality assessment should be incorporated in early stage throughout the fusion scheme, i.e. before degrading the signal in the quantization phase.

Literature results and our ones showed that approaches based on bit-level gives better performance than those at pixel-level in ideal conditions i.e. images with no imperfection such as segmentation errors, strong occlusions. However, this is not the case with images of low quality. Therefore, in scenario with non cooperative subject, we do not think that such approaches could be appropriate to enhance the performance of the recognition.

Chapter 7. Conclusions and perspectives

This PhD dissertation has addressed the problem of video-based iris recognition under less constrained environment. The authentication was performed in three challenging scenarios: at a distance and on the move, (ii) with intra-class variation (dilation, eyeglasses...) and (iii) at large distances in still positions. In such conditions, the captured images suffer from diverse degradations e.g. blur resulting from out-of-focus or/and motion blur, eyelids and eyelashes occlusions, specular reflections, shadows, off angles, uneven illumination, low contrasts between the boundaries and lack of resolution. All these perturbations dramatically affect the overall performance of the recognition system.

Taking advantage of disposing of several iris images in uncontrolled acquisition mode, we proposed to fuse the information available in each iris image of the sequence, in order to obtain a final optimized template, on which the recognition will be performed. More precisely, quality-based super-resolution methods in the pixel domain were elaborated in order to synthesize a clear high-quality iris image from multiple low-quality normalized iris images aiming at improving the recognition accuracy. Therefore, the main research focus of this thesis is two-fold: (i) designing a relevant quality measure and (ii) developing a fusion scheme based on super-resolution improved by taking into account this quality measure.

We have first elaborated a quality measurement algorithm able to locally measure the quality of the iris texture. This measure was later exploited in the proposed fusion scheme. Our quality measure is based on a Gaussian Mixture Model. The GMM was trained on highly textured sub-images free from any degradation. The choice of the input vectors to the model was guided by different experiments aiming at characterizing at best iris texture patterns. The quality measure is a value between 0 and 1. High values indicate regions well textured without artifacts. In contrast, low values are associated to regions containing perturbations such as artifacts, poorly textured region and pixels wrongly segmented. Consequently, we are able to distinguish between the high-quality and low-quality regions in normalized iris images. A global quality can be defined by using the different local quality measures estimated on different sub-parts of the normalized iris image.

To evaluate our quality measure, we followed the protocol defined in IREX II - IQCE report of NIST. A global pairwise quality is associated to each matching couple by taking the minimum between

the local qualities of the two normalized iris images. We have demonstrated the pertinence of our quality measure by showing its correlation to the recognition rate. Moreover, we have shown the strong relationship between our quality measure and (i) the amount of texture in non-occluded regions of the iris: we have proven the capacity of our quality measure to measure the amount of texture by discriminating highly textured regions from poorly textured ones and (ii) the usable iris area: we have shown that our quality metric supplies more pertinent information for classifying the images into low, medium, and high quality, than the usable iris area which is as far the most influential factor on the recognition rate as pointed in the IREX II - IQCE report. Moreover, by combining the information brought by the normalized iris mask and our quality measure further recognition improvements are observed by rejecting the couples of lowest quality.

These two factors considerably influence the accuracy of the recognition. Consequently, the developed quality measure can be considered as a relevant tool for estimating iris quality in the perspective of biometric verification.

As a second achievement, we have proposed quality-based super-resolution approaches for fusing iris sequences in order to improve the performance. This strategy can handle two types of issues for iris recognition which are the lack of resolution and the presence of various artifacts in the iris images. The fusion was carried out on the normalized iris images at the pixel-level. The super-resolution is based on a simple bilinear interpolation. As well known, SR techniques can remedy to poor resolution in the images. Despite the simplicity of the SR model implemented, the experimental results shown the effectiveness of this approach in improving the accuracy of the performance on several challenging iris databases. In order to further improve the previous results, we have proposed to exploit our quality measure in the fusion scheme. This quality measure can be considered globally or locally in order to decrease the effect of low quality images in the SR, which leads to a decrease in performance producing a rather counterproductive effect.

The global quality can be used in two ways: (i) as a selection tool: it allows performing the fusion using only the best images of the iris sequence and (ii) as a weighting factor in the same way as proposed in the literature. In this case, it permits to give less contribution to the low quality images of a given sequence in the reconstruction of the fused template. Compared to the state-of-the-art, the interest of our quality measure consists in the estimation of one unique quality measure avoiding a combination phase of various quality measures, which requires identifying a priori the nature of each degradation.

Our main novelty is the introduction of a local quality measure in the fusion scheme. Performing a local weighting in the image fusion scheme allows us to take into account the fact that degradations can be different in diverse parts of the iris image. This means that regions free from occlusions will contribute more in the reconstruction of the fused image than regions with artefacts. Using a local measure instead of a global one as done in the literature was motivated by our intuition that the quality in an iris image is not globally identical. In fact, eventual errors of the segmentation masks can occur in the normalized iris images especially in uncontrolled acquisition mode which is our case. Indeed, in general iris images that are captured at a distance or/and on-the-move suffer from blur and low contrast between the pupillary and limbic boundaries and from strong occlusions on the iris area. These degradations induce errors on iris localization, which particularly influence the precision of the iris segmentation and consequently the quality of the normalized iris texture. In this case, two normalized iris images resulting from different acquisitions of the same person, present a high discrepancy and consequently one must be very careful in fusing such images. Therefore, it is important to accurately consider the quality of the images in the fusion process in order to increase the recognition performance.

Extensive experiments were performed on several commonly used iris databases: MBGC portal and Casia-Iris-Thousand. We separately investigated the improvement brought by the super-resolution, the global quality and the local quality in the fusion process. In particular, the experimental results show the important improvement brought by the use of the global quality in the fusion process, improvement that is even increased using the local quality. These results confirm our intuition: the local quality is able to detect local noisy regions in the normalized iris images. By assigning small values to those regions, the reconstructed HR image is of better quality.

Moreover, the approaches were also evaluated on the new challenging database QFIRE, at three different distances: 5, 7 and 11 feet. Firstly, we have shown that SR enhances significantly the recognition rate when the images are of good quality. This is the case, when the fusion is applied on iris images taken from short distances or only on the best iris images coming from long distances. We believe that, thanks to the good quality of the images, there are fewer segmentation errors, and hence our image registration scheme in the SR is appropriate. Secondly, we have observed that the proposed method based on the incorporation of a local quality in the SR improves the performance mostly when the quality of the images decreases. For the short distances, we assume that, as the images are well segmented and present no artifact on the iris area, introducing a local quality measure is not really necessary. For the long distances, on the contrary, the local quality-based fusion scheme allows a high

improvement in the performance. Our explanation is that, at such distances, where many bad segmentations occur, the local quality measure is able to detect the bad-segmented pixels and to discard them from the fusion procedure. This way, the fusion procedure does not suffer too much from segmentation errors, thanks to the local quality weighting.

Finally, we have conducted a simple study to determine on which representation of the iris (pixel, feature or bit) our quality measure should be incorporated in the fusion scheme in order to obtain the best performance. The experimental results showed that the local quality led to better recognition rates when the measure is introduced at the pixel-level than at the bit-level. This fact pointed out that the degradations that can occur on the normalized iris images in the fusion should be handled at an early stage. In fact, the quantization of the features into binary codes leads to a loss of information that our local quality is not able to compensate.

This thesis opens up some perspectives and directions for future works:

A first point would be to improve the registration step in the super-resolution. Indeed, image alignment is an essential task in the fusion process as SR is very sensitive to registration errors. In this thesis, the normalization process was used to register the iris images. Indeed, this process performs a scaling of the iris zone dealing with pupil dilation, and thus allowing an alignment of the pixels. However, the blur can reduce the ability to accurately align the iris images. Indeed, the segmentation of blurred images can lead to small errors in the localization of the iris boundaries. As the normalization is based on these boundaries, the normalized iris images can present some distortions and disparities between them. In this case, using iris normalization may not be sufficient as the registration basis for SR. This can explain the fact that SR does not improve as much the recognition rate at long distances due to the blur. Better performances could be expected by performing more accurate registration as usually employed in SR methods such as cross correlation techniques.

Secondly, it would be interesting to investigate the possibility of performing a quality-based fusion scheme at the feature-level i.e. before the features quantization. We could combine our local quality to the response of the Gabor filters before the quantization into a binary code. In a weighted scheme, the phase numbers obtained from noisy regions detected by our local quality will have values near to zeros and occur close to the axes. Lowest weights will be assigned to those regions in the reconstruction of the fused feature template, on which the quantization will be done. Another possibility would be to directly estimate the quality of the iris features by a new quality metric at the

feature level. Then, this measure could be introduced in the fusion scheme at this level in order to give more importance to the features of good quality.

A final point to explore would be to perform a fusion scheme at the bit-level improved by a training phase aiming at optimizing the recognition rate. Each iris images of the sequence is segmented, normalized and then encoded. For fusing the resulting irisCodes, genetic algorithms could be used for finding the best bit-fusion strategy, which optimizes the verification performance. By this way, most relevant bits in the irisCodes of the sequence will be used to reconstruct an optimized fused irisCode.

Bibliography

[1] A. Ross, K. Nandakumar, and A. K. Jain, "Introduction to multibiometrics," in *Handbook of Biometrics*, Springer, 2008, pp. 271–292.

[2] K. W. Bowyer, K. Hollingsworth, and P. J. Flynn, "Image understanding for iris biometrics: A survey," *Comput. Vis. image Underst.*, vol. 110, no. 2, pp. 281–307, 2008.

[3] C. Rathgeb, A. Uhl, and P. Wild, "Iris Segmentation Methodologies," in *Iris Biometrics*, Springer, 2012, pp. 49–73.

[4] A. Ross, "Iris recognition: The path forward," *Computer (Long. Beach. Calif).*, no. 2, pp. 30–35, 2010.

[5] P. Kronfeld and G. Anatomy, "Embryology of the Eye," *Eye, Acad. Press. London*, 1962.

[6] M. Fairhurst and M. Erbilek, "Analysis of physical ageing effects in iris biometrics," *IET Comput. Vis.*, vol. 5, no. 6, pp. 358–366, 2011.

[7] J. Daugman and C. Downing, "Epigenetic randomness, complexity and singularity of human iris patterns," *Proc. R. Soc. London B Biol. Sci.*, vol. 268, no. 1477, pp. 1737–1740, 2001.

[8] A. Bertillon, *La couleur de l'iris*. Masson, 1886.

[9] J. H. Doggart, *Ocular signs in slit-lamp microscopy*. H. Kimpton, 1949.

[10] F. H. Adler, *Physiology of the eye: clinical application*. Mosby, 1959.

[11] L. Flom and A. U. S. Safir, "Patent No. 4641 349," *US Gov. Print. Off. Washington, DC*, 1987.

[12] J. G. Daugman, "Biometric personal identification system based on iris analysis." 1994.

[13] J. G. Daugman, "High confidence visual recognition of persons by a test of statistical independence," *Pattern Anal. Mach. Intell. IEEE Trans.*, vol. 15, no. 11, pp. 1148–1161, 1993.

[14] "UK Border Agency iris recognition immigration system." [Online]. Available: http://www.bbc.com/news/uk-england-17058448. [Accessed: 02-Dec-2015].

[15] "Iris scans at Amsterdam Airport Schiphol." [Online]. Available: http://www.schiphol.nl/Travellers/AtSchiphol/Privium.htm. [Accessed: 02-Dec-2015].

[16] "IRIS ID: Iris access in Action." [Online]. Available: http://www.irisid.com/productssolutions/irisaccessinaction/. [Accessed: 02-Dec-2015].

[17] "Alclear: Clear." [Online]. Available: https://www.clearme.com/. [Accessed: 02-Dec-2015].

[18] J. Daugman, "Iris recognition border-crossing system in the UAE," *Int. Airpt. Rev.*, vol. 8, no. 2, 2004.

[19] J. Daugman, "Iris recognition at 20 years: from zero to 150 trillion iris comparisons per day," in *Keynote Lecture, Biometrics (ICB), 2012 5th IAPR International Conference on*, 2012.

[20] "Unique Identification Authority of India." [Online]. Available: https://uidai.gov.in/. [Accessed: 02-Dec-2015].

[21] "UNHCR - Iris testing of returning Afghans passes 200,000 mark." [Online]. Available: http://www.unhcr.org/3f86b4784.html. [Accessed: 02-Dec-2015].

[22] "Canada Border Services Agency: NEXUS." [Online]. Available: http://www.cbsa-

asfc.gc.ca/prog/nexus/menu-eng.html. [Accessed: 02-Dec-2015].

[23] "Iris Exchange Program." [Online]. Available: http://www.nist.gov/itl/iad/ig/irex.cfm. [Accessed: 09-Dec-2015].

[24] G. W. Quinn, J. Matey, E. Tabassi, and P. Grother, "IREX V report," 2014.

[25] J. R. Matey, O. Naroditsky, K. Hanna, R. Kolczynski, D. J. LoIacono, S. Mangru, M. Tinker, T. M. Zappia, and W. Y. Zhao, "Iris on the move: Acquisition of images for iris recognition in less constrained environments," *Proc. IEEE*, vol. 94, no. 11, pp. 1936–1947, 2006.

[26] F. Bashir, P. Casaverde, D. Usher, and M. Friedman, "Eagle-eyes: a system for iris recognition at a distance," in *Technologies for Homeland Security, 2008 IEEE Conference on*, 2008, pp. 426–431.

[27] F. W. Wheeler, G. Abramovich, B. Yu, P. H. Tu, and others, "Stand-off iris recognition system," in *Biometrics: Theory, Applications and Systems, 2008. BTAS 2008. 2nd IEEE International Conference on*, 2008, pp. 1–7.

[28] W. Dong, Z. Sun, and T. Tan, "A design of iris recognition system at a distance," in *Pattern Recognition, 2009. CCPR 2009. Chinese Conference on*, 2009, pp. 1–5.

[29] S. Yoon, K. Bae, K. R. Park, and J. Kim, "Pan-tilt-zoom based iris image capturing system for unconstrained user environments at a distance," in *Advances in Biometrics*, Springer, 2007, pp. 653–662.

[30] S. Venugopalan, U. Prasad, K. Harun, K. Neblett, D. Toomey, J. Heyman, and M. Savvides, "Long range iris acquisition system for stationary and mobile subjects," in *Biometrics (IJCB), 2011 International Joint Conference on*, 2011, pp. 1–8.

[31] J. De Villar, R. W. Ives, J. R. Matey, and others, "Design and implementation of a long range iris recognition system," in *Signals, Systems and Computers (ASILOMAR), 2010 Conference Record of the Forty Fourth Asilomar Conference on*, 2010, pp. 1770–1773.

[32] J. Daugman, "How iris recognition works," *Circuits Syst. Video Technol. IEEE Trans.*, vol. 14, no. 1, pp. 21–30, 2004.

[33] N. Othman, B. Dorizzi, and S. Garcia-Salicetti, "OSIRIS: An open source iris recognition software," *Pattern Recognit. Lett.*, 2015.

[34] P. Grother and E. Tabassi, "Performance of biometric quality measures," *Pattern Anal. Mach. Intell. IEEE Trans.*, vol. 29, no. 4, pp. 531–543, 2007.

[35] "'Information Technology', Biometric Data Interchange Format. Part 6: Iris Image Data, ISO/IEC 19794-6.," 2005.

[36] "MBGC Portal Challenge Version 2 Preliminary Results. National Institute of Standards and Technology – MGBC 3rd Workshop." [Online]. Available: http://www.nist.gov/itl/iad/ig/mbgc-presentations.cfm. [Accessed: 02-Dec-2015].

[37] "Chinese Academy of Sciences' Institute of Automation, CASIA-Iris-Thousand," 2012. [Online]. Available: http://biometrics.idealtest.org/findTotalDbByMode.do?mode=Iris. [Accessed: 02-Dec-2015].

[38] S. Schuckers, P. Meyer Lopez, P. Johnson, N. Sazonova, F. Hua, R. Lazarick, C. Miles, E. Tabassi, E. Sazonov, A. Ross, and L. Hornak, "Quality--Face / Iris Research Ensemble (Q-FIRE) Data Collection Steps," 2010.

[39] S. Schuckers, P. Meyer Lopez, P. Johnson, N. Sazonova, F. Hua, R. Lazarick, C. Miles, E.

Tabassi, E. Sazonov, A. Ross, and L. Hornak, "Quality--Face / Iris Research Ensemble (Q-FIRE) Dataset Overview," 2010.

[40] P. A. Johnson, P. Lopez-Meyer, N. Sazonova, F. Hua, and S. Schuckers, "Quality in face and iris research ensemble (Q-FIRE)," in *Biometrics: Theory Applications and Systems (BTAS), 2010 Fourth IEEE International Conference on*, 2010, pp. 1–6.

[41] J. Liu, Z. Sun, and T. Tan, "Code-level information fusion of low-resolution iris image sequences for personal identification at a distance," in *Biometrics: Theory, Applications and Systems (BTAS), 2013 IEEE Sixth International Conference on*, 2013, pp. 1–6.

[42] P. A. Johnson, F. Hua, and S. Schuckers, "Comparison of quality-based fusion of face and iris biometrics," in *Biometrics (IJCB), 2011 International Joint Conference on*, 2011, pp. 1–5.

[43] "Biosecure Project." [Online]. Available: http://biosecure.it-sudparis.eu/AB/. [Accessed: 02-Dec-2015].

[44] M. Zhang, J. Liu, Z. Sun, T. Tan, W. Su, F. Alonso-Fernandez, V. Nemesin, N. Othman, K. Noda, P. Li, and others, "The first ICB* competition on iris recognition," in *Biometrics (IJCB), 2014 IEEE International Joint Conference on*, 2014, pp. 1–6.

[45] K. Revett, *Behavioral biometrics: a remote access approach*. John Wiley & Sons, 2008.

[46] H. Proenca, "Towards non-cooperative biometric iris recognition," *Univ. Beira Inter. Dep. Comput. Sci.*, 2006.

[47] "'Information Technology', Biometric performance testing and reporting -- Part 1: Principles and framework, ISO/IEC 19795-1.," 2006.

[48] G. Doddington, W. Liggett, A. Martin, M. Przybocki, and D. Reynolds, "Sheep, goats, lambs and wolves: A statistical analysis of speaker performance in the NIST 1998 speaker recognition evaluation," 1998.

[49] A. Hicklin, B. Ulery, and C. I. Watson, *The myth of goats: How many people have fingerprints that are hard to match?* US Department of Commerce, National Institute of Standards and Technology, 2005.

[50] E. Tabassi, "Image specific error rate: A biometric performance metric," in *Pattern Recognition (ICPR), 2010 20th International Conference on*, 2010, pp. 1124–1127.

[51] E. Tabassi, P. Grother, and W. Salamon, "IREX II-IQCE (Iris Quality Calibration and Evaluation: Performance of Iris Image Quality Assessment Algorithms) report," 2011.

[52] X. Li, Z. Sun, and T. Tan, "Predict and improve iris recognition performance based on pairwise image quality assessment," in *Biometrics (ICB), 2013 International Conference on*, 2013, pp. 1–6.

[53] J. Zuo, F. Nicolo, N. Schmid, H. Wechsler, and others, "Adaptive biometric authentication using nonlinear mappings on quality measures and verification scores," in *Image Processing (ICIP), 2010 17th IEEE International Conference on*, 2010, pp. 4077–4080.

[54] K. Nguyen, C. Fookes, S. Sridharan, and S. Denman, "Focus-score weighted super-resolution for uncooperative iris recognition at a distance and on the move," in *Image and Vision Computing New Zealand (IVCNZ), 2010 25th International Conference of*, 2010, pp. 1–8.

[55] P. J. Flynn, "Biometrics databases," in *Handbook of Biometrics*, Springer, 2008, pp. 529–548.

[56] P. J. Phillips, P. J. Flynn, J. R. Beveridge, W. T. Scruggs, A. J. O'toole, D. Bolme, K. W. Bowyer, B. A. Draper, G. H. Givens, Y. M. Lui, and others, "Overview of the multiple

biometrics grand challenge," in *Advances in Biometrics*, Springer, 2009, pp. 705–714.

[57] X. Tan, F. Song, Z.-H. Zhou, and S. Chen, "Enhanced pictorial structures for precise eye localization under incontrolled conditions," in *Computer Vision and Pattern Recognition, 2009. CVPR 2009. IEEE Conference on*, 2009, pp. 1621–1628.

[58] "Iris Challenge Evaluation." [Online]. Available: http://www.nist.gov/itl/iad/ig/ice.cfm. [Accessed: 02-Dec-2015].

[59] P. J. Phillips, K. W. Bowyer, P. J. Flynn, X. Liu, and W. T. Scruggs, "The iris challenge evaluation 2005," in *Biometrics: Theory, Applications and Systems, 2008. BTAS 2008. 2nd IEEE International Conference on*, 2008, pp. 1–8.

[60] P. J. Phillips, A. Martin, C. L. Wilson, and M. Przybocki, "An introduction evaluating biometric systems," *Computer (Long. Beach. Calif).*, vol. 33, no. 2, pp. 56–63, 2000.

[61] "SOCIA Lab, University of Beira Interior: Noisy Iris Challenge Evaluation Part I." [Online]. Available: http://nice1.di.ubi.pt/. [Accessed: 02-Dec-2015].

[62] "SOCIA Lab, University of Beira Interior: Noisy Iris Challenge Evaluation Part II." [Online]. Available: http://nice2.di.ubi.pt/. [Accessed: 02-Dec-2015].

[63] "UBIRIS: Noisy Visible Wavelength Iris Image Databases." [Online]. Available: URL: http://iris.di.ubi.pt/. [Accessed: 02-Dec-2015].

[64] T. Tan, Z. He, and Z. Sun, "Efficient and robust segmentation of noisy iris images for non-cooperative iris recognition," *Image Vis. Comput.*, vol. 28, no. 2, pp. 223–230, 2010.

[65] J. Daugman, *Biometric decision landscapes*, no. 482. University of Cambridge, Computer Laboratory, 2000.

[66] T. Tan, X. Zhang, Z. Sun, and H. Zhang, "Noisy iris image matching by using multiple cues," *Pattern Recognit. Lett.*, vol. 33, no. 8, pp. 970–977, 2012.

[67] "LivDet-Iris 2013: Iris Liveness Detection Competition 2013," 2013. [Online]. Available: http://iris2013.livdet.org/results.php. [Accessed: 03-Dec-2015].

[68] "MobILive 2014: Mobile Iris Liveness Detection Competition 2014.," 2014. [Online]. Available: http://mobilive2014.inescporto.pt/final-results. [Accessed: 03-Dec-2015].

[69] "MICHE-I: Mobile Iris Challenge Evaluation, Part I," 2014. [Online]. Available: http://biplab.unisa.it/MICHE/index_miche.htm. [Accessed: 03-Dec-2015].

[70] M. De Marsico, M. Nappi, D. Riccio, and H. Wechsler, "Mobile Iris Challenge Evaluation (MICHE)-I, biometric iris dataset and protocols," *Pattern Recognit. Lett.*, vol. 57, pp. 17–23, 2015.

[71] M. De Marsico, M. Nappi, H. Proença, and others, "Guest editorial introduction to the special executable issue on‘ Mobile Iris CHallenge Evaluation part I (MICHE I),'" *Pattern Recognit. Lett.*, no. 57, pp. 1–3, 2015.

[72] J. Daugman, "The importance of being random: statistical principles of iris recognition," *Pattern Recognit.*, vol. 36, no. 2, pp. 279–291, 2003.

[73] J. Daugman, "New methods in iris recognition," *Syst. Man, Cybern. Part B Cybern. IEEE Trans.*, vol. 37, no. 5, pp. 1167–1175, 2007.

[74] R. P. Wildes, "Iris recognition: an emerging biometric technology," *Proc. IEEE*, vol. 85, no. 9, pp. 1348–1363, 1997.

[75] S. J. K. Pedersen, “Circular hough transform,” *Aalborg Univ. Vision, Graph. Interact. Syst.*, 2007.

[76] L. Ma, T. Tan, Y. Wang, and D. Zhang, “Local intensity variation analysis for iris recognition,” *Pattern Recognit.*, vol. 37, no. 6, pp. 1287–1298, 2004.

[77] E. Krichen, S. Garcia-Salicetti, and B. Dorizzi, “A new probabilistic iris quality measure for comprehensive noise detection,” in *Biometrics: Theory, Applications, and Systems, 2007. BTAS 2007. First IEEE International Conference on*, 2007, pp. 1–6.

[78] E. Krichen, S. Garcia-Salicetti, and B. Dorizzi, “A new phase-correlation-based iris matching for degraded images,” *Syst. Man, Cybern. Part B Cybern. IEEE Trans.*, vol. 39, no. 4, pp. 924–934, 2009.

[79] L. Masek and P. Kovesi, “Matlab source code for a biometric identification system based on iris patterns, Master’s thesis,” *Sch. Comput. Sci. Softw. Eng. Univ. West. Aust.*, vol. 26, 2003.

[80] K. W. Bowyer, S. E. Baker, A. Hentz, K. Hollingsworth, T. Peters, and P. J. Flynn, “Factors that degrade the match distribution in iris biometrics,” *Identity Inf. Soc.*, vol. 2, no. 3, pp. 327–343, 2009.

[81] J. Zuo, N. Schmid, and others, “On a methodology for robust segmentation of nonideal iris images,” *Syst. Man, Cybern. Part B Cybern. IEEE Trans.*, vol. 40, no. 3, pp. 703–718, 2010.

[82] A. Uhl and P. Wild, “Weighted adaptive hough and ellipsopolar transforms for real-time iris segmentation,” in *Biometrics (ICB), 2012 5th IAPR International Conference on*, 2012, pp. 283–290.

[83] Z. He, T. Tan, Z. Sun, and X. Qiu, “Toward accurate and fast iris segmentation for iris biometrics,” *Pattern Anal. Mach. Intell. IEEE Trans.*, vol. 31, no. 9, pp. 1670–1684, 2009.

[84] M. Vatsa, R. Singh, and A. Noore, “Improving iris recognition performance using segmentation, quality enhancement, match score fusion, and indexing,” *Syst. Man, Cybern. Part B Cybern. IEEE Trans.*, vol. 38, no. 4, pp. 1021–1035, 2008.

[85] S. Shah and A. Ross, “Iris segmentation using geodesic active contours,” *Inf. Forensics Secur. IEEE Trans.*, vol. 4, no. 4, pp. 824–836, 2009.

[86] K. Roy, P. Bhattacharya, and C. Y. Suen, “Towards nonideal iris recognition based on level set method, genetic algorithms and adaptive asymmetrical SVMs,” *Eng. Appl. Artif. Intell.*, vol. 24, no. 3, pp. 458–475, 2011.

[87] D. Benboudjema, N. Othman, B. Dorizzi, and W. Pieczynski, “Challenging eye segmentation using triplet Markov spatial models,” in *Acoustics, Speech and Signal Processing (ICASSP), 2013 IEEE International Conference on*, 2013, pp. 1927–1931.

[88] S. J. Pundlik, D. L. Woodard, and S. T. Birchfield, “Non-ideal iris segmentation using graph cuts,” in *Computer Vision and Pattern Recognition Workshops, 2008. CVPRW’08. IEEE Computer Society Conference on*, 2008, pp. 1–6.

[89] C. Rathgeb, A. Uhl, and P. Wild, *Iris biometrics: from segmentation to template security*, vol. 59. Springer Science & Business Media, 2012.

[90] Z. Sun and T. Tan, “Ordinal measures for iris recognition,” *Pattern Anal. Mach. Intell. IEEE Trans.*, vol. 31, no. 12, pp. 2211–2226, 2009.

[91] D. M. Monro, S. Rakshit, and D. Zhang, “DCT-based iris recognition,” *Pattern Anal. Mach. Intell. IEEE Trans.*, vol. 29, no. 4, pp. 586–595, 2007.

[92] L. Ma, T. Tan, Y. Wang, and D. Zhang, "Efficient iris recognition by characterizing key local variations," *Image Process. IEEE Trans.*, vol. 13, no. 6, pp. 739–750, 2004.

[93] J. Thornton, M. Savvides, and B. Kumar, "An evaluation of iris pattern representations," in *Biometrics: Theory, Applications, and Systems, 2007. BTAS 2007. First IEEE International Conference on*, 2007, pp. 1–6.

[94] K. Miyazawa, K. Ito, T. Aoki, K. Kobayashi, and H. Nakajima, "A phase-based iris recognition algorithm," in *Advances in biometrics*, Springer, 2005, pp. 356–365.

[95] J. Thornton, M. Savvides, and V. Kumar, "A Bayesian approach to deformed pattern matching of iris images," *Pattern Anal. Mach. Intell. IEEE Trans.*, vol. 29, no. 4, pp. 596–606, 2007.

[96] B. V. K. Kumar, A. Mahalanobis, and D. W. Carlson, "Optimal trade-off synthetic discriminant function filters for arbitrary devices," *Opt. Lett.*, vol. 19, no. 19, pp. 1556–1558, 1994.

[97] L. Masek, "Recognition of human iris patterns for biometric identification," University of Western Australia, 2003.

[98] X. Liu, "Optimizations in iris recognition, Doctoral dissertation," University of Notre Dame, 2006.

[99] Y. Lee, R. J. Micheals, and J. Phillips, "Improvements in video-based automated system for iris recognition (VASIR)," in *Motion and Video Computing, 2009. WMVC'09. Workshop on*, 2009, pp. 1–8.

[100] R. Lienhart and J. Maydt, "An extended set of haar-like features for rapid object detection," in *Image Processing. 2002. Proceedings. 2002 International Conference on*, 2002, vol. 1, pp. I–900.

[101] J. R. Beveridge, G. H. Givens, P. J. Phillips, B. Draper, Y. M. Lui, and others, "Focus on quality, predicting FRVT 2006 performance," in *Automatic Face & Gesture Recognition, 2008. FG'08. 8th IEEE International Conference on*, 2008, pp. 1–8.

[102] E. Krichen, B. Dorizzi, Z. Sun, and S. Garcia-Salicetti, "Iris recognition," in *Guide to Biometric Reference Systems and Performance Evaluation*, Springer, 2009, pp. 25–49.

[103] C. Xu and J. L. Prince, "Snakes, shapes, and gradient vector flow," *Image Process. IEEE Trans.*, vol. 7, no. 3, pp. 359–369, 1998.

[104] G. Sutra, S. Garcia-Salicetti, and B. Dorizzi, "The viterbi algorithm at different resolutions for enhanced iris segmentation," in *Biometrics (ICB), 2012 5th IAPR International Conference on*, 2012, pp. 310–316.

[105] C.-T. Chou, S.-W. Shih, W.-S. Chen, V. W. Cheng, and D.-Y. Chen, "Non-orthogonal view iris recognition system," *Circuits Syst. Video Technol. IEEE Trans.*, vol. 20, no. 3, pp. 417–430, 2010.

[106] H. Proença and L. A. Alexandre, "Iris recognition: Analysis of the error rates regarding the accuracy of the segmentation stage," *Image Vis. Comput.*, vol. 28, no. 1, pp. 202–206, 2010.

[107] H. Proença, "Quality assessment of degraded iris images acquired in the visible wavelength," *Inf. Forensics Secur. IEEE Trans.*, vol. 6, no. 1, pp. 82–95, 2011.

[108] K. P. Hollingsworth, K. W. Bowyer, and P. J. Flynn, "The best bits in an iris code," *Pattern Anal. Mach. Intell. IEEE Trans.*, vol. 31, no. 6, pp. 964–973, 2009.

[109] H. J. Santos-Villalobos, D. R. Barstow, M. Karakaya, C. B. Boehnen, and E. Chaum, "Ornl biometric eye model for iris recognition," in *Biometrics: Theory, Applications and Systems*

(BTAS), 2012 IEEE Fifth International Conference on, 2012, pp. 176–182.

[110] S. Oishi, M. Ichino, and H. Yoshiura, "Fusion of iris and periocular user authentication by AdaBoost for mobile devices," in *Consumer Electronics (ICCE), 2015 IEEE International Conference on*, 2015, pp. 428–429.

[111] K. B. Raja, R. Raghavendra, V. K. Vemuri, and C. Busch, "Smartphone based visible iris recognition using deep sparse filtering," *Pattern Recognit. Lett.*, vol. 57, pp. 33–42, 2015.

[112] Y. Sanchez-Gonzalez, Y. Chacon-Cabrera, and E. Garea-Llano, "A Comparison of Fused Segmentation Algorithms for Iris Verification," in *Progress in Pattern Recognition, Image Analysis, Computer Vision, and Applications*, Springer, 2014, pp. 112–119.

[113] A. Czajka, "Influence of Iris Template Aging on Recognition Reliability," in *Biomedical Engineering Systems and Technologies*, Springer, 2014, pp. 284–299.

[114] D. Camara and V. C. da Rocha Jr, "Providing Higher Entropy Cryptographic Keys by the Use of Biometrics," 2010.

[115] M. V. C. Rodrigues, F. M. Masculo, F. M. de Assis, and B. B. Albert, "Biometrics-Based Secret Key Agreement by Public Discussion with RFID System."

[116] W. A. A. Torres, N. Bhattacharjee, and B. Srinivasan, "Effectiveness of Fully Homomorphic Encryption to Preserve the Privacy of Biometric Data," in *Proceedings of the 16th International Conference on Information Integration and Web-based Applications & Services*, 2014, pp. 152–158.

[117] I. Tomeo-Reyes, J. Liu-Jimenez, I. Rubio-Polo, and B. Fernandez-Saavedra, "Quality metrics influence on iris recognition systems performance," in *Security Technology (ICCST), 2011 IEEE International Carnahan Conference on*, 2011, pp. 1–7.

[118] C. Fancourt, L. Bogoni, K. Hanna, Y. Guo, R. Wildes, N. Takahashi, and U. Jain, "Iris recognition at a distance," in *Audio-and Video-Based Biometric Person Authentication*, 2005, pp. 187–200.

[119] F. Bashir, D. Usher, P. Casaverde, and M. Friedman, "Video surveillance for biometrics: long-range multi-biometric system," in *Advanced Video and Signal Based Surveillance, 2008. AVSS'08. IEEE Fifth International Conference on*, 2008, pp. 175–182.

[120] "Aoptix technologies, Insight-duo: Iris recognition and face capture system." [Online]. Available: http://www.airportsinternational.com/wp-content/directory/pdf/1343040479.pdf. [Accessed: 03-Dec-2015].

[121] "Morpho IAD: Iris at a distance solution." [Online]. Available: http://www.morpho.com/en/aviation-border-security/secure-and-manage-borders/check-traveler-id/control-stations/morpho-iad. [Accessed: 03-Dec-2015].

[122] J. Daugman, "Probing the uniqueness and randomness of IrisCodes: Results from 200 billion iris pair comparisons," *Proc. IEEE*, vol. 94, no. 11, pp. 1927–1935, 2006.

[123] B. J. Kang and K. R. Park, "A study on iris image restoration," in *Audio-and Video-Based Biometric Person Authentication*, 2005, pp. 31–40.

[124] L. Ma, T. Tan, Y. Wang, and D. Zhang, "Personal identification based on iris texture analysis," *Pattern Anal. Mach. Intell. IEEE Trans.*, vol. 25, no. 12, pp. 1519–1533, 2003.

[125] Z. Wei, T. Tan, Z. Sun, and J. Cui, "Robust and fast assessment of iris image quality," in *Advances in Biometrics*, Springer, 2005, pp. 464–471.

[126] G. Lu, J. Qi, and Q. Liao, "A new scheme of iris image quality assessment," in *Intelligent Information Hiding and Multimedia Signal Processing, 2007. IIHMSP 2007. Third International Conference on*, 2007, vol. 1, pp. 147–150.

[127] W. Dong, Z. Sun, T. Tan, and Z. Wei, "Quality-based dynamic threshold for iris matching," in *Image Processing (ICIP), 2009 16th IEEE International Conference on*, 2009, pp. 1949–1952.

[128] K. P. Hollingsworth, K. W. Bowyer, and P. J. Flynn, "The importance of small pupils: a study of how pupil dilation affects iris biometrics," in *Biometrics: Theory, Applications and Systems, 2008. BTAS 2008. 2nd IEEE International Conference on*, 2008, pp. 1–6.

[129] A. Czajka and K. W. Bowyer, "Statistical analysis of multiple presentation attempts in iris recognition," in *Cybernetics (CYBCONF), 2015 IEEE 2nd International Conference on*, 2015, pp. 483–488.

[130] T. Yang, J. Stahl, S. Schuckers, F. Hua, C. B. Boehnen, and M. Karakaya, "Gaze angle estimate and correction in iris recognition," in *Computational Intelligence in Biometrics and Identity Management (CIBIM), 2014 IEEE Symposium on*, 2014, pp. 132–138.

[131] J. Daugman and C. Downing, "Effect of severe image compression on iris recognition performance," *Inf. Forensics Secur. IEEE Trans.*, vol. 3, no. 1, pp. 52–61, 2008.

[132] R. W. Ives, D. A. D. Bishop, Y. Du, and C. Belcher, "Effects of image compression on iris recognition performance and image quality," in *Computational Intelligence in Biometrics: Theory, Algorithms, and Applications, 2009. CIB 2009. IEEE Workshop on*, 2009, pp. 16–21.

[133] S. Rakshit and D. M. Monro, "An evaluation of image sampling and compression for human iris recognition," *Inf. Forensics Secur. IEEE Trans.*, vol. 2, no. 3, pp. 605–612, 2007.

[134] T. Bergmueller, E. Christopoulos, M. Schnoell, and A. Uhl, "Recompression effects in iris segmentation," in *Biometrics (ICB), 2015 International Conference on*, 2015, pp. 1–8.

[135] N. D. Kalka, J. Zuo, N. Schmid, B. Cukic, and others, "Estimating and fusing quality factors for iris biometric images," *Syst. Man Cybern. Part A Syst. Humans, IEEE Trans.*, vol. 40, no. 3, pp. 509–524, 2010.

[136] J. Zuo, N. Schmid, and others, "Global and local quality measures for NIR iris video," in *Computer Vision and Pattern Recognition Workshops, 2009. CVPR Workshops 2009. IEEE Computer Society Conference on*, 2009, pp. 120–125.

[137] N. K. Mahadeo, A. P. Paplinski, and S. Ray, "Automated selection of optimal frames in nir iris videos," in *Digital Image Computing: Techniques and Applications (DICTA), 2013 International Conference on*, 2013, pp. 1–8.

[138] F. Alonso-Fernandez and J. Bigun, "Quality factors affecting iris segmentation and matching," in *Biometrics (ICB), 2013 International Conference on*, 2013, pp. 1–6.

[139] Y. Chen, S. C. Dass, and A. K. Jain, "Localized iris image quality using 2-d wavelets," in *Advances in Biometrics*, Springer, 2005, pp. 373–381.

[140] S. Cremer, B. Dorizzi, S. Garcia-Salicetti, and N. Lempérière, "How a local quality measure can help improving iris recognition," in *Biometrics Special Interest Group (BIOSIG), 2012 BIOSIG-Proceedings of the International Conference of the*, 2012, pp. 1–6.

[141] Y.-H. Li and M. Savvides, "An automatic iris occlusion estimation method based on high-dimensional density estimation," *Pattern Anal. Mach. Intell. IEEE Trans.*, vol. 35, no. 4, pp. 784–796, 2013.

[142] "'Information Technology', Biometric Data Interchange Format. Part 5: Face Image Data, ISO/IEC 19794.," 2004.

[143] D. Reynolds, R. C. Rose, and others, "Robust text-independent speaker identification using Gaussian mixture speaker models," *Speech Audio Process. IEEE Trans.*, vol. 3, no. 1, pp. 72–83, 1995.

[144] L. R. Rabiner, "A tutorial on hidden Markov models and selected applications in speech recognition," *Proc. IEEE*, vol. 77, no. 2, pp. 257–286, 1989.

[145] R. M. Haralick, K. Shanmugam, and I. H. Dinstein, "Textural features for image classification," *Syst. Man Cybern. IEEE Trans.*, no. 6, pp. 610–621, 1973.

[146] B. Mazaheri and H. Pourghassem, "Iris image classification based on texture and Fourier Mellin Transform features," in *Communication Software and Networks (ICCSN), 2011 IEEE 3rd International Conference on*, 2011, pp. 118–122.

[147] V. V. S. Tallapragada and E. G. Rajan, "Iris recognition based on combined feature of GLCM and Wavelet transform," in *Integrated Intelligent Computing (ICIIC), 2010 First International Conference on*, 2010, pp. 205–210.

[148] R. M. Sundaram and B. C. Dhara, "Neural network based Iris recognition system using Haralick features," in *Electronics Computer Technology (ICECT), 2011 3rd International Conference on*, 2011, vol. 3, pp. 19–23.

[149] A. Zaim, A. Sawalha, M. Quweider, J. Iglesias, and R. Tang, "A New Method for Iris Recognition using Gray-Level Coccurence Matrix," in *Electro/information Technology, 2006 IEEE International Conference on*, 2006, pp. 350–353.

[150] D. A. Clausi, M. E. Jernigan, and others, "A fast method to determine co-occurrence texture features," *IEEE Trans. Geosci. Remote Sens.*, vol. 36, no. 1, pp. 298–300, 1998.

[151] J. R. Ferguson, *Using the grey-level co-occurrence matrix to segment and classify radar imagery*. ProQuest, 2007.

[152] M. Hall-Beyer, "GLCM texture: a tutorial," *Natl. Counc. Geogr. Inf. Anal. Remote Sens. Core Curric.*, 2000.

[153] T. Ojala, M. Pietikainen, and D. Harwood, "Performance evaluation of texture measures with classification based on Kullback discrimination of distributions," in *Pattern Recognition, 1994. Vol. 1-Conference A: Computer Vision & Image Processing., Proceedings of the 12th IAPR International Conference on*, 1994, no. 1, pp. 582–585.

[154] T. Ojala, M. Pietikäinen, and T. Mäenpää, "Multiresolution gray-scale and rotation invariant texture classification with local binary patterns," *Pattern Anal. Mach. Intell. IEEE Trans.*, vol. 24, no. 7, pp. 971–987, 2002.

[155] J. MacQueen and others, "Some methods for classification and analysis of multivariate observations," in *Proceedings of the fifth Berkeley symposium on mathematical statistics and probability*, 1967, vol. 1, no. 14, pp. 281–297.

[156] A. P. Dempster, N. M. Laird, and D. B. Rubin, "Maximum likelihood from incomplete data via the EM algorithm," *J. R. Stat. Soc. Ser. B*, pp. 1–38, 1977.

[157] Y. Gong, D. Zhang, P. Shi, and J. Yan, "An optimized wavelength band selection for heavily pigmented iris recognition," *Inf. Forensics Secur. IEEE Trans.*, vol. 8, no. 1, pp. 64–75, 2013.

[158] B. J. Kang and K. R. Park, "Real-time image restoration for iris recognition systems," *Syst.*

Man, Cybern. Part B Cybern. IEEE Trans., vol. 37, no. 6, pp. 1555–1566, 2007.

[159] "Face Recognition Grand Challenge.," 2004. [Online]. Available: http://www.nist.gov/itl/iad/ig/frgc.cfm. [Accessed: 07-Dec-2015].

[160] E. Krichen, L. Allano, S. Garcia-Salicetti, and B. Dorizzi, "Specific texture analysis for iris recognition," in *Audio-and Video-Based Biometric Person Authentication*, 2005, pp. 23–30.

[161] N. Schmid, M. V Ketkar, H. Singh, B. Cukic, and others, "Performance analysis of iris-based identification system at the matching score level," *Inf. Forensics Secur. IEEE Trans.*, vol. 1, no. 2, pp. 154–168, 2006.

[162] K. Hollingsworth, T. Peters, K. W. Bowyer, and P. J. Flynn, "Iris recognition using signal-level fusion of frames from video," *Inf. Forensics Secur. IEEE Trans.*, vol. 4, no. 4, pp. 837–848, 2009.

[163] R. Jillela, A. Ross, and P. J. Flynn, "Information fusion in low-resolution iris videos using principal components transform," in *Applications of Computer Vision (WACV), 2011 IEEE Workshop on*, 2011, pp. 262–269.

[164] G. Fahmy, "Super-resolution construction of iris images from a visual low resolution face video," in *Signal Processing and Its Applications, 2007. ISSPA 2007. 9th International Symposium on*, 2007, pp. 1–4.

[165] K. Nguyen, C. Fookes, S. Sridharan, and S. Denman, "Quality-driven super-resolution for less constrained iris recognition at a distance and on the move," *Inf. Forensics Secur. IEEE Trans.*, vol. 6, no. 4, pp. 1248–1258, 2011.

[166] K. Nguyen, C. Fookes, S. Sridharan, and S. Denman, "Feature-domain super-resolution for iris recognition," *Comput. Vis. Image Underst.*, vol. 117, no. 10, pp. 1526–1535, 2013.

[167] K. Nguyen, S. Sridharan, S. Denman, and C. Fookes, "Feature-domain super-resolution framework for Gabor-based face and iris recognition," in *Computer Vision and Pattern Recognition (CVPR), 2012 IEEE Conference on*, 2012, pp. 2642–2649.

[168] H. Ren, Y. He, J. Pan, and L. Li, "Super resolution reconstruction and recognition for iris image sequence," in *Biometric Recognition*, Springer, 2012, pp. 193–201.

[169] N. Mahadeo, A. Paplinski, and S. Ray, "Optimization of Iris Codes for Improved Recognition," in *Computer Vision and Pattern Recognition Workshops (CVPRW), 2014 IEEE Conference on*, 2014, pp. 48–55.

[170] M. Bevilacqua, "Algorithms for super-resolution of images and videos based on learning methods," Rennes 1, 2014.

[171] S. C. Park, M. K. Park, and M. G. Kang, "Super-resolution image reconstruction: a technical overview," *Signal Process. Mag. IEEE*, vol. 20, no. 3, pp. 21–36, 2003.

[172] J. Yang and T. Huang, "Image super-resolution: Historical overview and future challenges," *Super-resolution imaging*, pp. 20–34, 2010.

[173] H. Ur and D. Gross, "Improved resolution from subpixel shifted pictures," *CVGIP Graph. Model. Image Process.*, vol. 54, no. 2, pp. 181–186, 1992.

[174] N. K. Bose, N. Ahuja, and others, "Superresolution and noise filtering using moving least squares," *Image Process. IEEE Trans.*, vol. 15, no. 8, pp. 2239–2248, 2006.

[175] M. Irani and S. Peleg, "Super resolution from image sequences," in *Pattern Recognition, 1990. Proceedings., 10th International Conference on*, 1990, vol. 2, pp. 115–120.

[176] A. J. Patti, M. I. Sezan, and others, "Superresolution video reconstruction with arbitrary sampling lattices and nonzero aperture time," *Image Process. IEEE Trans.*, vol. 6, no. 8, pp. 1064–1076, 1997.

[177] R. Y. Tsai and T. S. Huang, "Multiframe image restoration and registration," *Adv. Comput. Vis. Image Process.*, vol. 1, no. 2, pp. 317–339, 1984.

[178] S. Rhee and M. G. Kang, "DCT-based regularized algorithm for high-resolution image reconstruction," in *Image Processing, 1999. ICIP 99. Proceedings. 1999 International Conference on*, 1999, vol. 3, pp. 184–187.

[179] N. Woods, N. P. Galatsanos, A. K. Katsaggelos, and others, "Stochastic methods for joint registration, restoration, and interpolation of multiple undersampled images," *Image Process. IEEE Trans.*, vol. 15, no. 1, pp. 201–213, 2006.

[180] N. Nguyen and P. Milanfar, "An efficient wavelet-based algorithm for image superresolution," in *Image Processing, 2000. Proceedings. 2000 International Conference on*, 2000, vol. 2, pp. 351–354.

[181] S. E. El-Khamy, M. M. Hadhoud, M. I. Dessouky, B. M. Salam, and F. E. A. El-Samie, "Wavelet fusion: A tool to break the limits on LMMSE image super-resolution," *Int. J. Wavelets, Multiresolution Inf. Process.*, vol. 4, no. 01, pp. 105–118, 2006.

[182] H. Ji and C. Fermüller, "Wavelet-based super-resolution reconstruction: theory and algorithm," in *Computer Vision--ECCV 2006*, Springer, 2006, pp. 295–307.

[183] J. Tian and K.-K. Ma, "Stochastic super-resolution image reconstruction," *J. Vis. Commun. Image Represent.*, vol. 21, no. 3, pp. 232–244, 2010.

[184] K. Nguyen, C. Fookes, and S. Sridharan, "Robust mean super-resolution for less cooperative NIR iris recognition at a distance and on the move," in *Proceedings of the 2010 Symposium on Information and Communication Technology*, 2010, pp. 122–127.

[185] K. Y. Shin, K. R. Park, B. J. Kang, and S. J. Park, "Super-resolution method based on multiple multi-layer perceptrons for iris recognition," in *Ubiquitous Information Technologies & Applications, 2009. ICUT'09. Proceedings of the 4th International Conference on*, 2009, pp. 1–5.

[186] L. Ma, Y. Wang, and T. Tan, "Iris recognition using circular symmetric filters," in *Pattern Recognition, 2002. Proceedings. 16th International Conference on*, 2002, vol. 2, pp. 414–417.

[187] J. Huang, L. Ma, T. Tan, and Y. Wang, "Learning Based Resolution Enhancement of Iris Images.," in *BMVC*, 2003, pp. 1–10.

[188] S. Geman and D. Geman, "Stochastic relaxation, Gibbs distributions, and the Bayesian restoration of images," *Pattern Anal. Mach. Intell. IEEE Trans.*, no. 6, pp. 721–741, 1984.

[189] W. T. Freeman, T. R. Jones, and E. C. Pasztor, "Example-based super-resolution," *Comput. Graph. Appl. IEEE*, vol. 22, no. 2, pp. 56–65, 2002.

[190] N. Wiener, *Extrapolation, interpolation, and smoothing of stationary time series*, vol. 2. MIT press Cambridge, MA, 1949.

[191] M. E. Schuckers, *Computational Methods in Biometric Authentication: Statistical Methods for Performance Evaluation*. Springer Science & Business Media, 2010.

[192] R. M. Bolle, S. Pankanti, J. H. Connell, and N. K. Ratha, "Iris individuality: A partial iris model," in *Pattern Recognition, 2004. ICPR 2004. Proceedings of the 17th International*

Conference on, 2004, vol. 2, pp. 927–930.

[193] Y. Du, B. Bonney, R. Ives, D. Etter, and R. Schultz, "Analysis of partial iris recognition using a 1D approach," in *Acoustics, Speech, and Signal Processing, 2005. Proceedings.(ICASSP'05). IEEE International Conference on*, 2005, vol. 2, pp. ii–961.

[194] K. P. Hollingsworth, K. W. Bowyer, and P. J. Flynn, "Improved iris recognition through fusion of hamming distance and fragile bit distance," *Pattern Anal. Mach. Intell. IEEE Trans.*, vol. 33, no. 12, pp. 2465–2476, 2011.

[195] G. Dozier, K. Frederiksen, R. Meeks, M. Savvides, K. Bryant, D. Hopes, and T. Munemoto, "Minimizing the number of bits needed for iris recognition via bit inconsistency and grit," in *Computational Intelligence in Biometrics: Theory, Algorithms, and Applications, 2009. CIB 2009. IEEE Workshop on*, 2009, pp. 30–37.

[196] C. Rathgeb, A. Uhl, and P. Wild, "On combining selective best bits of iris-codes," in *Biometrics and ID Management*, Springer, 2011, pp. 227–237.

[197] C. Rathgeb, A. Uhl, and P. Wild, "Incremental iris recognition: A single-algorithm serial fusion strategy to optimize time complexity," in *Biometrics: Theory Applications and Systems (BTAS), 2010 Fourth IEEE International Conference on*, 2010, pp. 1–6.

[198] J. E. Gentile, N. Ratha, and J. Connell, "SLIC: Short-length iris codes," in *Biometrics: Theory, Applications, and Systems, 2009. BTAS '09. IEEE 3rd International Conference on*, 2009, pp. 1–5.

[199] "Multimedia University, MMU iris image database," 2004.

[200] J. E. Gentile, N. Ratha, and J. Connell, "An efficient, two-stage iris recognition system," in *Biometrics: Theory, Applications, and Systems, 2009. BTAS'09. IEEE 3rd International Conference on*, 2009, pp. 1–5.

[201] W. Dong, Z. Sun, and T. Tan, "Iris matching based on personalized weight map," *Pattern Anal. Mach. Intell. IEEE Trans.*, vol. 33, no. 9, pp. 1744–1757, 2011.

[202] H. Proenca, "Iris Recognition: What Is Beyond Bit Fragility?," *Inf. Forensics Secur. IEEE Trans.*, vol. 10, no. 2, pp. 321–332, 2015.

[203] E. Krichen, "Reconnaissance des personnes par l'iris en mode dégradé," Evry, Institut national des télécommunications, 2007.

Appendix A: Personal publications

International conferences:

- Nadia Othman, Nesma Houmani, Bernadette Dorizzi: *Improving Video-based Iris Recognition Via Local Quality Weighted Super Resolution*, in International Conference on Pattern Recognition Applications and Methods (ICPRAM), Barcelona, Spain, 2013.
- Dalila Benboudjema, Nadia Othman, Bernadette Dorizzi, Wojciech Pieczynski: *Challenging eye segmentation using Triplet Markov spatial models*, in International Conference on Acoustics, Speech and Signal Processing (ICASSP), Vancouver, Canada, 2013.
- M. Zhang, J. Liu, Z. Sun, T. Tan, W. Su, F. Alonso-Fernandez, V. Nemesin, N. Othman, K. Noda, P. Li, E. Hoyle, A. Josh: *The First ICB Competition on Iris Recognition*, in international Joint Conference on Biometrics (IJCB), Florida, USA, 2014.

National conference:

- Dalila Benboudjema, Nadia Othman, Bernadette Dorizzi, Wojciech Pieczynski: *Segmentation d'images des yeux par champs de markov triplets: Application à la biométrie*, in proceedings to Colloque GRETSI, 2013.

Book chapter:

- Nadia Othman, Nesma Houmani, and Bernadette Dorizzi: Quality-Based Super Resolution for Degraded Iris Recognition, in Advances in Intelligent Systems and Computing, Series "Pattern Recognition Applications and Methods", vol. 318, Springer, Jan. 2015.

International journals:

- Nadia Othman, and Bernadette Dorizzi: Impact of Quality-Based Fusion Techniques for Video-Based Iris Recognition at a Distance, in Information Forensics and Security, IEEE Transactions on , vol.10, no.8, pp.1590-1602, Aug. 2015.
- Nadia Othman, Bernadette Dorizzi, and Sonia Garcia-Salicetti: OSIRIS: An Open Source Iris Recognition Software, in Pattern Recognition Letters (accepted in Sept 2015).

Appendix B: QFIRE subset and protocols

The subset is available upon request. See CITER website:

http://clarkson.edu/citer/research/collections/face_iris_research.html

The protocols are available online:

http://svnext.it-sudparis.eu/svnview2-eph/ref_syst/QFIRE_protocols/

Quality Face and Iris Research Ensemble (QFIRE) [1] [2] is a multimodal database composed of iris and face videos, recorded at Clarkson University. The acquisition was funded by the Department of Homeland Security (DHS) Science and Technology (S&T) Directorate in cooperation with the National Science Foundation. QFIRE contains a large number of various acquisition scenarios. The sequences are collected at varying distances and different quality levels, entirely controlled during the acquisition.

As we address the problem of iris recognition at a distance, we have selected 3 subsets from the QFIRE database which seem to us interesting for our context. More precisely, we have proposed in [3] several systems aiming at improving the poor performance resulting from image degradations (low resolution, blur, and lack of texture) obtained from such distant acquisitions. Our approaches are based on simple super-resolution techniques applied at the pixel level on the different frames of a video, improved by taking into account some quality criteria.

The 3 selected subsets correspond to the scenario “illumination” at the medium quality level, and at different distances: 5, 7 and 11 feet of QFIRE database. This variability in the distance was introduced to produce high, medium and low resolution iris images. The quality factor "resolution" is defined as the number of pixels across the horizontal diameter of the iris. In addition, during the acquisition procedure of QFIRE, an intentional defocus blur was added to each sequence by manually turning the focus ring of the iris camera in order to generate some non-uniformity in each video sequence. Note that the subjects are static.

To study the contribution of our fusion approaches, we benchmarked them on these 3 distances by comparing videos against videos as protocol.

Dataset overview:

To build the dataset, we first tracked right and left eyes in the NIR videos. In particular, the sequences contain entire (at long distances) or partial faces (at close distance). To localize the eyes, in the case of

entire faces, we used the MATLAB code developed in [4] based on an enhanced pictorial structure model for precise eye localization. In order to track the eyes in partial faces, we used a simple implementation based on a Hough transform. Due to the intentional defocus blur added at the beginning and the end during the sequence acquisition, we have discarded unusable frames and for this, we used wavelet transform. To increase the number of videos, long sequences were divided into sequences of 10 frames. In order to increase the number of intra-class comparisons, we divided the sequences with a large number of usable frames into multiple sequences of 10 frames. We give in TABLE 1 a summary of the dataset we obtained after all these pre-processing processes.

Those interested in these datasets can request a copy from Clarkson University at the following email address: citer@clarkson.edu. Any questions related to requesting the dataset can also be directed to: sschucke@clarkson.edu.

TABLE 1: CHARACTERISTICS OF EACH OF THE 3 SUBSETS OF QFIRE DATABASE USED IN [3].

Acquisition distance	*5 feet*	*7 feet*	*11 feet*
Database nomination	*QFIRE05*	*QFIRE07*	*QFIRE11*
Number of sequences	*662*	*453*	*361*
Number of frames per sequence	*10*	*10*	*10*
Number of class	*166*	*160*	*113*
Number of sequence per class	*2 to 6*	*2 to 6*	*2 to 6*
Image size	*680 x520 (mostly)*	*640x480 (mostly)*	*280x440*
Format	*bmp*	*bmp*	*bmp*
Iris Resolution	*280 to 300*	*200 to 220*	*100 to 120*
Quality level (resolution)	*High*	*Medium*	*Low*
Subset comparable to	*Higher quality of UBIRIS datasets*	*Medium quality of CASIA and BioSecure datasets*	*Low quality MBGC dataset (NIR face camera)*
Illumination level	*Medium*	*Medium*	*Medium*
Number of session	*2*	*2*	*2*
Sensor	*Dalsa 4M30 infrared camera*	*Dalsa 4M30 infrared camera*	*Dalsa 4M30 infrared camera*
Other information	*Possible presence of blur, spot light and occlusion*	*Possible presence of blur, spot light and occlusion*	*Possible presence of blur, spot light and occlusion*

The convention name of the images is as follows:

(Subject Number)_illumination_(Distance)_ft_M(Sequence Number)-F(Frame Number)-(Iris).bmp

where:

Distance: [05, 07, 11]

Iris: [LEFT, RIGHT]

Protocols:

The protocols are available online:

http://svnext.it-sudparis.eu/svnview2-eph/ref_syst/QFIRE_protocols/

List of images:

The lists of the images are available in the folder: *"./List of images/*". For example, the file: "*ImList_05ft_session1.txt*" lists the images of QFIRE05 subset, acquired during the first session. Each line represents the ten used images for each sequence.

List of matching:

The matching protocol is based on a comparison of *N* fused frames (session1) vs. *N* fused frames (session2). TABLE 2 reports the number of comparisons for each subset.

TABLE 2: NUMBER OF COMPARISONS FOR EACH SUBSET OF QFIRE DATABASE USED IN [3].

Database nomination	***QFIRE05***	***QFIRE07***	***QFIRE11***
Intra-class comparisons	*670*	*320*	*293*
Inter-class comparisons	*108722*	*50676*	*32231*

The matching lists are available in the folder: *"./List of matching/*". For example the text file *"InterMatchingList_05ft.txt"* gives the inter-class comparisons of QFIRE05. The first and second column respectively represents the name of the fused template obtained from the sequence acquired in the first and second session. The convention name of the fused template is as follows:

(Subject Number)_illumination_(Distance)_ft_M(Sequence Number)-(Iris)_(Session).bmp

where:

Distance: [05, 07, 11]

Iris: [LEFT, RIGHT]

Session: [1, 2]

References

Please cite the following references on any work made public based directly or indirectly on the data we have presented in this document:

"N. Othman, and B. Dorizzi: Impact of Quality-Based Fusion Techniques for Video-Based Iris Recognition at a Distance, in Information Forensics and Security, IEEE Transactions on , vol.10, no.8, pp.1590-1602, Aug. 2015."

Please, do not forget also to cite the references of the original QFIRE database, as indicated by its owners.

Contact:

Questions regarding these datasets and protocols can be directed toward:

Nadia Othman: nadia.othmane@gmail.com

Bernadette Dorizzi: Bernadette.dorizzi@telecom-sudparis.eu

Bibliography:

[1] S. Schuckers, P. Meyer Lopez, P. Johnson, N. Sazonova, F. Hua, R. Lazarick, C. Miles, E. Tabassi, E. Sazonov, A. Ross, and L. Hornak, "Quality--Face / Iris Research Ensemble (Q-FIRE) Data Collection Steps," 2010.

[2] S. Schuckers, P. Meyer Lopez, P. Johnson, N. Sazonova, F. Hua, R. Lazarick, C. Miles, E. Tabassi, E. Sazonov, A. Ross, and L. Hornak, "Quality--Face / Iris Research Ensemble (Q-FIRE) Dataset Overview," 2010.

[3] N. Othman, and B. Dorizzi: Impact of Quality-Based Fusion Techniques for Video-Based Iris Recognition at a Distance, in Information Forensics and Security, IEEE Transactions on , vol.10, no.8, pp.1590-1602, Aug. 2015.

[4] X. Tan, F. Song, Z.-H. Zhou, and S. Chen, "Enhanced pictorial structures for precise eye localization under incontrolled conditions," in Computer Vision and Pattern Recognition, 2009. CVPR 2009. IEEE Conference on, 2009, pp. 1621–1628.